

# Robustness-Aware 3D Object Detection in Autonomous Driving: A Review and Outlook

Ziying Song, Lin Liu, Feiyang Jia, Yadan Luo, Caiyan Jia, Guoxin Zhang, Lei Yang, Li Wang

**Abstract**—In the realm of modern autonomous driving, the perception system is indispensable for accurately assessing the state of the surrounding environment, thereby enabling informed prediction and planning. The key step to this system is related to 3D object detection that utilizes vehicle-mounted sensors such as LiDAR and cameras to identify the size, the category, and the location of nearby objects. Despite the surge in 3D object detection methods aimed at enhancing detection precision and efficiency, there is a gap in the literature that systematically examines their resilience against environmental variations, noise, and weather changes. This study emphasizes the importance of robustness, alongside accuracy and latency, in evaluating perception systems under practical scenarios. Our work presents an extensive survey of camera-only, LiDAR-only, and multi-modal 3D object detection algorithms, thoroughly evaluating their trade-off between accuracy, latency, and robustness, particularly on datasets like KITTI-C and nuScenes-C to ensure fair comparisons. Among these, multi-modal 3D detection approaches exhibit superior robustness, and a novel taxonomy is introduced to reorganize the literature for enhanced clarity. This survey aims to offer a more practical perspective on the current capabilities and the constraints of 3D object detection algorithms in real-world applications, thus steering future research towards robustness-centric advancements.

**Index Terms**—3D Object Detection, Perception, Robustness, Autonomous Driving

## I. INTRODUCTION

**A**UTONOMOUS driving systems, fundamental to the future of transportation, heavily rely on advanced perception, decision-making, and control technologies. These systems employ a range of sensors [1] such as camera, LiDAR and radar as depicted in Fig. 1, to effectively perceive surrounding environments. This capability is crucial for recognizing road signs, detecting and tracking vehicles,

This work was supported in part by the National Key R&D Program of China (2018AAA0100302), supported by the STI 2030-Major Projects under Grant 2021ZD0201404. (Corresponding author: Caiyan Jia.)

Ziying Song, Lin Liu, Feiyang Jia, Caiyan Jia are with School of Computer Science & Technology, Beijing Key Lab of Traffic Data Analysis and Mining, Beijing Jiaotong University, Beijing 100044, China (e-mail: 22110110@bjtu.edu.cn, liulin010811@gmail.com, feiyangjia@bjtu.edu.cn, cyjia@bjtu.edu.cn)

Yadan Luo is with the School of Information Technology and Electrical Engineering, The University of Queensland, St Lucia, QLD 4072, Australia (e-mail: uqyluo@uq.edu.au)

Guoxin Zhang is with School of Computer Science, Beijing University of Posts and Telecommunications, Beijing 100876, China (e-mail: zhangguoxins@gmail.com)

Lei Yang is with the State Key Laboratory of Intelligent Green Vehicle and Mobility, and the School of Vehicle and Mobility, Tsinghua University, Beijing 100084, China (e-mail: yanglei20@mails.tsinghua.edu.cn).

Li Wang is with School of Mechanical Engineering, Beijing Institute of Technology, Beijing 100081, China (e-mail: wangli\_bit@bit.edu.cn)

and predicting pedestrian behaviors, enabling safe operations amidst complex traffic conditions [2].

The primary task of perception is to accurately understand the surrounding environment and minimize collision risks [3]. This is where 3D object detection methods become essential. These approaches enable the autonomous systems to accurately identify objects in the vicinity, including their position, shape, and category [4]. Such detailed environmental perception enhances the system’s ability to comprehend the driving context and make more informed decisions.

The advancement of autonomous driving technologies has spared a wave of research in 3D object detection, leading to the development of diverse and innovative methods. These approaches are typically categorized based on their input types, including camera-only [5]–[35], LiDAR-only [36]–[98], and multi-modal methods [65], [99]–[122]. The current landscape of 3D object detection methods is prolific, necessitating a comprehensive summarization to offer intriguing insights to the research community. While comprehensive, prior surveys, such as [4], [123], often overlook the safety aspects of autonomous driving perception, particularly in terms of the system’s robustness against varying testing data following deployment.

In real-world testing scenarios, the conditions encountered usually greatly differ from those during training. The environmental variability, sensor discrepancies or noise, and spatial misalignment can cause a shift in the input sensory data distribution, leading to a significant drop in detector performance [108], [111], [124], [125]. We identify and discuss three major factors critical for assessing detection **robustness**.

- **Environmental Variability.** A detection algorithm needs to perform well under different environmental conditions, including variations in lighting, weather, and seasons. The algorithms should exhibit adaptability, ensuring that it does not fail due to changes in the environment.
- **Sensor Noise.** This includes handling noise introduced by sensor malfunctions, such as motion blur in a camera. An algorithm must possess the capability to effectively manage hardware noise, ensuring the accurate processing of input data.
- **Misalignment.** In real-world scenarios, sensor calibration errors can complicate the synchronization of multi-modal input data, causing misalignment due to external factors (e.g., uneven road surfaces) or internal factors (e.g., system clock misalignment). An algorithm should be fault-tolerant and may incorporate an elastic alignment to mitigate the impact of misalignment on detection performance.

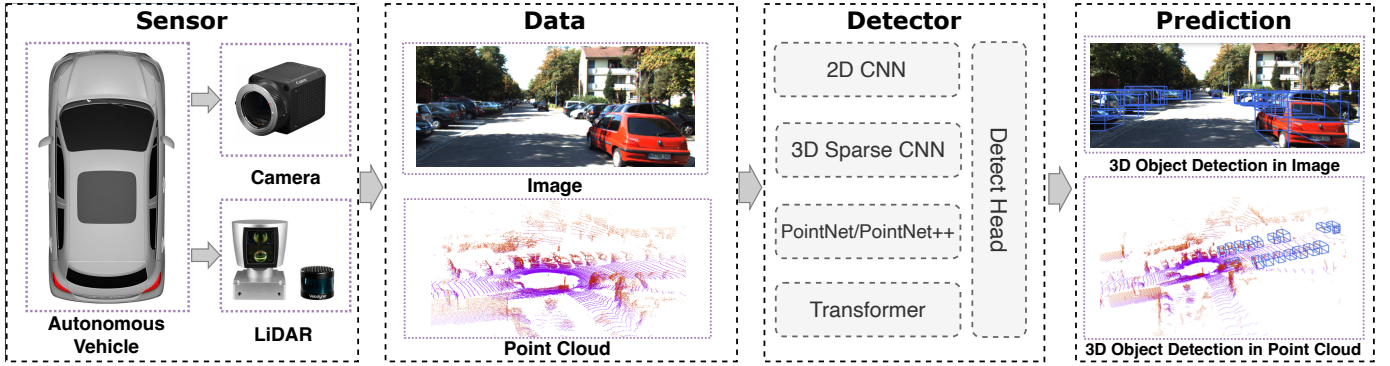


Fig. 1: An illustration of 3D object detection in autonomous driving scenarios with different sensors.

To ensure safe operation in varying test environments, assessing the robustness of 3D object detection algorithms is essential. They must maintain efficient, accurate, and reliable performance across diverse scenarios. In this survey, we conduct extensive experimental comparisons among existing algorithms. Centered around ‘Accuracy, Latency, Robustness’, we delve into existing solutions, offering insightful guidance for practical deployment in autonomous driving.

- **Accuracy:** Current researches often prioritize accuracy as a key performance metric. However, a deeper understanding of these methods’ performance in complex environments and extreme weather conditions is needed to ensure real-world reliability. A more detailed analysis of false positives and false negatives is necessary for improvement.
- **Latency:** Real-time capability is vital for autonomous driving. The latency of a 3D object detection method impacts the system’s ability to make timely decisions, particularly in emergencies.
- **Robustness:** Robustness refers to the system’s stability under various conditions, including weather, lighting, sensory and alignment changes. Many existing evaluations may not fully consider the diversity of real-world scenarios, necessitating a more comprehensive adaptability assessment.

Through an in-depth analysis of extensive experimental results, with a focus on ‘Accuracy, Latency, Robustness’, we have identified significant advantages in safety perception with Multi-modal 3D detection in safety perception. By integrating information from diverse sensors or data sources, Multi-modal methods provide a richer and more diverse perception capability for autonomous driving systems, thereby enhancing the understanding and responding to the surrounding environment. Our research provides practical guidance for the future deployment of autonomous driving technology. By discussing these key areas, we aim to align the technology more closely with real-world needs and enhance its societal benefits effectively.

The structure of this paper is organized as follows: First, we introduce the datasets and evaluation metrics for 3D object detection, with a particular focus on robustness in Section II. Subsequent sections systematically examine existing 3D object detection methods, including camera-only approaches (Section III), LiDAR-only approaches (Section IV), and multi-

TABLE I: Advantages and limitations of different modalities.

Type	Sensor	Hardware Cost(\$)	Advantages	Limitations
Image	Camera	$10^2$ - $10^3$	+ The dense data incorporates additional color and texture information.	- Missing depth information and affected by light, weather, etc.
Point cloud	LiDAR	$10^4$ - $10^5$	+ With accurate depth information less affected by light and larger field of view	- High computational cost for sparse and disordered point cloud data and no color information.
Multi-modal	Camera, LiDAR	$10^4$ - $10^5$	+ Simultaneous color and depth information	- Fusion methods can produce noise interference

modal approaches (Section V). The paper concludes with a comprehensive summary of our findings in Section VII.

## II. DATASETS

Currently, autonomous driving systems primarily rely on sensors such as cameras, and LiDAR, generating data in two modalities, point clouds and images. Based on these data types, existing public benchmarks predominantly manifest in three forms: camera-only, LiDAR-only, and multi-modal. Table I delineates the advantages and the disadvantages of each of these three forms. Among them, there are many reviews [123], [126]–[132] providing a comprehensive overview of **clean** autonomous driving datasets as shown in Table II. The most notable ones include KITTI [133], nuScenes [134], and Waymo [135].

In recent times, the pioneering work on clean autonomous driving datasets has provided rich resources for 3D object detection. As autonomous driving technology transitions from breakthrough stages to practical implementation, we have conducted some guided researches to systematically review the currently available robustness datasets. We have focused more on noisy scenarios and systematically reviewed datasets related to the robustness of 3D detection. Many studies have collected new datasets to evaluate model robustness under different conditions. Early research explored camera-only approaches under adverse conditions [136], [137], with datasets that were notably small in scale and exclusively applicable to camera-only visual tasks, rather than multi-modal sensor stacks that include LiDAR. Subsequently, a series of multi-modal datasets [138]–[141] have focused on noise concerns. For instance, the GROUNDED dataset [138] focuses on ground-penetrating

radar localization under varying weather conditions. Additionally, the ApolloScape open dataset [140] incorporates LiDAR, camera, and GPS data, encompassing cloudy and rainy conditions as well as brightly lit scenarios. The Ithaca365 dataset [141] is designed for robustness in autonomous driving research, providing scenarios under various challenging weather conditions, such as rain and snow.

Due to the prohibitive cost of collecting extensive noisy datasets from the real world, rendering the formation of large-scale datasets impractical, many studies have shifted their focus to synthetic datasets. ImageNet-C [142] is a seminal work in corruption robustness research, benchmarking classical image classification models against prevalent corruptions and perturbations. This line of research has subsequently been extended to include robustness datasets tailored for 3D object detection in autonomous driving. Additionally, there are adversarial attacks [143]–[145] designed for studying the robustness of 3D object detection. However, these attacks may not exclusively concentrate on natural corruption, which is less common in autonomous driving scenarios.

To better emulate the distribution of noise data in the real world, several studies [124], [125], [146]–[149] have developed toolkits for robustness benchmarks. These benchmark toolkits [124], [125], [146]–[149] enable the simulation of various scenarios using clean autonomous driving datasets, such as KITTI [133], nuScenes [134], and Waymo [135]. Among them, Dong et al. [125] systematically designed 27 common corruptions in 3D object detection to benchmark the corruption robustness of existing detectors. By applying these corruptions comprehensively on public datasets, they established three corruption-robust benchmarks: KITTI-C, nuScenes-C, and Waymo-C. [125] denotes model performance on the original validation set as  $AP_{\text{clean}}$ . For each corruption type  $c$  at each severity  $s$ , [125] adopts the same metric to measure model performance as  $AP_{c,s}$ . The corruption robustness of a model is calculated by averaging over all corruption types and severities as

$$\Lambda P_{\text{cor}} = \frac{1}{|\mathcal{C}|} \sum_{c \in \mathcal{C}} \frac{1}{5} \sum_{s=1}^5 \Lambda P_{c,s}. \quad (1)$$

Where  $\mathcal{C}$  is the set of corruptions in evaluation. It should be noticed that for different kinds of 3D object detectors, the set of corruptions can be different (e.g., [125] has not evaluated camera noises for LiDAR-only models). Thus, the results of  $\Lambda P_{\text{cor}}$  are not directly comparable between different kinds of models, and [125] performs a fine-grained analysis under each corruption. It also calculates relative corruption error (RCE) by measuring the percentage of performance drop as

$$\text{RCE}_{c,s} = \frac{AP_{\text{clean}} - AP_{c,s}}{AP_{\text{clean}}}; \text{RCE} = \frac{AP_{\text{clean}} - \Lambda P_{\text{cor}}}{AP_{\text{clean}}}. \quad (2)$$

Unlike KITTI-C and Waymo-C, nuScenes-C primarily assesses performance using the mean Average Precision (mAP) and nuScenes Detection Score (NDS) computed across ten object categories. The mAP is determined using the 2D center distance on the ground plane instead of the 3D Intersection over Union (IoU). The NDS metric consolidates mAP with

TABLE II: Public datasets for 3D object detection in autonomous driving. ‘C’, ‘L’ and ‘R’ denote Camera, LiDAR and Radar, respectively.

Dataset	Year	Sensors	Data Size		Diversity	
			Frame	Annotation	Scenes	Category
KITTI [133]	2012	CL	15K	200K	50	3
nuScenes [134]	2019	CLR	40K	1.4M	1000	10
Lyft L5 [150]	2019	CL	46K	1.3M	366	9
H3D [151]	2019	L	27K	1.1M	160	8
Applo [152]	2019	CL	140K	-	103	27
Argoverse [153]	2019	CL	46K	993K	366	9
A*3D [154]	2019	CL	39K	230K	-	7
Waymo [135]	2020	CL	230K	12M	1150	3
A2D2 [155]	2020	CL	12.5K	43K	-	38
PandaSet [156]	2020	CL	14K	-	179	28
KITTI-360 [157]	2020	CL	80K	68K	11	19
Cirrus [158]	2020	CL	6285	-	12	8
ONCE [159]	2021	CL	15K	417K	-	5
OpenLane [160]	2022	CL	200K	-	1000	14

other aspects, such as scale and orientation, into a unified score. Analogous to KITTI-C, [125] denotes the model’s performance on the validation set as  $mAP_{\text{clean}}$  and  $NDS_{\text{clean}}$ , respectively. The corruption robustness metrics,  $mAP_{\text{cor}}$  and  $NDS_{\text{cor}}$ , are evaluated by averaging over all corruption types and severities. Additionally, [125] calculates the Relative Corruption Error (RCE) under both mAP and NDS metrics, similar to the formulation in Eq.2.

Additionally, some studies [143], [146], [161] examine robustness in single-modal contexts. For instance, [146] proposes a LiDAR-only benchmark that utilizes physically-aware simulation methods to simulate degraded point clouds under various real-world common corruptions. This benchmark, tailored for point cloud detectors, includes 1,122,150 examples across 7,481 scenes, covering 25 common corruption types with six severity levels. Moreover, [146] devises a novel evaluation metric, including  $CE_{\text{AP}}(\%)$  and  $mCE$ , and calculates corruption error (CE) to assess performance degradation based on Overall Accuracy (OA) by

$$CE_{c,s}^m = OA_{\text{clean}}^m - OA_{c,s}^m, \quad (3)$$

where  $OA_{c,s}^m$  is the overall accuracy of detector  $m$  under corruption  $c$  of severity level  $s$  (excluding “clean,” i.e., severity level 0) and clean represents the clean data. For detector  $m$ , we can calculate the mean CE (mCE) for each detector by

$$mCE^m = \frac{\sum_{s=1}^5 \sum_{c=1}^{25} CE_{c,s}^m}{5C}. \quad (4)$$

### III. CAMERA-ONLY 3D OBJECT DETECTION

In this section, we introduce the Camera-only 3D object detection methods. Compared to LiDAR-only methods, the camera solution is more cost-effective and the images obtained from cameras require no complex preprocessing. Therefore, it is favored by many automotive manufacturers, particularly in the context of multi-view applications such as BEV (bird’s-eye view) systems. Generally, as shown in Fig. 2, Camera-only methods can be categorized into three types, monocular, stereo-based, and multi-view (bird’s-eye view). Due to the excellent cost-effectiveness of Camera-only methods, there

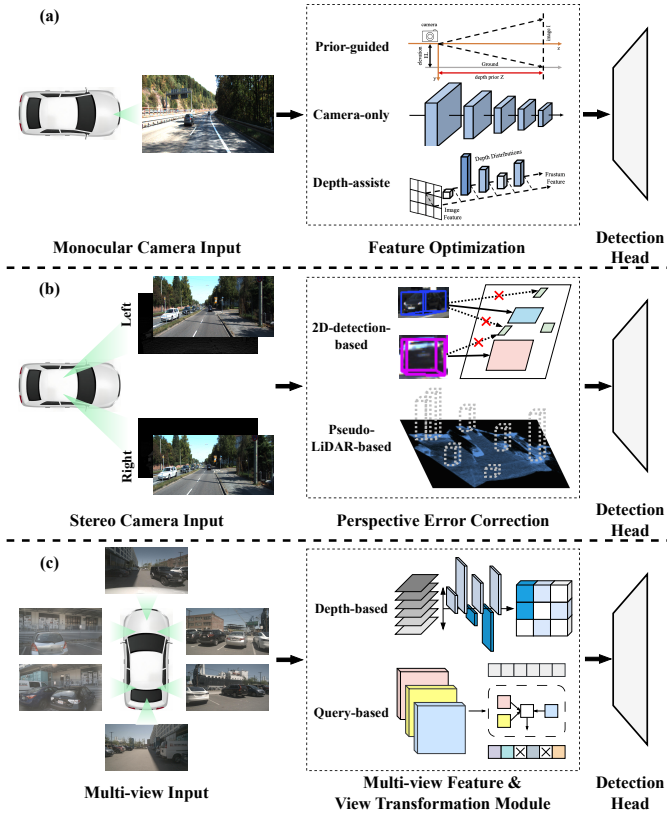


Fig. 2: The general pipeline of Camera-only methods.

have been numerous reviews and investigations conducted to summarize and explore them. However, the majority of existing reviews on 3D object detection are limited to specific methodologies, with a predominant focus on accuracy. This survey aims to revisit the fundamental considerations of safety-perception deployment, redefining the discourse around existing categorizations, and exploring ‘Accuracy, Latency, and Robustness’, as the core dimensions for an in-depth analysis of current methodologies. The objective is to provide additional insights to guide the development of existing technologies.

### A. Monocular 3D object detection

Monocular 3D object detection refers to performing 3D object detection using only one camera, which aims to infer the 3D positions, sizes, and orientations of objects from a single image [131]. In recent years, monocular 3D object detection has gained increasing attention due to its advantages of low cost, low power consumption, and ease of deployment in real-world applications. However, monocular methods face many challenges, owing to the insufficient 3D information in monocular pictures, such as accurately localizing 3D positions, handling occluded scenes, and so on. Overcoming these challenges relies on leveraging depth information to supplement the missing 3D information in monocular images. Typically, most approaches employ depth estimation tasks to acquire depth information from images. However, monocular depth estimation is an ill-posed and highly challenging task, prompting researchers to dedicate significant efforts to optimizing the accuracy and stability of depth estimation.

1) **Prior-guided monocular 3D object detection:** In recent years, prior-guided monocular methods [7], [8], [11]–[13], [18], [19], [21], [26], [162]–[170], [184], [352] have continuously explored how to utilize the hidden prior knowledge of object shapes and scene geometry in images to address the challenges of monocular 3D object detection. The effective integration of this prior knowledge is crucial for mitigating the uncertainty and ill-posed nature of inherent in monocular 3D object detection problems. By introducing pre-trained subnetworks or auxiliary tasks, prior knowledge can provide additional information or constraints to assist in the accurate localization of 3D objects and enhance detection precision and robustness.

Widely adopted prior knowledge in 3D objects includes object shapes [163], [166], [167], [353]–[355], geometric consistency [7], [8], [12], [19], [19], [170], [356], temporal constraints [180], [357], and segmentation information [166]. Object shape provides insights into the appearance and structure of an object, aiding in more accurate inference of the spatial position and pose of the object. Geometric consistency knowledge assists the model in better understanding the relative positional relationships between objects in the scene, thereby improving detection consistency and robustness. Temporal constraints consider the continuity and stability of an object across different frames, providing vital clues for object detection. Additionally, leveraging segmentation information enables the model to better comprehend semantic information in images, facilitating precise localization and identification of objects. As a result, current works are dedicated to further exploring and utilizing prior knowledge to enhance the performance and robustness of monocular 3D object detection by integrating prior knowledge with deep learning approaches, thus driving continuous development and innovation in this field.

2) **Camera-only monocular 3D object detection:** Camera-only monocular 3D object detection [7]–[9], [11], [18], [22], [24]–[26], [169], [179]–[184] is a kind of methods that utilize images captured by a single camera to detect and localize 3D objects. Camera-only monocular methods employ convolutional neural networks (CNNs) to directly regress 3D bounding box parameters from images, enabling the estimation of the spatial dimensions and poses of objects in three dimensions. Inspired by 2D detection networks, this direct regression methods can be trained end-to-end, facilitating holistic learning and inference for 3D objects. The unique challenge of monocular 3D object detection lies in inferring objects’ 3D positions, dimensions, and orientations solely from a single image without relying on additional depth maps or point cloud data. Consequently, the direct regression approaches demonstrate practicality and broad applicability. By learning features from images, CNNs can predict the 3D information of objects. The network gradually optimizes its parameters through end-to-end training to enhance the accurate extraction of 3D information. These direct regression methods streamline the entire detection process and reduce the reliance on supplementary information, improving the algorithms’ robustness and generalization capability. Nevertheless, monocular 3D object detection still presents challenges, such as occlusion, viewpoint variations,

TABLE III: Camera-only 3D object detection methods.

Input Type	Keypoint	Methods
Monocular	<b>Prior-guided:</b> Direct regression using geometric prior knowledge.	Deep MANTA [CVPR2017] [162], Mono3D++ [AAAI2019] [163], 3D-RCNN [CVPR2018] [164], ROI-10D [CVPR2019] [165], MonoDR [ECCV2020] [166], Autolabeling [CVPR2020] [167], MonoPSR [CVPR2019] [21], 3DVP [CVPR2015] [168], MultiBin [CVPR2017] [169], M3D-RPN [ICCV2019] [11], SHIFT R-CNN [ICIP2019] [170], RTM3D [ECCV2020] [7], UR3D [ECCV2020] [19], Decoupled-3D [AAAI2020] [12], GUP Net [ICCV2021] [26], MonoFlex [CVPR2021] [8], Mix-Teaching [TCSVT2023] [28], MonoPair [CVPR2020] [13], MonoJSG [CVPR2022] [10], Geo Aug [CVPR2022] [171], Monoground [CVPR2022] [172], MonoPGC [ICRA2023] [173], MonoEdge [WACV2023] [174], GPro3D [Neurocomputing2023] [175], MonoGAE [arXiv2023] [176], GUPNet++ [arXiv2023] [177], NeurOCS [CVPR2023] [178].
	<b>Camera-only:</b> uses the RGB image information captured by the monocular.	Smoke [CVPR2020] [179], Kinematic3D [ECCV2020] [180], FQNet [CVPR2019] [18], FCOS3D [CVPR2021] [24], PGD [CoRL2022] [25], CaDDN [CVPR2021] [22], MoVi-3D [ECCV2020] [181], MonoDIS [ICCV2019] [9], GS3D [CVPR2019] [182], MonoGRNet [TPAMI2021] [183], MonoRCNN [ICCV2021] [184], MonoFENet [TIP2019] [185], MonoCon [AAAI2022] [186], MonoXiver [ICCV2023] [187], SGM3D [RAL2022] [188], MonoDETR [ICCV2023] [29], MonoDTR [CVPR2022] [23], DiD-M3D [ECCV2022] [189], MonoNeRD [ICCV2023] [190], MonoSAID [IRS2024] [191], WeakMono3D [CVPR2023] [192], DDCCDC [Neurocomputing2023] [193], Obmo [TIP2023] [194], Shape-Aware [TITS2023] [195], Lite-FPN [KBS2023] [196], OOD-M3D [TCE2024] [197], MonoTDP [arXiv2023] [198], Cube R-CNN [CVPR2023] [199], M2S [TIP2023] [200].
	<b>Depth-assisted:</b> extracting depth information via camera parallax.	PatchNet [ECCV2020] [201], DD3D [ICCV2021] [27], Pseudo-LiDAR [CVPR2019] [6], DeepOptics [ICCV2019] [202], AM3D [ICCV2019] [20], MonoTAKD [arXiv2024] [203], MonoPixel [TITS2022] [204], DDMP-3D [CVPR2021] [205], D4LCN [CVPRW2020] [206], ADD [AAAI2023] [207], PDR [TCSVT2023] [208], Pseudo-Mono [ECCV2022] [209], Deviant [ECCV2022] [210], CMAN [TITS2022] [5], ODM3D [WACV2024] [211], MonoGAE [arXiv2023] [176], FD3D [AAAI2023] [212], MonoSKD [arXiv2023] [213].
Stereo	<b>2D-Detection-based:</b> Integrate 2D information about the object into the image.	Disp R-CNN [CVPR2020] [214], TL-Net [CVPR2019] [215], ZoomNet [AAAI2020] [216], IDA-3D [CVPR2020] [217], YOLOStereo3D [ICRA2021] [14], SIDE [WACV2022] [218], VPFNet [TMM2022] [219], FCNet [Entropy2022] [220], MC-Stereo [arXiv2023] [221], PCW-Net [ECCV2022] [222], ICVP [ICIP2023] [223], MoCha-Stereo [arXiv2024] [224], UCFNet [TPAMI2023] [225], IGEV-Stereo [CVPR2023] [226], NMRF-Stereo [arXiv2024] [227].
	<b>Pseudo-LiDAR-only:</b> incorporate additional information from pseudo-LiDAR to simulate LiDAR depth.	Pseudo-LiDAR [CVPR2019] [6], Pseudo-LiDAR++ [ICLR2020] [228], E2E-PL [CVPR2020] [229], CG-Stereo [IROS2020] [230], SGM3D [RAL2022] [188], RTS3D [AAAI2023] [231], RT3DStereo [ITSS2019] [232], RT3D-GMP [ITSC2020] [233], CDN [NIPS2020] [234].
	<b>Volume-based:</b> perform 3D object detection directly on 3D stereo volumes.	GC-Net [ICCV2017] [235], ESGN [TCSVT2022] [236], DSGN [CVPR2020] [17], DSGN++ [TPAMI2022] [237], LIGA-Stereo [ICCV2021] [238], PLUMENet [IROS2021] [239], Selective-IGEV [arXiv2024] [240], ViTAS [arXiv2024] [241], LaC+GANet [AAAI2022] [242], DMIO [arXiv2024] [243], HCR [IVC2024] [244], LEAStereo [NIPS2020] [245], CREStereo [CVPR2022] [246], Abc-Net [TVC2022] [247], AcfNet [AAAI2020] [248], CAL-Net [ICASSP2021] [249], CFNet [CVPR2021] [250], PFSMNet [TITS2021] [251], DCVSMNet [arXiv2024] [252], DPCF [TIP2021] [253], ACVNet [CVPR2022] [254], .
Multi-view	<b>Depth-based:</b> Convert 2D spatial features into 3D spatial features through depth estimation.	BEVDepth [AAAI2023] [15], BEVDet [arXiv2021] [255], BEVDet4D [arXiv2022] [33], LSS [ECCV2020] [256], BEVHeight [CVPR2023] [257], BEVHeight++ [arXiv2023] [35], BEV-SAN [CVPR2023] [258], BEVUDA [arXiv2022] [259], BEVPoolv2 [arXiv2022] [260], BEVStereo [AAAI2023] [261], BEVStereo++ [arXiv2023] [262], TiG-BEV [arXiv2022] [263], DG-BEV [CVPR2023] [264], HotBEV [NeurIPS2024] [265], BEVNeXt [CVPR2024] [266].
	<b>Query-based:</b> Influenced by the transformer technology stack, there is a trend to explicitly or implicitly query Bird's Eye View (BEV) features.	PolarFormer [AAAI2023] [267], SparseBEV [ICCV2023] [34], BEVFormer [ECCV2022] [16], PETR [ECCV2022] [31], PETRv2 [ICCV2023] [32], M3DETR [WACV2022] [84], FrustumFormer [CVPR2023] [268], DETR4D [arXiv2022] [269], Sparse4D [arXiv2022] [270], Sparse4D v2 [arXiv2023] [271], Sparse4D v3 [arXiv2023] [272], SOLOFusion [ICLR2022] [273], CAPE [CVPR2023] [274], VEDet [CVPR2023] [275], Graph-DETR3D [ACMMM] [276], 3DPPE [CVPR2023] [277], BEVDistill [ICLR2023] [278], StreamPETR [ICCV2023] [279], Far3D [ICCV2023] [280], CLIP-BEVFormer [CVPR2024] [281], BEVFormer v2 [CVPR2023] [282].

and lighting conditions, which may affect the accuracy of 3D detection. The representative work Smoke [179] abandons the regression of 2D bounding boxes and predicts the 3D box for each detected object by combining the estimation of individual key points with the regression of 3D variables.

3) **Depth-assisted monocular 3D object detection:** Depth estimation plays a crucial role in depth-assisted monocular 3D object detection. To achieve more accurate monocular detection results, numerous studies [20], [27], [201], [202] leverage pre-trained auxiliary depth estimation networks. Specifically, the process begins by transforming monocular images into depth images using pre-trained depth estimators, such as MonoDepth [358]. Subsequently, two primary methodologies are employed to handle depth images and monocular images. Remarkable progress has been made in Pseudo-LiDAR detectors that use a pre-trained depth estimation network to generate Pseudo-LiDAR representations [201], [359]. However, there is a significant performance gap between Pseudo-LiDAR and LiDAR-only detectors due to the errors in image-to-LiDAR generation. Thus, Hong *et al.* [360] attempted to transfer deeper structural information from point clouds to assist monocular image detection. By leveraging the mean-teacher framework, they aligned the outputs of the LiDAR-only teacher model and the Camera-only student model at both the

feature-level and the response-level, aiming to achieve cross-modal knowledge transfer. Such depth-assisted monocular 3D object detection, by effectively integrating depth information, not only enhances detection accuracy but also extends the applicability of monocular vision to tasks involving 3D scene understanding.

### B. Stereo-based 3D object detection

Stereo-based 3D object detection is designed to identify and localize 3D objects using a pair of stereo images. Leveraging the inherent capability of stereo cameras to capture dual perspectives, stereo-based methods excel in acquiring highly accurate depth information through stereo matching and calibration. This is a feature that distinguishes them from monocular camera setups. Despite these advantages, stereo-based methods still face a considerable performance gap when compared to LiDAR-only counterparts. Furthermore, the realm of 3D object detection from stereo images remains relatively underexplored, with only limited research efforts dedicated to this domain. Specifically, these approaches involve the utilization of image pairs captured from distinct viewpoints to estimate the 3D spatial depth of each object.

1) **2D-detection-based methods:** Traditional 2D object detection frameworks can be modified to address stereo detection

TABLE IV: A comprehensive performance analysis of various categories of Camera-only 3D object detection methods across different datasets. We report the inference time (ms) originally reported in the papers, and report AP<sub>3D</sub>(%) for 3D car detection on the KITTI test benchmark, mAP (%) and NDS scores on the nuScenes test set. ‘R.E.P.’ denotes ‘Representation’. ‘PUB’ denotes ‘Publication’. ‘M.V.’ denotes ‘Multi-view’.

Method	R.E.P.	PUB	L.T.	GPU	KITTI Car Easy Mod. Hard	nuScenes mAP NDS
FQNet [18]		CVPR2019	500	1080Ti	2.77 1.51 1.01	- -
ROI-10D [165]		CVPR2019	200	-	4.32 2.02 1.46	- -
MonoGRNet [183]		AAAI2019	60	TITANX	9.61 5.74 4.25	- -
MonoDIS [9]		CVPR2019	100	V100	10.37 7.94 6.40	30.4 38.4
MonoPair [13]		CVPR2020	60	1080Ti	13.04 9.99 8.65	- -
SMOKE [179]		CVPR2020	30	TITANX	14.03 9.76 7.84	- -
PatchNet [201]		ECCV2020	400	1080	15.68 11.12 10.17	- -
CaDDN [22]		CVPR2021	-	-	19.17 13.21 11.46	- -
FCOS3D [24]		CVPR2021	-	-	- - -	35.8 42.8
MonoFlex [8]		CVPR2021	30	2080Ti	19.94 13.89 12.07	- -
PGD [25]		CVPR2022	28	1080Ti	- - -	38.6 44.8
MonoDTR [23]		CVPR2022	37	V100	21.99 15.39 12.73	- -
NeurOCS [178]		CVPR2023	-	-	29.89 18.94 15.90	- -
MonoATT [283]		CVPR2023	56	3090	24.72 17.37 15.00	- -
MonoDETR [29]		ICCV2023	38	3090	25.00 16.47 13.58	- -
MonoCD [284]		CVPR2024	36	2080Ti	25.53 16.59 14.53	- -
RT3DStereo [232]		ITS2019	79	TITANX	29.90 23.28 18.96	- -
Stereo R-CNN [285]		CVPR2019	420	TITANXp	47.58 30.23 23.72	- -
Pseudo-LiDAR [6]		CVPR2019	-	-	54.53 34.05 28.25	- -
OC-Stereo [286]		ICRA2020	350	TITANXp	55.15 37.60 30.25	- -
ZoomNet [216]		AAAI2020	-	-	55.98 38.64 30.97	- -
Disp R-CNN [287]		CVPR2020	-	-	58.53 37.91 31.93	- -
DSGN [17]		CVPR2020	682	V100	73.50 52.18 45.14	- -
CG-Stereo [230]		ROS2020	570	2080Ti	74.39 53.58 46.50	- -
YoloStereo3D [14]		ICRA2021	80	1080Ti	65.68 41.25 30.42	- -
LIGA-Stereo [238]		ICCV2021	400	TITANXp	81.39 64.66 57.22	- -
PLUMENet [239]		ROS2021	150	V100	83.00 66.30 56.70	- -
ESGN [236]		TCSVT2022	62	3090	65.80 46.39 38.42	- -
SNVC [288]		AAAI2022	-	-	78.54 61.34 54.23	- -
DSGN++ [237]		TPAMI2022	281	2080Ti	83.21 67.37 59.91	- -
StereoDistill [289]		AAAI2023	-	-	81.66 66.39 57.39	- -
BEVDet [255]		arXiv2021	526	3090	- - -	42.2 48.2
DETR3D [30]		PMLR2022	-	-	- - -	41.2 47.9
Graph-DETR3D [276]		ACMMM2022	-	-	- - -	42.5 49.5
BEVDet4D [33]		arXiv2022	526	3090	- - -	42.1 54.5
PETR [31]		ECCV2022	93	V100	- - -	44.1 50.4
BEVFormer [16]		ECCV2022	588	V100	- - -	48.1 56.9
Sparse4D [270]		arXiv2022	164	3090	- - -	51.1 59.5
PolarFormer [267]		AAAI2023	-	-	- - -	49.3 57.2
BEVDistill [278]		ICLR2023	-	-	- - -	49.8 59.4
VEDet [275]		CVPR2023	-	-	- - -	50.5 58.5
PETrv2 [32]		ICCV2023	53	3090	- - -	51.9 60.1
BEVDepth [15]		AAAI2023	-	-	- - -	52.0 60.9
BEVStereo [261]		AAAI2023	-	-	- - -	52.5 61.0
DistillBEV [290]		ICCV2023	-	-	- - -	52.5 61.2
BEVStereo++ [262]		arXiv2023	-	-	- - -	54.6 62.5
SparseBEV [34]		ICCV2023	43	3090	- - -	55.6 63.6
CAPE [274]		CVPR2023	-	-	- - -	52.5 61.0
Sparse4Dv2 [271]		arXiv2023	49	3090	- - -	55.7 63.8
Sparse4Dv3 [272]		arXiv2023	51	3090	- - -	57.0 65.6
StreamPETR [279]		CVPR2023	32	3090	- - -	62.0 67.6
Far3D [280]		ICCV2023	-	-	- - -	63.5 68.7
BEVNeXt [266]		CVPR2024	227	3090	- - -	55.7 64.2
CLIP-BEVFormer [281]		CVPR2024	-	-	- - -	44.7 54.7

problems. Stereo R-CNNs [285] employ an image-based 2D detector to predict 2D proposals, generating left and right regions of interest (RoIs) for the corresponding left and right images. Subsequently, in the second stage, they directly estimate the parameters of 3D objects based on the previously generated RoIs. This paradigm has been widely adopted by subsequent works [14], [195], [214]–[218].

2) *Pseudo-LiDAR-only methods*: The disparity map predicted from stereo images can be transformed into a depth map and further converted into pseudo-LiDAR points. Consequently, similar to monocular detection methods, pseudo-LiDAR representations can also be employed in stereo-based 3D object detection approaches. These methods aim to enhance disparity estimation in stereo matching to achieve more accurate depth predictions. Regarding the contribution of depth in 3D detection, Wang et al. [6] are pioneers in introducing

TABLE V: A comprehensive performance analysis of various categories of LiDAR-only 3D object detection methods across different datasets. ‘P.V.’ denotes ‘Point-Voxel based’. The other settings are the same as TABLE IV.

Method	R.E.P.	PUB	L.T.	GPU	KITTI Car Easy Mod. Hard	nuScenes mAP NDS
PIXOR [291]		CVPR2018	35	TitanXp	81.70 77.05 72.95	- -
HDNet [292]		CoRL2018	-	-	89.14 86.57 78.32	- -
BirdNet [293]		ITSC2018	-	-	75.52 50.81 50.00	- -
RCD [88]		arXiv2020	301	V100	85.37 82.61 77.80	- -
RangeRCNN [87]		arXiv2020	45	V100	88.47 81.33 77.09	- -
RangeUoDet [89]		CVPR2021	22	V100	88.60 79.80 76.76	- -
RangeDet [90]		ICCV2021	83	2080Ti	85.41 77.36 72.60	- -
IPOD [70]		arXiv2018	-	-	71.40 53.46 48.34	- -
PointRGCN [294]		arXiv2019	262	1080Ti	85.97 75.73 70.60	- -
StarNet [295]		arXiv2019	-	-	81.63 73.99 67.07	- -
PointRCNN [45]		CVPR2019	-	-	85.94 75.76 68.32	- -
STD [98]		ICCV2019	80	TITANv	87.95 79.71 75.09	- -
PI-RCNN [296]		AAAI2020	11	TITAN	84.37 74.82 70.03	- -
Point-GNN [44]		CVPR2020	643	1070	88.33 79.47 72.29	- -
3DSSD [40]		CVPR2020	38	TITANv	88.36 79.57 74.55	- -
3D-CenterNet [297]		PR2021	19	TITANXp	86.83 80.17 75.96	- -
DGCNN [80]		NeurIPS2021	-	-	- - -	53.3 63.0
PC-RGNN [298]		AAAI2021	-	-	89.13 79.90 75.54	- -
Pointformer [66]		CVPR2021	-	-	87.13 77.06 69.25	- -
IA-SSD [299]		CVPR2022	12	2080Ti	88.34 80.13 75.04	- -
SASA [94]		AAAI2022	36	V100	88.76 82.16 77.16	- -
SVGA-Net [63]		AAAI2022	-	-	87.33 80.47 75.91	- -
PG-RCNN [300]		TGRS2023	60	3090	89.38 82.13 77.33	- -
SECOND [43]		Sensors2018	50	1080Ti	83.13 73.66 66.20	- -
VoxelNet [42]		CVPR2018	220	TITANX	77.47 65.11 57.73	- -
PointPillars [51]		CVPR2019	16	1080Ti	79.05 74.99 68.30	- -
CBGS [301]		arXiv2019	-	-	- - -	52.8 63.3
PartA2 [302]		TPAMI2020	71	ITANXp	85.94 77.86 72.00	- -
Voxel-FPN [48]		Sensors2020	20	1080Ti	85.64 76.70 69.44	- -
TANet [303]		AAAI2020	35	TITANv	83.81 75.38 67.66	- -
CVC-Net [304]		NIPS2020	-	-	- - -	55.8 64.2
SegVoxelNet [305]		ICRA2020	40	1080Ti	84.19 75.81 67.80	- -
HotSpotNet [306]		ECCV2020	40	V100	87.60 78.31 73.34	59.3 66.0
Associate-3Ddet [71]		CVPR2020	60	1080Ti	85.99 77.40 70.53	- -
CenterPoint [57]		CVPR2021	70	TITAN	- - -	58.0 65.5
CIA-SSD [77]		AAAI2021	31	ITANXp	89.59 80.28 72.87	- -
SIEV-NET [307]		TGRS2021	45	1080Ti	85.21 76.18 70.06	- -
VoTr-TSD [58]		ICCV2021	139	V100	89.90 82.09 79.14	- -
Voxel R-CNN [47]		AAAI2021	40	2080Ti	90.90 81.62 77.06	- -
PillarNet [93]		ECCV2022	-	-	- - -	66.0 71.4
VoxelNeXt [46]		CVPR2023	-	-	- - -	64.5 70.0
PV-RCNN [308]		CVPR2020	80	1080Ti	90.25 81.43 76.82	- -
SA-SSD [309]		CVPR2020	40	2080Ti	88.75 79.79 74.16	- -
HVPR [83]		CVPR2021	28	2080Ti	86.38 77.92 73.04	- -
VIC-NET [310]		ICRA2021	-	-	88.60 81.57 77.09	- -
PVGNet [82]		CVPR2021	-	-	89.94 81.81 77.09	- -
CT3D [67]		ICCV2021	-	-	87.83 81.77 77.16	- -
Pyramid R-CNN [86]		ICCV2021	-	-	88.39 82.08 77.49	- -
PV-RCNN++ [50]		IJCV2023	-	-	90.14 81.88 77.15	- -
VP-Net [36]		TGRS2023	59	2080Ti	90.46 82.03 79.65	- -
SASAN [311]		TNNLS2023	104	V100	90.40 81.90 77.20	- -
PVT-SSD [312]		CVPR2023	49	3080Ti	90.65 82.29 76.85	- -
HCPVF [313]		TCSVT2023	70	3090	89.34 82.63 77.72	- -
APVR [314]		TAI2023	-	-	91.45 82.17 78.08	58.6 65.9
HPV-RCNN [315]		TCSS2023	81	A100	89.33 80.61 75.53	- -

the Pseudo-LiDAR representation. This representation is generated by using an image with a depth map, requiring the model to perform a depth estimation task to assist in detection. Subsequent works have followed this paradigm and made optimizations by introducing additional color information to augment pseudo point cloud [20], auxiliary tasks (instance segmentation [361], foreground and background segmentation [362] and domain adaptation [363]) and coordinate transform scheme [201], [364]. To achieve both high accuracy and high responsiveness, Meng et al. [365] propose a lightweight Pseudo-LiDAR 3D detection system. These studies indicate that the power of the pseudo LiDAR representation stems from the coordinate transformation rather than the point cloud representation itself.

3) *Volume-based methods*: The general procedure of volume-based methods is to generate a cost volume from the left and the right images to represent disparity information, which is then utilized in the subsequent detection process.

TABLE VI: A comprehensive performance analysis of various categories of multi-modal 3D object detection methods across different datasets. ‘P.P.’ denotes Point-Projection. ‘F.P.’ denotes Feature-Projection. ‘A.P.’ denotes Auto-Projection. ‘D.P.’ denotes Decision-Projection. ‘Q.L.’ denotes Query-Learning. ‘U.F.’ denotes Unified-Feature. The other settings are the same as TABLE IV.

Method	R.E.P.	PUB	L.T.	GPU	KITTI Car			nuScenes	
					Easy	Mod.	Hard	mAP	NDS
MVX-Net [316]		ICRA2019	-	-	85.50	73.30	67.40	-	-
RoarNet [317]		IV2019	-	-	83.71	73.04	59.16	-	-
ComplexerYOLO [318]		CVPRW2019	16	1080i	55.63	49.44	44.13	-	-
PointPainting [100]		CVPR2020	-	-	82.11	71.70	67.08	46.4	58.1
EPNet [104]		ECCV2020	-	-	89.81	79.28	74.59	-	-
PointAugmenting [319]	P.P.	CVPR2021	542	1080Ti	-	-	-	66.8	71.0
FusionPainting [320]		ITSC2021	-	-	-	-	-	66.5	70.7
MVP [321]		NeurIPS2021	-	-	-	-	-	66.4	70.5
Centerfusion [322]		WACV2021	-	-	-	-	-	-	-
EPNet++ [105]		TPAMI2022	-	-	91.37	81.96	76.71	-	-
MSF [323]		TGRS2024	63	V100	-	-	-	68.2	71.6
PPF-Det [324]		TITS2024	29	TITANX	89.51	84.46	78.91	-	-
Cont Fuse [325]		ECCV2018	60	-	82.54	66.22	64.04	-	-
MMF [326]		CVPR2019	80	-	86.81	76.75	68.41	-	-
Focals Conv [110]		CVPR2022	125	2080Ti	90.55	82.28	77.59	67.8	71.8
VFF [327]		CVPR2022	-	-	89.50	82.09	79.29	68.4	72.4
LargeKernel3D [328]		CVPR2023	145	2080ti	-	-	-	71.2	74.2
SupFusion [329]	F.P.	ICCV2023	-	-	-	-	-	56.6	64.6
VoxelNextFusion [122]		TGRS2023	54	A6000	90.90	82.93	80.6	68.8	72.5
RoboFusion [330]		IJCAI2024	32	A100	91.75	84.08	80.71	69.9	72.0
PI-RCNN [296]		AAAI2020	90	TITAN	84.37	74.82	70.03	-	-
3D-CVF [41]		ECCV2020	75	1080Ti	89.20	80.05	73.11	-	-
3D Dual-Fusion [331]		Arxiv2022	-	-	91.01	82.40	79.39	70.6	73.1
AutoAlignV2 [332]		ECCV2022	208	V100	-	-	-	68.4	72.4
HMFI [120]	A.P.	ECCV2022	-	-	88.90	81.93	77.30	-	-
LoGoNet [121]		ICCV2023	-	-	91.80	85.06	80.74	-	-
GraphAlign [111]		ICCV2023	26	A6000	90.96	83.49	80.14	66.5	70.6
GraphAlign++ [112]		TCSVT2024	149	V100	90.98	83.76	80.16	68.5	72.2
CLOCs [333]		IROS2020	-	-	83.68	68.78	61.67	-	-
AVOD [334]		IROS2018	100	TITANXp	81.94	71.88	66.38	-	-
MV3D [335]		CVPR2017	240	TitanX	71.09	62.35	55.12	-	-
F-PointNets [336]		CVPR2018	-	-	81.20	70.39	62.19	-	-
F-ConvNet [96]	D.P.	ICCV2019	-	-	82.11	71.70	67.08	46.4	58.1
F-PointPillars [337]		ICCV2021	-	-	88.90	79.28	78.07	-	-
Fast-CLOCs [338]		WACV2022	-	-	89.11	80.34	76.98	-	-
Graph R-CNN [113]		ECCV2022	13	1080Ti	91.89	83.27	77.78	-	-
TransFusion [108]		CVPR2022	265	V100	-	-	-	68.9	71.7
DeepInteraction [116]		NeurIPS2022	204	A100	-	-	-	70.8	73.4
SparseFusion [101]		ICCV2023	188	A6000	-	-	-	72.0	73.8
AutoAlign [339]	Q.L.	IJCAI2022	-	-	-	-	-	65.8	70.9
SparseLIF [340]		arXiv2024	340	A100	-	-	-	75.9	77.7
FusionFormer [341]		arXiv2024	263	A100	-	-	-	71.4	74.1
FSF [342]		TPAMI2024	141	3090	-	-	-	70.6	74.0
BEVFusion-PKU [109]		NeurIPS2022	-	-	-	-	-	69.2	71.8
BEVFusion-MIT [343]		ICRA2023	119	3090	-	-	-	70.2	72.9
EA-BEV [344]		arXiv2023	195	V100	-	-	-	71.2	73.1
BEVFusion4D [345]		arXiv2023	500	V100	-	-	-	72.0	73.5
FocalFormer3D [346]		ICCV2023	109	V100	-	-	-	71.6	73.9
FUTR3D [106]		CVPR2023	-	-	-	-	-	69.4	72.1
UniTR [347]		ICCV2023	107	A100	-	-	-	70.9	74.5
VirConv [99]		CVPR2023	92	V100	92.48	87.20	82.45	68.7	72.3
MSMD Fusion [348]	U.F.	CVPR2023	265	V100	-	-	-	71.5	74.0
SFD [114]		CVPR2022	10	2080Ti	91.73	84.76	77.92	-	-
CMT [103]		ICCV2023	167	A100	-	-	-	72.0	74.1
UVTR [65]		NeurIPS2022	-	-	-	-	-	67.1	71.1
ObjectFusion [117]		ICCV2023	274	V100	-	-	-	71.0	73.3
GraphBEV [349]		arXiv2024	141	A100	-	-	-	71.7	73.6
ContrastAlign [350]		arXiv2024	154	A100	-	-	-	71.8	73.8
IS-Fusion [351]		CVPR2024	-	-	-	-	-	73.0	75.2

Volume-based methods bypass the pseudo-LiDAR representation and perform 3D object detection directly on 3D stereo volumes. These methods have inherited the traditional matching idea, but most computations now rely on 3D convolutional networks, such as those found in references [17], [235], [236], [238], [242], [245], [254], [366]. For example, the pioneering work GC-Net [235] uses an end-to-end neural network for stereo matching, obviating the need for any post-processing steps, and regressively computes disparity from a cost volume constructed by a pair of stereo features. GwcNet [366] employs a proposed group-wise correlation method to construct the cost volume. LEAStereo [245] utilizes NAS technology to select

the optimal structure for the 3D cost volume. GANet [242] designs a semi-global aggregation layer and a local guidance aggregation layer to further improve accuracy. ACVNet [254] introduces an attention concatenation unit to generate more accurate similarity metrics. DSGN [17] proposes a 3D geometric volume derived from stereo matching networks and applies a grid-based 3D detector on the volume for 3D object detection. LIGA-Stereo [238] uses a LiDAR-based detector as a teacher model to guide geometry-aware feature learning. ESGN [236] achieves efficient stereo matching through the efficient geometry-aware feature generation (EGFG) module. Due to the benefits of large-scale training data and end-to-end training, deep learning-based stereo methods have achieved outstanding results [243].

### C. Multi-view 3D object detection

Recently, multi-view 3D object detection has demonstrated superior accuracy and robustness compared to monocular and stereo 3D object detection approaches. In contrast to LiDAR-only 3D object detection, the latest panoramic Bird’s Eye View (BEV) approaches eliminate the need for high-precision maps, elevating the detection from 2D to 3D. This advancement has led to significant developments in multi-view 3D object detection. In comparison to previous reviews [4], [123], [126], [130], [131], there has been extensive research on effectively leveraging multi-view images for 3D object detection. A key challenge in multi-camera 3D object detection is recognizing the same object across different images and aggregating object features from multiple view inputs. The current approach, a common practice, involves uniformly mapping multi-view to the Bird’s Eye View (BEV) space. Therefore, multi-view 3D object detection, also called BEV-camera-only 3D object detection, revolves around the core challenge of unifying 2D views into the BEV space. Based on different spatial transformations, this can be categorized into two main methods. Ones are depth-based methods [15], [33], [35], [255]–[259], [263], [264], [268], [367], [368], represented by the LSS [256], also known as 2D to 3D transformation. The others are query-based methods [16], [31], [32], [34], [84], [267]–[280], [369], represented by DETR3D [30], making a query from 3D to 2D.

1) **Depth-based Multi-view methods:** The direct transformation from 2D to BEV space poses a significant challenge. LSS [256] was the first to propose a depth-based method, utilizing 3D space as an intermediary. This approach involves initially predicting the grid depth distribution of 2D features and then elevating these features to voxel space. This method holds promise for achieving the transformation from 2D to BEV space more effectively. Following LSS [256], CaDDN [22] adopted a similar depth representation approach. It employed a network structure akin to LSS, primarily for predicting categorical depth distribution. By compressing voxel-space features into BEV space, it performed the final 3D detection. It is worth noting that CaDDN is not part of multi-view 3D object detection but rather single-view 3D object detection, which has influenced subsequent research on depth. The main distinction between LSS [256] and CaDDN [22] lies in CaDDN’s use of actual ground truth depth values to supervise

its prediction of categorical depth distribution, resulting in a superior depth network capable of more accurately extracting 3D information from 2D space. This line of research has sparked a series of subsequent studies, such as BEVDet [255], its temporal version BEVDet4D [33], and BEVDepth [15]. These studies are significant in advancing the transformation from 2D to 3D space and enabling more accurate object detection in the BEV space, providing valuable insights and directions for the field’s development. Furthermore, some studies have addressed the issue of insufficient depth solely by encoding height information. These studies have found that with increasing distance, the depth disparity between the car and the ground rapidly diminishes [35], [257].

2) **Query-based Multi-view methods:** Under the influence of Transformer technology, such as in the works [370]–[373], query-based Multi-view methods retrieve 2D spatial features from 3D space. Inspired by Tesla’s perception system, DETR3D [30] introduces 3D object queries to address the aggregation of multi-view features. It achieves this by extracting image features from different perspectives and projecting them into 2D space using learned 3D reference points, thus obtaining image features in the Bird’s Eye View (BEV) space. Query-based Multi-view methods, as opposed to Depth-based Multi-view methods, acquire sparse BEV features by employing a reverse querying technique, fundamentally impacting subsequent query-based developments [16], [31], [32], [34], [84], [267]–[280], [369]. However, due to the potential inaccuracies associated with explicit 3D reference points, PETR [31], influenced by DETR [374] and DETR3D [30], adopts an implicit positional encoding method for constructing the BEV space, influencing subsequent works [32], [279].

#### D. Analysis: Accuracy, Latency, Robustness

Currently, the 3D object detection solutions based on Bird’s Eye View (BEV) perception are rapidly advancing. Despite the existence of numerous reviews [4], [123], [126], [130], [131], a comprehensive review of this field remains inadequate. It is noteworthy that Shanghai AI Lab and SenseTime Research have provided a thorough review [375] of the technical roadmap for BEV solutions. However, unlike existing reviews [4], [123], [126], [130], [131], which primarily focus on the technical roadmap and the current state of the art, we consider crucial aspects such as autonomous driving safety perception. Following an analysis of the technical roadmap and the current state of development for Camera-only solutions, we intend to base our discussion on the foundational principles of ‘Accuracy, Latency, and Robustness’. We will integrate the perspectives of safety perception to guide the practical implementation of safety perception in autonomous driving.

1) **Accuracy:** Accuracy is a focal point of interest in most research articles and reviews and is indeed of paramount importance. While accuracy can be reflected through AP (average precision), considering AP alone for comparison may not provide a comprehensive view, as different methodologies may exhibit substantial differences due to differing paradigms.

As shown in Fig. 3 (a), we selected ten representative methods (including classic and latest research) for comparison,

and it is evident that there are significant metric disparities between monocular 3D object detection [10], [13], [23], [28], [29], [179], [183], [184] and stereo-based 3D object detection [14], [17], [216], [231], [234], [236], [237], [286], [378]. The current scenario indicates that the accuracy of monocular 3D object detection is far lower than that of stereo-based 3D object detection. Stereo-based 3D object detection leverages the capture of images from two different perspectives of the same scene to obtain depth information. The greater the baseline between cameras, the wider the range of depth information captured. As shown in Fig. 3 (b), there were monocular 3D object detection methods [9], [24], [25], [27], [379] on the nuScenes dataset [134], but no related research on stereo-based 3D object detection.

Starting from 2021, monocular methods have gradually been supplanted by multi-view (bird’s-eye-view perception) 3D object detection methods [15], [16], [30]–[32], [272], [273], [279], [280], [282], leading to a significant improvement in mAP. The emergence of the novel bird’s-eye-view paradigm and the increase in sensor quantity have substantially impacted mAP. It can be observed that initially, the disparity between DD3D [27] and DETR3D [30] is not prominent, but with the continuous enhancement of multi-view 3D object detection, particularly with the advent of novel works such as Far3D [280], the gap has widened. In other words, camera-only 3D object detection methods on multi-camera datasets like nuScenes [134] are predominantly based on bird’s-eye-view perception. If we consider accuracy solely from this single dimension, the increase in sensor quantity has significantly improved accuracy metrics (including mAP, NDS, AP, etc.).

2) **Latency:** In 3D object detection, latency (frames per second, FPS) and accuracy are critical metrics for evaluating algorithm performance [386]. As shown in Table IV, Monocular-based 3D object detection, which relies on data from a single camera, typically achieves higher FPS due to lower computational requirements. However, its accuracy is often inferior to stereo or multi-view systems due to the absence of depth information. Stereo-based detection, leveraging disparity information from dual cameras, enhances depth estimation accuracy but introduces greater computational complexity, potentially reducing FPS. Multi-view detection provides richer scene information and improved accuracy but demands extensive data processing, computational power, and algorithmic optimization for reasonable FPS levels. Notably, the nuScenes dataset lacks representation of stereo-based methods, with the monocular method FCOS3D [24] standing out as emblematic, introduced in 2021. Over time, multi-view 3D object detection has rapidly evolved in terms of accuracy and latency. In practice, real-time performance is also an important consideration when deploying a robust 3D object detection system. For example, ER3D [387] takes stereo images as input and predicts 3D bounding boxes, which leverages a fast but inaccurate method of semi-global matching for depth estimation. Li et al. [388] propose a lightweight Pseudo-LiDAR 3D detection system that achieves high accuracy and responsiveness. RTS3D [231] proposes a novel framework for faster and more accurate 3D object detection using stereo images. FastFusion [389], a three-stage stereo-LiDAR deep fusion scheme, integrates



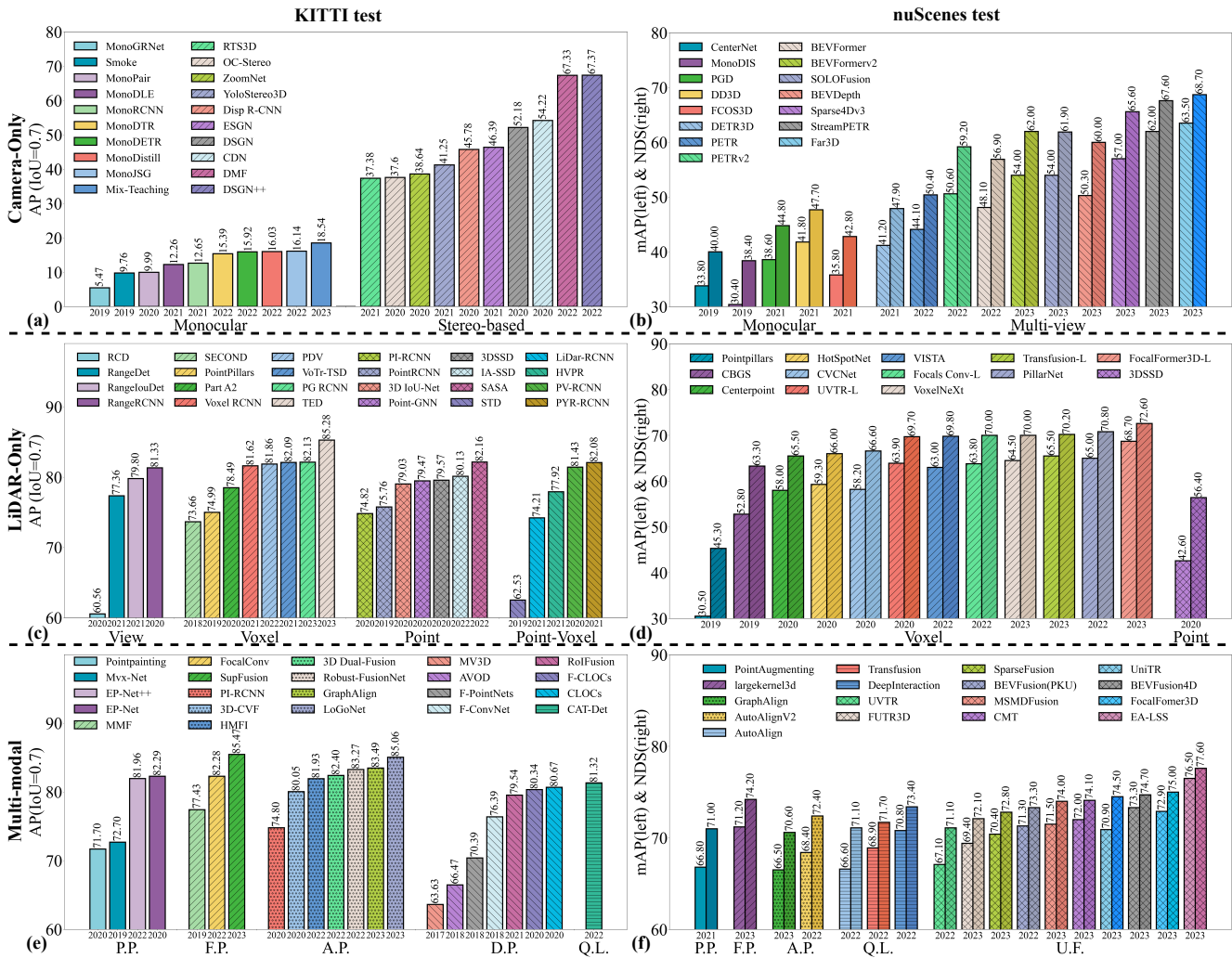


Fig. 3: (a) The  $AP_{3D}$  comparison of monocular-based methods [10], [13], [23], [28], [29], [179], [183], [184], [376], [377] and stereo-based methods [14], [17], [214], [216], [231], [234], [236], [237], [286], [378] on KITTI test dataset. (b) The mAP (left) and NDS (right) comparison of monocular-based methods [9], [24], [25], [27], [379] and Multi-view methods [15], [16], [30]–[32], [272], [273], [279], [280], [282] on the nuScenes test dataset. (c) The  $AP_{3D}$  comparison of View-based methods [87]–[90], Voxel-based methods [43], [47], [51], [53], [54], [58], [300], [302], Point-based [40], [44], [45], [94], [296], [299], [380], and Point-Voxel-based methods [83], [86], [98], [308], [381] on KITTI test dataset. (d) The mAP (left) and NDS (right) comparison of Voxel-based methods [46], [51], [57], [65], [93], [108], [110], [346], [379] and Point-based methods [40] on the nuScenes test dataset. (e) The  $AP_{3D}$  comparison of Point-Projection-based (P.P.) methods [100], [104], [105], [316], Feature-Projection-based (F.P.) methods [110], [118], [326], Auto-Projection-based (A.P.) methods [41], [111], [120], [121], [296], [331], [382], Decision-Projection-based (D.P.) methods [96], [334], [335], [337], [338], [383], [384], and Query-Learning-based (Q.L.) methods [385] on KITTI test dataset. (f) The mAP (left) and NDS (right) comparison of Point-Projection-based (P.P.) methods [319], Feature-Projection-based (F.P.) methods [60], Auto-Projection-based (A.P.) methods [111], [332], Query-Learning-based (Q.L.) methods [108], [116], [339] and Unified-Feature-based (U.F.) methods [65], [101], [103], [106], [109], [344]–[348] on the nuScenes test dataset.

LiDAR priors into each step of the classical stereo-matching taxonomy, thereby gaining high-precision dense depth sensing in real-time. In conclusion, achieving safe autonomous driving necessitates balancing latency and accuracy in 3D object detection algorithms. While monocular detection is faster, it lacks precision. Stereo and multi-view methods are accurate but slower. Future research should focus on maintaining high precision while emphasizing increased FPS and reduced latency to meet the dual requirements of real-time responsiveness and safety in autonomous driving.

3) **Robustness**: Robustness constitutes a pivotal factor in the safety perception of autonomous driving, representing a topic of significant attention that has been previously overlooked in comprehensive reviews. In the current meticulously designed clean datasets and benchmarks, such as KITTI [133], nuScenes [134], and Waymo [135], this aspect is not commonly addressed. Presently, research works [124], [125], [147], [148], [390]–[392] like RoboBEV [124], Robo3D [148] on 3D object detection incorporate considerations of robustness, exemplified by factors such as sensor misses, as illustrated in Fig. 4. They have adopted a methodology involving the introduction of disturbances into datasets relevant to 3D object detection to assess robustness. This includes introducing various types of noise, such as variations in weather conditions, sensor malfunctions, motion disturbances, and object-related perturbations, aimed at unraveling the distinct impacts of different noise sources on the model. Typically, most papers investigating robustness conduct evaluations by introducing noise to the validation sets of clean datasets, such as KITTI [133], nuScenes [134], and Waymo [135]. Additionally, we highlight findings from Ref. [125], where KITTI-C [125] and nuScenes-C [125] are emphasized as examples to illustrate the results of Camera-Only 3D object detection methods. Tables VII and VIII provide an overall comparison, revealing that, in general, Camera-Only methods are less robust compared to LiDAR-Only and multi-modal fusion methods. They are highly susceptible to various types of noise. In KITTI-C, three representative works—SMOKE [179], PGD [25], and ImVoxelNet [393]—show consistently lower overall performance and reduced robustness to noise. In nuScenes-C, noteworthy methods such as DETR3D [30] and BEVFormer [16] exhibit greater robustness compared to FCOS3D [24] and PGD [25], suggesting that as the number of sensors increases, overall robustness improves. In conclusion, future Camera-Only methods need to consider not only cost and accuracy metrics (mAP, NDS, etc.) but also factors related to safety perception and robustness. Our analysis aims to provide valuable insights for the safety of future autonomous driving systems.

#### IV. LiDAR-ONLY 3D OBJECT DETECTION

LiDAR-only methods capture precise 3D information, leading to higher detection accuracy and robustness, particularly in extreme weather conditions [125]. Because in comparison to optical radiation, the laser beams emitted by LiDAR systems can penetrate certain weather disturbances, such as raindrops and haze, with slight interference. However, the high cost of

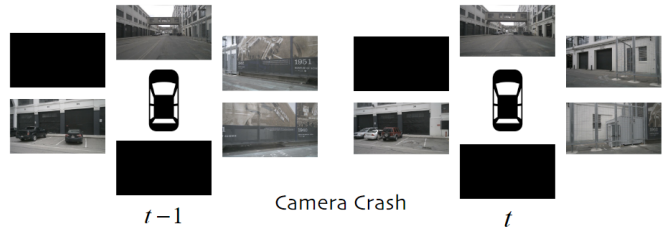


Fig. 4: Corruption Examples in the RoboBEV [124] Benchmark: Simulating Camera Malfunction.

LiDAR remains one of the main barriers to large-scale adoption of LiDAR-only methods. Generally, as shown in Fig. 5, LiDAR-only methods can be categorized into four types: (1) view-based 3D object detection, (2) voxel-based 3D object detection, (3) point-based 3D object detection, (4) point-voxel-based 3D object detection. In contrast to previous reviews [4], [123], [126], [130], [131], our survey extends beyond the conventional classifications of LiDAR-only methods. We adopt a more foundational idea to class LiDAR-only methods based on their core **data representations** (BEV, Voxel, Pillars.) and underlying **model structure** (CNNs, Transformers, PointNet). We provide a comprehensive understanding of the technological paradigms at LiDAR-only methods, analyzing and classifying these systems from a more essential, technical lineage perspective.

##### A. View-based 3D object detection

View-based methods transform point clouds into pseudo-images using BEV and range views. Based on the different data representation views, the view-based methods can be divided into two categories: 1) **Range View**, 2) **BEV View**. In these representations, each pixel contains 3D spatial information rather than RGB values. Due to the dense representation of pseudo-images, traditional or specialized 2D convolutions can be seamlessly applied to range images, making the feature extraction process highly efficient. However, compared to other LiDAR-only methods, detection using range views is more susceptible to occlusion and scale variations.

1) **Range View**: Due to the sparsity of point cloud data, projecting it directly onto an image plane results in a sparse 2D point map. Therefore, most methods [87]–[90], [394], [395] project the point cloud into the cylinder coordinate to generate a dense front-view representation by using the following projection function:

$$\begin{aligned} \theta &= \text{atan2}(y, x), \\ \phi &= \arcsin(z/\sqrt{x^2 + y^2 + z^2}), \\ r &= \lfloor \theta/\Delta\theta \rfloor, \\ c &= \lfloor \phi/\Delta\phi \rfloor, \end{aligned} \quad (5)$$

where  $p = (x, y, z)^T$  denotes a 3D point and  $(r, c)$  denotes the 2D map position of its projection.  $\theta$  and  $\phi$  denote the azimuth and elevation angle when observing the point.  $\Delta\theta$  and  $\Delta\phi$  are the average horizontal and vertical angle resolution between consecutive beam emitters, respectively. VeloFCN [396] is an influential work that first introduces

TABLE VII: Comparison with SOTA methods on **KITTI-C validation** set. The results are evaluated based on the **car** class with AP of  $R_{40}$  at **moderate** difficulty. ‘RCE’ denotes Relative Corruption Error from Ref. [125].

Corruptions		LiDAR-Only						Camera-Only			Multi-modal			
		SECOND <sup>†</sup>	PointPillars <sup>†</sup>	PointRCNN <sup>†</sup>	PV-RCNN <sup>†</sup>	Part-A <sup>2</sup> <sup>†</sup>	3DSSD <sup>†</sup>	SMOKE <sup>†</sup>	PGD <sup>†</sup>	ImVoxelNet <sup>†</sup>	EPNet <sup>†</sup>	Focals Conv <sup>†</sup>	LoGoNet <sup>†</sup>	VirConv-S <sup>*</sup>
None(AP <sub>clean</sub> )		81.59	78.41	80.57	84.39	82.45	80.03	7.09	8.10	11.49	82.72	85.88	86.07	91.95
Weather	Snow	52.34	36.47	50.36	52.35	42.70	27.12	2.47	0.63	0.22	34.58	34.77	51.45	51.17
	Rain	52.55	36.18	51.27	51.58	41.63	26.28	3.94	3.06	1.24	36.27	41.30	55.80	50.57
	Fog	74.10	64.28	72.14	79.47	71.61	45.89	5.63	0.87	1.34	44.35	44.55	67.53	75.63
	Sunlight	78.32	62.28	62.78	79.91	76.45	26.09	6.00	7.07	10.08	69.65	80.97	75.54	63.62
Sensor	Density	80.18	76.49	80.35	82.79	80.53	77.65	-	-	-	82.09	84.95	83.68	80.70
	Cutout	73.59	70.28	73.94	76.09	76.08	73.05	-	-	-	76.10	78.06	77.17	75.18
	Crosstalk	80.24	70.85	71.53	82.34	79.95	46.49	-	-	-	82.10	85.82	82.00	75.67
	Gaussian (L)	64.90	74.68	61.20	65.11	60.73	59.14	-	-	-	60.88	82.14	61.85	63.16
	Uniform (L)	79.18	77.31	76.39	81.16	77.77	74.91	-	-	-	79.24	85.81	82.94	70.74
	Impulse (L)	81.43	78.17	79.78	82.81	80.80	78.28	-	-	-	81.63	85.01	84.66	80.50
	Gaussian (C)	-	-	-	-	-	-	1.56	1.71	2.43	80.64	80.97	84.29	82.55
	Uniform (C)	-	-	-	-	-	-	2.67	3.29	4.85	81.61	83.38	84.45	82.56
Impulse (C)	-	-	-	-	-	-	1.83	1.14	2.13	81.18	80.83	84.20	82.54	
Motion	Moving Obj.	52.69	50.15	50.54	54.60	79.57	77.96	1.67	2.64	5.93	55.78	49.14	14.44	32.28
	Motion Blur	-	-	-	-	-	-	3.51	3.36	4.19	74.71	81.08	84.52	82.58
Object	Local Density	75.10	69.56	74.24	77.63	79.57	77.96	-	-	-	76.73	80.84	78.63	78.73
	Local Cutout	68.29	61.80	67.94	72.29	75.06	73.22	-	-	-	69.92	76.64	64.88	71.01
	Local Gaussian	72.31	76.58	69.82	70.44	77.44	75.11	-	-	-	75.76	82.02	55.66	72.85
	Local Uniform	80.17	78.04	77.67	82.09	80.77	78.64	-	-	-	81.71	84.69	79.94	79.61
	Local Impulse	81.56	78.43	80.26	84.03	82.25	79.53	-	-	-	82.21	85.78	84.29	82.07
	Shear	41.64	39.63	39.80	47.72	37.08	26.56	1.68	2.99	1.33	41.43	45.77	-	-
	Scale	73.11	70.29	71.50	76.81	75.90	75.02	0.13	0.15	0.33	69.05	69.48	-	-
	Rotation	76.84	72.70	75.57	79.93	75.50	76.98	1.11	2.14	2.57	74.62	77.76	-	-
Alignment	Spatial	-	-	-	-	-	-	-	-	-	35.14	43.01	-	-
Average(AP <sub>cor</sub> )		70.45	65.48	67.74	72.59	69.92	60.55	2.68	2.42	3.05	67.81	71.87	80.93	85.66
RCE (%) ↓		13.65	16.49	15.92	13.98	15.20	24.34	62.20	70.12	73.46	22.03	18.02	5.97	6.84

<sup>†</sup>: Results from Ref. [125].

\* denotes the result of our re-implementation.

TABLE VIII: Comparison with SOTA methods on **nuScenes-C validation** set with **mAP**. ‘D.I.’ refers to DeepInteraction [116]. ‘RCE’ denotes Relative Corruption Error from Ref. [125].

Corruptions		LiDAR-Only			Camera-Only				Multi-modal			D.I.*
		PointPillars <sup>†</sup>	SSN <sup>†</sup>	CenterPoint <sup>†</sup>	FCOS3D <sup>†</sup>	PGD <sup>†</sup>	DETR3D <sup>†</sup>	BEVFormer <sup>†</sup>	FUTR3D <sup>†</sup>	TransFusion <sup>†</sup>	BEVFusion <sup>†</sup>	
None(AP <sub>clean</sub> )		27.69	46.65	59.28	23.86	23.19	34.71	41.65	64.17	66.38	68.45	69.90
Weather	Snow	27.57	46.38	55.90	2.01	2.30	5.08	5.73	52.73	63.30	62.84	62.36
	Rain	27.71	46.50	56.08	13.00	13.51	20.39	24.97	58.40	65.35	66.13	66.48
	Fog	24.49	41.64	43.78	13.53	12.83	27.89	32.76	53.19	53.67	54.10	54.79
	Sunlight	23.71	40.28	54.20	17.20	22.77	34.66	41.68	57.70	55.14	64.42	64.93
Sensor	Density	27.27	46.14	58.60	-	-	-	-	63.72	65.77	67.79	68.15
	Cutout	24.14	40.95	56.28	-	-	-	-	62.25	63.66	66.18	66.23
	Crosstalk	25.92	44.08	56.64	-	-	-	-	62.66	64.67	67.32	68.12
	FOV lost	8.87	15.40	20.84	-	-	-	-	26.32	24.63	27.17	42.66
	Gaussian (L)	19.41	39.16	45.79	-	-	-	-	58.94	55.10	60.64	57.46
	Uniform (L)	25.60	45.00	56.12	-	-	-	-	63.21	64.72	66.81	67.42
	Impulse (L)	26.44	45.58	57.67	-	-	-	-	63.43	65.51	67.54	67.41
	Gaussian (C)	-	-	-	3.96	4.33	14.86	15.04	54.96	64.52	64.44	66.52
Uniform (C)	-	-	-	8.12	8.48	21.49	23.00	57.61	65.26	65.81	65.90	
Impulse (C)	-	-	-	3.55	3.78	14.32	13.99	55.16	64.37	64.30	65.65	
Motion	Compensation	3.85	10.39	11.02	-	-	-	-	31.87	9.01	27.57	39.95
	Moving Obj. Motion Blur	19.38 -	35.11 -	44.30 -	10.36 10.19	10.47 9.64	16.63 11.06	20.22 19.79	45.43 55.99	51.01 64.39	51.63 64.74	- 65.45
Obeject	Local Density	26.70	45.42	57.55	-	-	-	-	63.60	65.65	67.42	67.71
	Local Cutout	17.97	32.16	48.36	-	-	-	-	61.85	63.33	63.41	65.19
	Local Gaussian	25.93	43.71	51.13	-	-	-	-	62.94	63.76	64.34	64.75
	Local Uniform	27.69	46.87	57.87	-	-	-	-	64.09	66.20	67.58	66.44
	Local Impulse	27.67	46.88	58.49	-	-	-	-	64.02	66.29	67.91	67.86
	Shear	26.34	43.28	49.57	17.20	16.66	17.46	24.71	55.42	62.32	60.72	-
	Scale	27.29	45.98	51.13	6.75	6.57	12.02	17.64	55.42	62.32	60.72	-
Rotation	27.80	46.93	54.68	17.21	16.84	27.28	33.97	59.64	63.36	65.13	-	
Alignment	Spatial	-	-	-	-	-	-	-	63.77	66.22	68.39	-
	Temporal	-	-	-	-	-	-	-	51.43	43.65	49.02	-
Average(AP <sub>cor</sub> )		23.42	40.37	49.81	10.26	10.68	18.60	22.79	56.99	58.73	61.03	62.92
RCE (%) ↓		15.42	13.46	15.98	57.00	53.95	46.89	46.41	11.45	11.52	10.84	11.09

<sup>†</sup>: Results from Ref. [125].

\* denotes the result of our re-implementation.

the projection method in cylindrical coordinates. It has then followed by [87]–[90]. LaserNet [394] utilizes DLA-Net [397] to obtain multi-scale features and detect 3D objects from this representation. Inspired by LaserNet, some works have borrowed models from 2D object detection to handle range images. For example, U-Net [398] is applied in [87], [395],

[399], RPN [400] is employed in [87], [88], and FPN [401] is leveraged in [90]. Considering the limitations of traditional 2D CNNs in extracting features from range images, some works have resorted to novel operators, including range dilated convolutions [88], graph operators [402], and meta-kernel convolutions [90]. Furthermore, some works have focused on

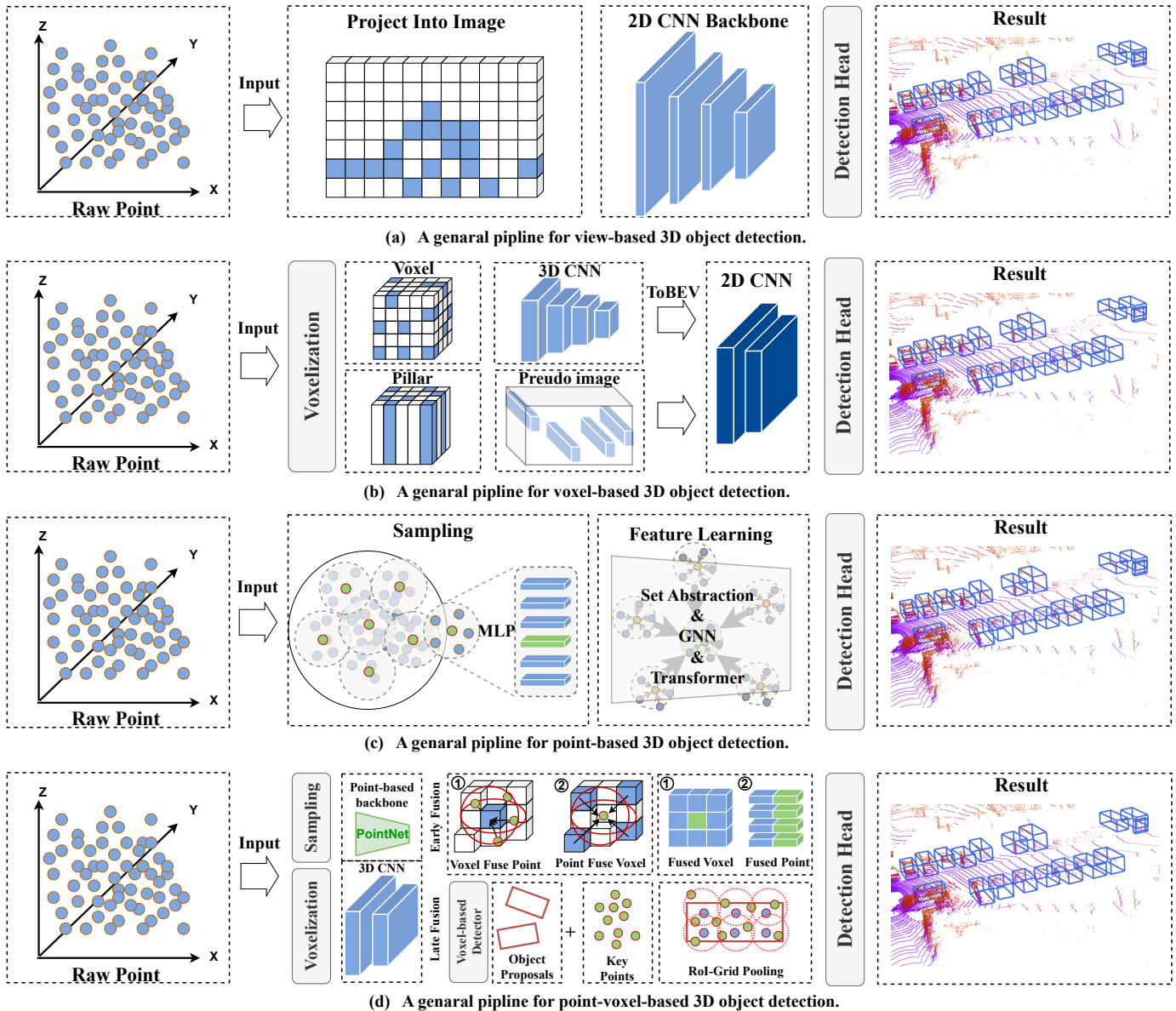


Fig. 5: The general pipelines for LiDAR-only 3D object detection.

addressing issues of occlusion and scale variation in range view. Specifically, these methods [87], [89] construct feature transformation structures from the range view to the point view and from the point view to the BEV (Bird’s Eye View) perspective to convert range features into BEV perspective.

2) **BEV View**: Comparison to range view detection, BEV-based detection is more robust to occlusion and scale variation challenges. Hence, feature extraction from the range view and object detection from the BEV become the most practical solution for range-based 3D object detection. The BEV representation is encoded by height, intensity, and density. Point clouds are discretized into a regular 2D grid. To encode more detailed height information, point clouds are evenly divided into  $M$  slices, resulting in  $M$  height maps where each grid cell stores the maximum height value of the point clouds. The intensity feature represents the reflectance value of the point within each grid cell, and the point cloud density

indicates the number of points in each cell. PIXOR [291], which outputs oriented 3D object estimates decoded from pixel-wise neural network predictions, is a pioneering work in this field, followed by [89], [90], [293], [403]. These methods usually entail three stages. First, point clouds are projected into a novel cell encoding for BEV projection. Next, both the object’s location on the plane and its heading are estimated through a convolutional neural network originally designed for image processing. Considering scale variation and occlusion, RangeRCNN [87] and RangeIOUdet [89] introduce a point view that serves as a bridge from RV to BEV, which provides pointwise features for the models.

### B. Voxel-based 3D object detection

Voxel-based methods segment sparse point clouds into regular voxels, achieving a dense representation through voxelization. Despite spatial convolution enhancing 3D information

perception, challenges persist in achieving high detection accuracy. These challenges include 1) **high computational complexity**, which demands substantial memory and computational resources due to the numerous voxels representing 3D space, 2) **spatial information loss** that occurs during voxelization, leading to difficulties in accurately detecting small objects, 3) **inconsistencies in scale and density**, inherent to specific voxel grids, which pose challenges in adapting to diverse scenes with varying object scales and point cloud densities. Overcoming these challenges requires addressing limitations in data representation, enhancing network feature capacity, improving object localization accuracy, and enhancing the model’s understanding of complex scenes. Ensuring safety perception in autonomous driving is crucial, and despite varying optimization strategies, these methods converge on common perspectives of model optimization, focusing on 1) **data representation** and 2) **model structure**.

1) **Data representation**: Voxel-based methods first rasterize point clouds into discrete grid representations. Grid representations are closely related to accuracy, computational complexity, and memory requirements. Using a voxel size that is too large results in significant information loss, while using a voxel size that is too small increases the burdens of computation and memory. As shown in Fig. 5 (b), according to the height along the z-axis, the types of grid representations can be categorized into voxels and pillars.

a) **Voxel**: Voxel process divides the 3D space into regular voxel grids with size ( $d_L \times d_W \times d_H$ ) in the x, y, and z directions, respectively. Only non-empty voxel units that contain points are stored and used for feature extraction. However, due to the sparse distribution of point clouds, the majority of voxel units are empty. As a pioneering work in voxel-based methods [36]–[40], [42], [43], [46]–[48], [54], [57], [60], [61], [65], [69], [77], [92], [108], VoxelNet [42] proposes a novel voxel feature encoding (VFE) layer to extract features from the points inside a voxel cell. Then, following works [38], [39], [47], [57], [75], [80] have extended the VoxelNet network by adopting similar voxel encoding approaches. Existing methods often perform local partitioning and feature extraction uniformly across all positions in the point cloud. This approach limits the receptive field for distant regions and information truncation. Therefore, some works have proposed different approaches to voxel partitioning: 1) **Different coordinate systems**: some approaches have reexamined voxel partitioning from different coordinate system perspectives, e.g. [78], [404] from cylindrical and [62] from spherical coordinate systems. Spheroformer [62] facilitates the aggregation of information from sparsely distant points by dividing the 3D space into multiple non-overlapping radial windows using spherical coordinates ( $r, \theta, \phi$ ), thereby enhancing information integration from dense point regions. 2) **Multi-scale voxels**: some works generate voxels of different scales [48], [76] or use reconfigurable voxels [79], e.g., HVNet [76] proposes a hybrid voxel network which integrates different scales in the point-level voxel feature encoder (VFE).

b) **Pillars**: Pillars can be considered a special form of voxels. Specifically, point clouds are discretized into a grid uniformly distributed on the x-y plane without binning

along the z-axis. Pillar features can be aggregated from points through a PointNet [405] and then scattered back to construct a 2D BEV image for feature extraction. As the pioneering work in this series [51], [52], [55], [64], [91], [93], PointPillar [51] first introduces the pillar representation. Following works have extended the ideas from 2D detection to PointPillars. PillarNet [93] adopts the ‘encoder-neck-head’ detection architecture to enhance the performance of pillar-based methods. SWFormer [64] and ESS [55] draw inspiration from the Swin Transformer [371] and apply a hierarchical window mechanism to pseudo-images, thereby enabling the network to maintain a global receptive field. PillarNeXt [52] integrates a series of mature 2D detection techniques and achieves performance comparable to voxel-based methods.

2) **Model Structure**: There are three major types of neural networks in voxel-based methods: 1) 2D CNNs for processing BEV feature maps and pillars. 2) 3D Sparse CNNs for processing voxels. 3) Transformers for handling both voxels and pillars.

a) **2D CNNs**: 2D CNNs are primarily used to detect 3D objects from a bird’s-eye view perspective, including processing BEV (Bird’s Eye View) feature maps and pillars [51], [52], [64], [91], [93]. Specifically, the 2D CNNs used for processing BEV feature maps often come from well-developed 2D object detection networks, such as Darknet [406], ResNet [407], FPN [401], and RPN [400]. One significant advantage of 2D CNNs compared to 3D CNNs is their faster speed. However, due to their difficulty in capturing spatial relationships and shape information, 2D CNNs typically exhibit lower accuracy.

b) **3D Sparse CNNs**: 3D Sparse CNNs consist of two core operators: sparse convolution and submanifold convolution [408], which ensure that the convolutional operation is performed only on non-empty voxels. SECOND [43] implements efficient computation of sparse convolution [408] and submanifold convolution [409] operators to gain fast inference speed by constructing a hash table. It is followed by [39], [46], [47], [57], [122]. However, the limited receptive field of 3D Sparse CNNs, which leads to information truncation, restricts the model’s feature extraction capabilities. Meanwhile, the sparse representation of features makes it challenging for the model to capture fine-grained object boundaries and detailed information. To optimize these issues, main optimization strategies have emerged: 1) Expanding the model’s receptive field. Some methods [60], [61] extend the concept of large kernel convolution from 2D to 3D space or introduce additional downsampling layers in the model [46]. 2) Combining sparse and dense representations. Methods in this category typically utilize dense prediction heads to prevent information loss [42], [43], [47], [57], [302] or retrieve lost 3D information from the detection process [37], [47], [57], [86], [302], or they add additional auxiliary tasks to the model [38], [39], [77], [302], [305]. Methods employing dense prediction heads typically require high-resolution Bird’s Eye View (BEV) feature maps for conducting dense predictions on them. Considering computational complexity, some recent methods aim to establish global sparse and local dense prediction relationships [56].

c) **Transformer**: Due to the amazing performance of transformers [371], [372], many efforts have been made to

adapt Transformers to 3D object detection. Particularly, recent studies [124], [125] have confirmed the excellent robustness of transformer-based models, which will further advance research in the domain of safety perception for autonomous driving. Compared with CNNs, the query-key-value design and the self-attention mechanism allow transformers to model global relationships, resulting in a larger receptive field. However, the primary limitation for efficiently applying Transformer-based models is the quadratic time and space complexity of the global attention mechanism. Hence, designing specialized attention mechanisms for Transformer-based 3D object detectors is critical. Transformer [370], DETR [374], and ViT [372] are the works that have most significantly influenced 3D transformer-based methods [55], [58], [59], [64], [91], [101], [108]. They have each inspired subsequent 3D detection works in various aspects: the design of attention mechanisms, the architecture of encoders and decoders, and the development of patch-based inputs and architectures similar to visual transformers. Inspired by transformer [370], VoTr [58] is the first work to incorporate a transformer into a voxel-based backbone network, composed of sparse attention and sparse submanifold attention modules. Subsequent works [59] have continued to build on the foundation of voxel-transformer, further optimizing the temporal complexity of the attention mechanism. DETR [374] has inspired a range of networks to adopt an encoder-decoder structure akin to DETR's. TransFusion [108] is a notable work that generates object queries from initial detections, applying cross-attention to LiDAR and image features within the Transformer decoder for 3D object detection. Meanwhile, many papers [55], [64], [91] are exploring and refining the patch-based input mechanism from ViT [372] and the window attention mechanism from Swin Transformer [371], e.g., SST [55] and SWFormer [64] group local regions of voxels into patches, apply sparse regional attention, and then apply region shift to change the grouping. Notably, SEFormer [91] is the first to introduce object structure encoding into the transformer module.

### C. Point-based 3D object detection

Unlike voxel-based methods, point-based methods retain the original information to the maximum extent, facilitating fine-grained feature acquisition. However, the performance of point-based methods is still affected by two crucial factors: 1) the number of contextual points in the point cloud sampling stage and 2) the context radius used in the point-based backbone. These factors significantly impact the speed and accuracy of point-based methods, including the detection of small objects, which is critical for safety considerations. Therefore, optimizing these two factors is paramount, based on existing literature. In this regard, we primarily focus on elucidating 1) **Point Cloud Sampling** and 2) **Point-based Backbone**.

1) **Point Cloud Sampling**: As an extensively utilized method, FPS (Farthest Point Sampling) aims to select a set of representative points from the raw points, such that their mutual distances are maximized, thereby optimally covering the entire spatial distribution of the point cloud.

PointRCNN [45], a pioneering two-stage detector in point-based methods, utilizes the PointNet++ [410] with multi-scale grouping as the backbone network. In the first stage, it generates 3D proposals from point clouds in a bottom-up manner. The second stage network refines the proposals by combining semantic features and local spatial features. However, existing methods relying on FPS still face several issues: 1) Points irrelevant to detection also participate in the sampling process, leading to additional computational burden. 2) The distribution of points across different parts of an object is uneven, resulting in suboptimal sampling strategies. Subsequent works have attempted various optimization strategies, such as segmentation-guided background point filtering [94], random sampling [295], feature space sampling [40], voxel-based sampling [44], [113], coordinate refinement [66], and ray-based grouping sampling [95].

2) **Point-based Backbone**: The feature learning stage in point-based methods aims to extract discriminative feature representations from raw points. The neural network used in the feature learning phase should possess the ability of to local be awareness locally aware and integrating to integrate contextual information. Based on the aforementioned motivations, a multitude of detectors have been designed for processing raw points. However, most methods can be categorized according to the core operators they utilize: 1) PointNet-based methods [45], [94], [98], [297]. 2) Graph Neural Network-based methods [44], [63], [294], [295], [411]. 3) Transformer-based methods [66], [412].

a) **PointNet-based**: PointNet-based methods [45], [94], [98], [297] primarily rely on the Set Abstraction [405] to perform downsampling on raw points, aggregation of local information, and integration of contextual information, while preserving the symmetry invariance of the raw points. PointRCNN [45], as the first two-stage work in point-based methods, achieved amazing performance at its time; however, it still faces the issue of high computational cost. Subsequent work [70], [94] has addressed this issue by introducing an additional semantic segmentation task during the detection process to filter out background points that contribute minimally to detection. Furthermore, some efforts have focused on resolving the issue of the uncontrolled receptive field in PointNet & PointNet++, such as through the use of GNN [80] or Transformer [66] techniques.

b) **Graph-based**: GNNs (Graph Neural Networks) possess key elements such as an adaptive structure, dynamic neighborhood, the capability to construct both local and global contextual relationships, and robustness against irregular sampling. These characteristics naturally endow GNNs with an advantage in handling irregular point clouds. Point-GNN [44], a pioneering work, designs a one-stage graph neural network to predict objects with an auto-registration mechanism, merging, and scoring operations, which demonstrate the potential of using graph neural networks as a new approach for 3D object detection. Most graph-based, point-based methods [44], [294], [295], [298], [411] aim to fully utilize contextual information. This motivation has led to further improvements in subsequent works [298], [411].

c) **Transformer-based:** Up to this point, a series of methods [66], [412]–[414] have explored the use of transformers for feature learning in point clouds, achieving excellent results. Pointformer [66] introduced local and global attention modules for processing 3D point clouds. The local transformer module models interactions among points within local areas, with the aim of learning contextually relevant regional features at the object level. The global transformer, on the other hand, focuses on learning context-aware representations at the scene level. Subsequently, the local-global Transformer combines local features with high-resolution global features to further capture dependencies between multi-scale representations. Group-free [412] adapted the Transformer to suit 3D object detection, enabling it to model both object-to-object and object-to-pixel relationships and to extract object features without manual grouping. Moreover, by iteratively refining the spatial encoding of objects at different stages, the detection performance is further enhanced. Point-based transformers directly process unstructured and unordered raw point clouds, which results in significantly higher computational complexity compared to structured voxel data.

#### D. Point-Voxel based 3D object detection

Point-voxel methods aim to leverage the fine-grained information capture capabilities of point-based methods and the computational efficiency of voxel-based methods. By integrating these methods, point-voxel based methods enable a more detailed processing of point cloud data, capturing both the global structure and micro-geometric details. This is critically important for safety perception in autonomous driving, as the accuracy of decisions made by autonomous driving systems depends on high-precision detection results.

The key goal of point-voxel methods is to enable feature interplay between voxels and points via point-to-voxel or voxel-to-point transformations. The idea of leveraging point-voxel feature fusion in backbones has been explored by many works [49], [50], [53], [67], [72], [82]–[84], [86], [97], [308], [381], [415]. These methods fall into two categories: 1) **Early Fusion.** Early fusion methods [49], [72], [82]–[84], [97] fuse voxel features and point features within the backbone network. 2) **Late Fusion.** Late fusion methods [50], [53], [67], [86], [308], [381], [415] typically employ a two-stage detection approach, using voxel-based methods for initial proposal box generation, followed by sampling and refining key point features from the point cloud to enhance 3D proposals.

a) **Early Fusion:** Some methods [49], [72], [82]–[84], [97] have explored using new convolutional operators to fuse voxel and point features, with PVCNN [49] potentially being the first work in this direction. In this method, the voxel-based branch initially converts points into a low-resolution voxel grid and aggregates neighboring voxel features through convolution. Then, the voxel-level features are transformed back into point-level features and fused with the features obtained from the point-based branch. Following closely, SPVCNN [97], which builds upon PVCNN, extends PVCNN to the domain of object detection. Other methods attempt to make improvements from other perspectives, such as auxiliary tasks [72] or multi-scale feature fusion [82]–[84].

b) **Late Fusion:** The methods in this series predominantly adopt a two-stage detection framework. Initially, voxel-based methods are employed to generate preliminary object proposals. This is followed by a refinement phase, where point-level features are leveraged for the precise delineation of detection boxes. As a milestone in PV-based methods, PV-RCNN [308] utilizes SECOND [43] as the first-stage detector and proposes a second-stage refinement stage with a RoI grid pool for the fusion of keypoint features. Subsequent works have followed the aforementioned paradigm, focusing on advancements in second-stage detection. Notable developments include the use of attention mechanisms [67], [85], [86], scale-aware pooling [381], and point density-aware refinement modules [53].

PV-based methods simultaneously possess the computational efficiency of voxel-based approaches and the capability of point-based methods to capture fine-grained information. However, constructing point-to-voxel or voxel-to-point relationships, along with the feature fusion of voxels and points, incurs additional computational overhead. Consequently, compared to voxel-based methods, PV-based methods can achieve better detection accuracy and robustness, but at the cost of increased inference time.

#### E. Analysis: Accuracy, Latency, Robustness

In the autonomous driving sector, the development of LiDAR-only 3D object detection solutions is advancing rapidly. A series of works [1], [4], [123], [126], [130], [131] have comprehensively summarized the current technological roadmaps, such as the extensive review of LiDAR-only solutions by the Shanghai AI Lab and SenseTime Research [126]. However, there is a lack of summarization and guidance from the perspective of safety perception and cost impact in autonomous driving. Therefore, in this section, following an analysis of the technological roadmaps and the current state of LiDAR-only solutions, we intend to base our discussion on the fundamental principles of ‘Accuracy, Latency, and Robustness.’ It aims to guide the practical implementation of economically efficient and safe sensing in autonomous driving.

1) **Accuracy:** Referring to Section III on Camera-only methods, we investigated the core factors influencing LiDAR-only methods. Representative methods from each category underwent comparative performance analysis on the KITTI [133] and nuScenes [134] datasets, as shown in Fig 3 (c, d). The current scenario indicates that the latest view-based methods exhibit lower performance compared to other categories. View-based approaches transform point clouds into pseudo-images for processing with 2D detectors, which favors inference speed but sacrifices 3D spatial information. Therefore, an effective representation of 3D spatial information is pivotal for LiDAR-only methods. Initially, point-based and PV-based methods outperformed voxel-based approaches in LiDAR-only detection. Over time, methods like Voxel RCNN [47], which utilize ROI pool modules for fine-grained information aggregation, have achieved comparable or superior performance. Voxel RCNN’s ROI pooling module effectively addresses the loss of detailed 3D spatial information resulting from voxelization.

2) **Latency**: Section III highlights latency’s importance in autonomous driving safety and user experience. While Camera-only methods tend to outperform LiDAR-only methods in terms of inference speed, the latter still maintain a competitive edge due to their accurate 3D perception. We conducted tests using an A100 graphics card to measure the FPS of significant LiDAR-only approaches, and evaluated their performance using the original research’s AP and NDS metrics. As shown in Table V, it indicates that view-based methods excel in model latency due to the reduction in point cloud dimensions and the efficiency of 2D CNNs. Voxel-based methods achieve exceptional inference speed due to the use of structured voxel data and well-optimized 3D sparse convolutions. However, point-based methods face challenges in applying efficient operators during data preprocessing and feature extraction stages due to the irregular representation of point clouds. Point-GNN [44] is an extreme example of this, with model latency nearly several times that of contemporary voxel algorithms. Transformer-based methods [67] face significant challenges in real-time inference. The current research trend in transformer-based methods is the development of efficient attention operators, like [55], [64], [371]. Moreover, for PV-based methods, the construction of point-to-voxel or voxel-topoint relationships, along with the feature fusion of voxels and points, incurs additional computational overhead. To conclude, common accuracy optimization strategies, such as two-stage optimization or attention mechanisms, typically compromise inference speed in autonomous driving models. Achieving a balance between accuracy and speed is an evolving challenge in this field. Future studies should prioritize the simultaneous improvement of accuracy, as well as the reduction of FPS (frames per second) and latency, in order to meet the urgent requirements of real-time response and safety in autonomous driving.

3) **Robustness**: Previous comprehensive reviews have not focused significantly on the topic of robustness. Presently, research works [124], [125], [147], [148], [390]–[392] like RoboBEV [124], Robo3D [148] on 3D object detection incorporate considerations of robustness, exemplified by factors such as sensor misses. Robo-LiDAR [146] represents the first comprehensive exploration solely dedicated to the robustness of LiDAR-only methods. In a manner akin to BR3D [125], this method evaluates robustness by integrating disturbances into datasets pertinent to 3D object detection, such as KITTI [133]. The method involves proposing a variety of noise types and 25 typical degradations associated with object and scene-level natural weather conditions, noise interferences, density variations, and object transformations. In this section, we will combine the work of Ref. [125] and Robo-LiDAR [146] with the aim of systematically analyzing the robustness of LiDAR-only methods. As shown in the Table VII, generally, LiDAR-only methods exhibit higher robustness to noise compared to Camera-only methods. In Multi-modal methods [99], [105], [106], [108], [110], [116], [121], the complementary interplay of data types becomes evident when disturbances are limited to LiDAR sensor data. In such scenarios, image data can partially mitigate the impact on point cloud integrity, consequently elevating the performance of fusion methods above that of

methods relying solely on LiDAR. when disturbances affect both image and point cloud data concurrently, the efficacy of most Multi-modal methods significantly diminishes. It is worth noting that DTS [416] and Bi3D [417] enhance model robustness through domain adaptation methods.

As shown in Table IX, under various noise conditions, LiDAR-only methods experience varying degrees of accuracy decline, with the most significant reduction observed in extreme weather noise scenarios. These results indicate an urgent need in the field of autonomous driving to address the robustness issue of point cloud detectors. For most types of corruptions, voxel-based methods generally exhibit greater robustness than point-based methods, as shown in Table VII, VIII, IX. A plausible explanation is that voxelization, through the spatial quantization of a group of adjacent points, mitigates the local randomness and spatial information disruption caused by noise and density degradation. Specifically, for severe corruptions (e.g., shear, FFD in the transformation), the point-voxel-based method [308] exhibits greater robustness. PointRCNN [45] does not show the highest robustness against any form of corruption, highlighting potential limitations inherent in point-based methods. In conclusion, future works should explore robustness optimization from the perspectives of data representation and model architecture. The above analysis aims to offer valuable insights for future work related to robustness.

TABLE IX: Comparison with LiDAR-only detectors on corrupted validation sets of KITTI from Ref. [146] on Car detection with  $CE_{AP}(\%)$ .  $CE_{AP}(\%)$  denotes **Corruption Error** from Ref. [146]. The best one is highlighted in **bold**. ‘T.F.’ denotes Transformation.

Corruption		PV	Point	Voxel			Avg.
		PV-RCNN	PointRCNN	SECOND	SE-SSD	CenterPoint	
Weather	rain	25.11	23.31	<b>21.81</b>	29.51	25.83	26.45
	snow	44.23	37.74	<b>34.84</b>	49.19	38.74	45.64
	fog	1.59	3.52	1.60	1.59	<b>1.11</b>	1.88
Noise	uniform_rad	10.19	8.32	9.51	9.34	8.15	7.82
	gaussian_rad	13.02	9.98	12.13	11.02	10.17	9.65
	impulse_rad	2.20	3.86	2.23	<b>1.18</b>	1.8	2.46
	background	2.93	6.49	2.41	2.14	1.86	2.46
	upsample	0.81	1.84	<b>0.31</b>	0.55	0.46	0.75
Density	cutout	3.75	3.97	4.27	4.26	4.11	4.0
	local_dec	14.04	-	13.88	17.01	14.64	14.44
	local_inc	1.40	3.34	1.33	<b>0.90</b>	0.95	1.68
	beam_del	0.58	0.79	0.73	1.07	<b>0.47</b>	0.73
	layer_del	2.94	3.46	3.10	3.37	<b>2.67</b>	3.17
Noise	uniform	15.44	12.95	9.48	6.99	6.51	8.94
	gaussian	20.48	17.62	12.98	9.56	9.49	12.42
	impulse	3.3	4.7	2.53	2.2	<b>2.11</b>	3.26
	upsample	1.12	1.95	0.67	0.22	0.16	0.74
Density	cutout	15.81	15.62	14.99	16.51	<b>14.06</b>	15.47
	local_dec	14.38	14.16	13.23	15.08	<b>12.52</b>	13.84
	local_inc	13.93	14.19	13.74	<b>11.03</b>	11.64	12.81
T.F.	shear	<b>37.27</b>	40.96	40.35	40.35	40.0	39.71
	FFD	<b>32.42</b>	38.88	33.15	37.96	32.86	34.93
	rotation	0.60	0.47	0.31	<b>0.27</b>	0.38	0.52
	scale	<b>5.78</b>	8.13	6.96	6.53	7.50	6.97
	translation	3.82	3.03	3.24	<b>1.37</b>	3.91	3.77
mCE		11.49	11.64	10.60	11.17	<b>10.09</b>	11.01

## V. MULTI-MODAL 3D OBJECT DETECTION

Multi-modal 3D object detection refers to the technique of using data features from different sensors and integrating these features to achieve complementarity, thus enabling the



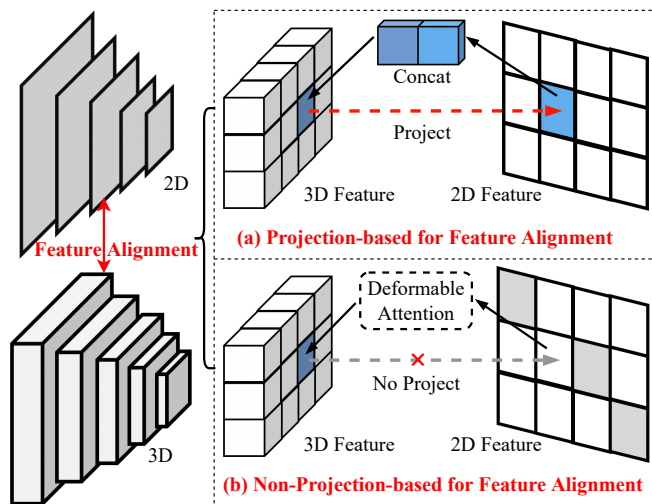


Fig. 6: Projection-based for Feature Alignment vs. Non-Projection-based for Feature Alignment.

detection of 3D objects. As shown in Fig. 6, the approach particularly emphasizes the combination of image data and point cloud data. Image data is rich in semantic features, such as color and texture, but often lacks depth information. In contrast, point cloud data provides depth information and geometric structure, which is crucial for accurately perceiving and interpreting the 3D characteristics of a scene. Since a single type of sensor cannot fully and accurately perceive the 3D environment, multi-modal 3D object detection acquires features with rich semantic information by fusing various types of data.

In the field of autonomous driving, there are a variety of fusion methods for multi-modal 3D object detection. Previous reviews [4], [123], [126], [130], [131] have mostly classified these methods based on different stages of fusion (early, middle, late), but this classification is overly simplistic and does not fully consider the special requirements of autonomous driving. Given the fundamental differences between the two heterogeneous modalities of point clouds and images, the alignment step in multi-modal fusion is particularly critical. It ensures the consistency and accuracy of information from different sensors and data sources during the fusion process. In autonomous driving, the key to achieving feature alignment lies in whether to use a calibration matrix (also known as a projection matrix). However, the inherent error of the calibration matrix, being a type of prior knowledge, poses a challenge. Some works, like [115], [339], avoid using the projection matrix and reduce projection errors by adopting learning methods.

Therefore, based on different methods of feature alignment, we can categorize multi-modal 3D object detection methods into two types: (1) projection-based for feature alignment, and (2) model-based for feature alignment. This taxonomy is more detailed and scientific, better reflecting the characteristics and progress of multi-modal 3D object detection methods in the field of autonomous driving.

### A. Projection-based 3D object detection

Projection-based 3D object detection refers to the use of projection matrices during the feature fusion stage to achieve the integration of point cloud and image features. It is important to clarify that the focus here is on projection during the feature fusion period, rather than projections in other stages of the fusion process, which include projections needed for processes such as data augmentation. As shown in Fig. 7, we have developed a more detailed classification of projection-based 3D object detection based on the different types of projection used in the fusion stage, including Point-Projection-based [100], [104], [105], [316]–[322], [418], Feature-Projection-based [110], [122], [325]–[329], [419], [420], Auto-Projection-based [41], [111], [112], [120], [121], [296], [331], [332], [382], and Decision-Projection-based methods [96], [113], [333]–[338], [383].

1) **Point-Projection-based 3D object detection:** Point-Projection-based 3D object detection methods [100], [317]–[322], [418] involve projecting image features onto raw point clouds to enhance the representational capability of the original point cloud data, as shown in Fig. 7 (a). The initial step in these methods is to establish a strong correlation between LiDAR points and image pixels, which is achieved using calibration matrices. Following this, the point cloud features are enhanced by augmenting them with additional data. This augmentation takes two forms: either through the incorporation of segmentation scores [100], [320], [323] or by using CNN features [104], [105], [316], [319], [321] from the correlated pixels. PointPainting [100] and PointAugmenting [319] represent advancements in multi-modal 3D object detection methods by enhancing the traditional cut-and-paste augmentation. These techniques aim to seamlessly integrate data from different domains, such as point clouds and 2D imagery, while carefully managing potential overlaps or collisions between objects in both domains. PointPainting enhances LiDAR points by appending segmentation scores. However, it has limitations in effectively capturing the color and texture details present in images. To address these shortcomings, more sophisticated approaches like FusionPainting [320] have been developed, following a similar paradigm. MVP [321] builds upon the concept of PointPainting [100]. It initially utilizes image instance segmentation and establishes an alignment between the segmentation masks and the point cloud using a projection matrix. The key distinction of MVP lies in its approach to sampling: it randomly selects pixels within each range, ensuring consistency with the points in the point cloud. These selected pixels are then linked to their nearest neighbors in the point cloud. The depth value of the LiDAR point in this linkage is assigned as the depth of the corresponding pixel. Subsequently, these points are projected back to the LiDAR coordinate system, resulting in the generation of virtual LiDAR points.

2) **Feature-Projection-based 3D object detection:** In contrast to Point-Projection-based methods, Feature-Projection-based 3D object detection methods [60], [110], [118], [122], [326], [327], [419], [420], [432], as shown in Fig. 7 (b), primarily focus on fusing point cloud features with image

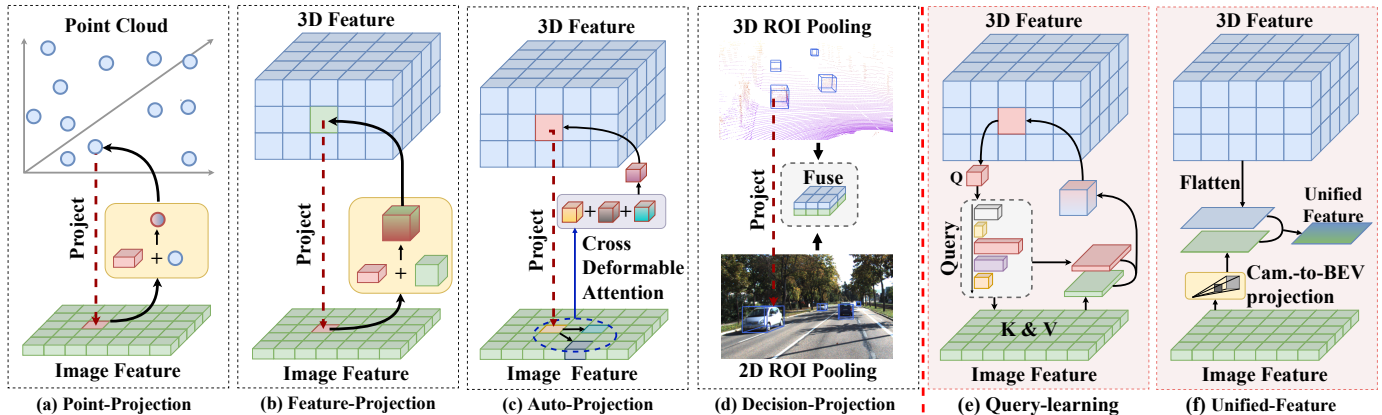


Fig. 7: Projection-based 3D object detection: (a) Point-Projection-based methods [100], [104], [105], [316]–[324], [418], (b) Feature-Projection-based methods [110], [122], [325]–[330], [419]–[421], (c) Auto-Projection-based methods [41], [111], [112], [120], [121], [296], [331], [332], [382], [385], [422]–[424], (d) Decision-Projection-based methods [96], [113], [333]–[338], [383]. Non-Projection-based 3D object detection: (e) Query-Learning-based methods [101], [108], [115], [116], [339], [340], [425]–[427], (f) Unified-Feature-based methods [65], [99], [102], [103], [106], [109], [114], [117], [344]–[351], [428]–[431].

features during the feature extraction phase of the point clouds. During this fusion process, point cloud features are projected onto corresponding image features, and subsequently, these image and point cloud features are integrated together. This process is achieved by applying a calibration matrix to transform the voxel’s three-dimensional coordinate system into the pixel coordinate system of the image, thereby facilitating the effective fusion of point cloud and image modalities. Specifically, the projection of a three-dimensional point cloud onto the image plane can be articulated as follows:

$$z_c \begin{bmatrix} u \\ v \\ 1 \end{bmatrix} = h\mathcal{K} \begin{bmatrix} R & T \end{bmatrix} \begin{bmatrix} P_x \\ P_y \\ P_z \\ 1 \end{bmatrix}, \quad (6)$$

where,  $P_x$ ,  $P_y$ , and  $P_z$  represent the three-dimensional spatial coordinates of the LiDAR points, while  $u$  and  $v$  denote the corresponding two-dimensional coordinates. The term  $z_c$  indicates the depth of the point’s projection on the image plane. Additionally,  $\mathcal{K}$  represents the intrinsic parameters of the camera, and  $R$  and  $T$  signify the rotation and translation of the LiDAR relative to the camera’s reference frame, respectively. The factor  $h$  accounts for the scale change due to downsampling.

A quintessential example of the Feature-Projection-based method, ContFuse [432], employs continuous convolution to amalgamate multi-scale convolutional feature maps from each sensor. Within this technique, the projection of the point cloud facilitates the correspondence between the image and the Bird’s Eye View (BEV). In essence, Feature-Projection-based 3D object detection method is accomplished during the point cloud feature extraction phase. Compared to Point-Projection-based methods, they do not perform fusion on the original point cloud but achieve a profound depth feature fusion, resulting in more robust performance.

3) **Auto-Projection-based 3D object detection:** As shown in Fig. 8, a partial image from the KITTI [133] dataset



Fig. 8: Examples of misalignment between point clouds and images.

exemplifies that projection inaccuracies persist even in this classic clean dataset. Consequently, the issue of projection errors cannot be completely eliminated through manual calibration; instead, they can only be mitigated. This is a frequent challenge in practical dataset deployments. Many studies, like Point & Feature-Projection-based methods, have performed fusion through direct projection without addressing the projection error issue. A few works [41], [111], [112], [120], [121], [331], [332], [382], have sought to mitigate these errors through approaches such as projection offsets and neighboring projections. For instance, Deformable Cross Attention [373] has been employed to learn offsets in the context of already projected data. We have systematically reviewed and synthesized methods that tackle projection errors, designating them as Auto-projection-based 3D object detection methods, as shown in Fig. 7 (c). As representative works addressing feature alignment, HMF1 [120], GraphAlign [111], and GraphAlign++ [112] utilize a priori knowledge of projection calibration matrices to project onto corresponding images for local graph modeling. This approach simulates intermodal relationships, enabling Multi-modal 3D object detectors to effectively identify more appropriate alignment relationships, thereby achieving faster and more accurate feature alignment between modalities. AutoAlignV2 [332] focuses on sparse learnable sampling points for cross-modal relational model-

ing, enhancing calibration error tolerance and significantly accelerating feature aggregation across different modalities. In summary, Auto-Projection-based 3D object detection methods mitigate errors arising from feature alignment by leveraging neighbor relationships or neighbor offsets, thereby enhancing robustness in Multi-modal 3D object detection.

#### 4) *Decision-Projection-based 3D object detection:*

Decision-Projection-based 3D object detection methods [96], [113], [333]–[338], [383], as early implementations of Multi-modal 3D object detection schemes, use projection matrices to align features in Regions of Interest (RoI) or specific results, as shown in Fig. 7 (d). These methods are primarily focused on the alignment of features in localized areas of interest or specific detection outcomes.

Graph-RCNN [113] projects the graph node to the location in the camera image and collects the feature vector at that pixel in the camera image through bilinear interpolation. F-PointNet [336] performs detection on the 2D image to determine the class and localization of the object, and for each detected object, the corresponding point clouds in 3D space are obtained through the conversion matrix of calibrated sensor parameters and 3D space. MV3D [335] employs a transformation of the LiDAR point cloud into Bird’s Eye View (BEV) and Front View (FV) projections for generating proposals. During this process, a specialized 3D proposal network is used to create precise 3D candidate boxes. These 3D proposals are then projected onto feature maps from multiple perspectives to facilitate feature alignment between the two modalities. Differing from MV3D [335], AVOD [334] streamlines this approach by omitting the FV component and introducing a more refined region proposal mechanism. In summary, Decision-Projection-based 3D object detection methods primarily achieve feature fusion at a high level through projection, with limited interaction between heterogeneous modalities. This often leads to the alignment and fusion of erroneous features, resulting in issues of reduced accuracy and robustness.

### B. *Non-Projection-based 3D object detection*

Non-Projection-based 3D object detection methods achieve fusion without relying on feature alignment, thereby yielding robust feature representations. They circumvent the limitations of camera-to-LiDAR projection, which often reduces the semantic density of camera features and impacts the effectiveness of techniques like Focals Conv [110] and PointPainting [100]. Non-Projection-based methods typically employ cross-attention mechanisms or the construction of a unified space to address the inherent misalignment issues in direct feature projection. These methods are primarily divided into two categories: (1) Query-Learning-based [108], [115], [116], [339], [385], [425] and (2) Unified-feature-based [65], [99], [101], [103], [106], [109], [114], [344]–[348]. Query-Learning-based methods entirely negate the need for alignment during the fusion process. Conversely, Unified-Feature-based methods, though constructing a unified feature space, do not completely avoid projection; it usually occurs within a single modality context. For example, BEVFusion [109] utilizes LSS [256] for camera-to-BEV projection. This process, taking place before

fusion, demonstrates considerable robustness in scenarios with feature misalignment.

1) *Query-Learning-based 3D object detection:* Query-Learning-based 3D object detection methods, as exemplified by works such as [108], [115], [116], [339], [385], [425], [433], eschew the necessity for projection within the feature fusion process, as shown in Fig. 7 (e). Instead, they attain feature alignment through cross-attention mechanisms before engaging in the fusion of features. Point cloud features are typically employed as queries, while image features serve as keys and values, facilitating a global feature query to acquire highly robust Multi-modal features. Furthermore, DeepInteraction [116] incorporates multimodality interaction, wherein point cloud and image features are utilized as distinct queries to enable further feature interaction. In comparison to the exclusive use of point cloud features as queries, the comprehensive incorporation of image features leads to the acquisition of more resilient Multi-modal features. Overall, Query-Learning-based 3D object detection methods employ a transformer-based structure for feature querying to achieve feature alignment. Ultimately, the Multi-modal features are integrated into LiDAR-only pipelines, such as CenterPoint [57].

2) *Unified-Feature-based 3D object detection:* Unified-feature-based 3D object detection methods, represented by works such as [65], [99], [101], [103], [106], [109], [114], [344]–[348], generally employ projection before feature fusion, achieving the pre-fusion unification of heterogeneous modalities, as shown in Fig. 7 (f). In the BEV fusion series, which utilizes LSS for depth estimation [101], [109], [344], [345], the front-view features are transformed into BEV features, followed by the fusion of BEV image and BEV point cloud features. Alternatively, CMT [103] and UniTR [347] employ transformers for tokenization of point clouds and images, constructing an implicit unified space through transformer encoding. CMT [103] utilizes projection in the position encoding process, but entirely avoids dependency on projection relations at the feature learning level. FocalFormer3D [346], FUTR3D [106], and UVTR [65] leverage transformers’ queries to implement schemes similar to DETR3D [30], constructing a unified sparse BEV feature space through queries, thus mitigating the instability introduced by direct projection. VirConv [99], MSMDFusion [348], and SFD [114] construct a unified space through pseudo-point clouds, with the projection occurring before feature learning. The issues introduced by direct projection are addressed through subsequent feature learning. In summary, Unified-feature-based 3D object detection methods [65], [99], [101], [103], [106], [109], [114], [344]–[348] currently represent high-precision and robust solutions. Although they incorporate projection matrices, such projection does not occur between Multi-modal fusion, distinguishing them as Non-Projection-based 3D object detection methods. Unlike Auto-Projection-based 3D object detection approaches, they do not directly address projection error issues but instead opt for unified space construction, considering multiple dimensions for Multi-modal 3D object detection, thereby obtaining highly robust Multi-modal features.

### C. Analysis: Accuracy, Latency, Robustness

In the preceding Sections III-D, IV-E, we have conducted a comprehensive analysis of ‘Accuracy, Latency, Robustness’ for camera-only and LiDAR-only approaches. Subsequently, we extend our examination to Multi-modal 3D object detection methods, employing a similar analytical framework.

1) **Accuracy:** As shown in Fig.3 (e) and (f), we conducted comparative evaluations on both the KITTI and nuScenes test datasets. The majority of Projection-based 3D object detection methods have predominantly undergone experimentation on the KITTI dataset, with only a minority extending their evaluation to nuScenes. As shown in Fig.3 (e), it is evident that Feature-Projection-based and Auto-Projection-based methods exhibit superior overall performance, while Decision-Projection-based methods, primarily dated prior to 2020, tend to manifest relatively lower Average Precision (AP) metrics. A scant few Non-Projection-based 3D object detection methods, such as CAT-Det [385], have been experimented with on the KITTI dataset. As shown in Fig.3 (f), the latest methods predominantly belong to the Unified-Feature-based methods, underscoring the suitability of the panoramic camera offered by nuScenes for achieving modality-unifying strategies like BEVFusion [109]. Overall, it is discernible that Non-Projection-based methods present more effective solutions in terms of Accuracy metrics (e.g., AP, mAP, NDS, etc.).

2) **Latency:** As shown in Table V, we conducted a comparative analysis of mono-modal 3D object detection methods (LiDAR-only and Camera-only) and Multi-modal 3D object detection on the KITTI and nuScenes datasets, presenting scatter plots for Latency (FPS) and Accuracy metrics (AP, mAP, NDS, etc.). It is noteworthy that, in comparison to mono-modal 3D object detection methods (LiDAR-only and Camera-only), Multi-modal 3D object detection approaches generally exhibit lower FPS. The results on the KITTI dataset indicate that GraphAlign excels in both AP and FPS metrics. Additionally, LoGoNet [121], Focals Conv [110], and EPNet [104] demonstrate outstanding performance. GraphAlign [111] maintains its position as having the highest FPS, but its NDS performance is suboptimal on the nuScenes dataset. In contrast, UniTR performs exceptionally well in both NDS and FPS metrics. Overall, it can be observed that within Projection-based methods, Auto-Projection-based and Feature-Projection-based methods exhibit superior overall performance, while within Unified-Feature-based methods, the overall performance is more outstanding. In the meticulous evaluation of the KITTI and nuScenes datasets, emphasis is placed on the trade-off between FPS and NDS metrics.

3) **Robustness:** In the previous sections III-D3 and IV-E3, we analyzed the robustness of mono-modal 3D object detection (Camera-only and LiDAR-only). In this section, based on Tables VII and VIII, we analyze the robustness of Multi-modal 3D object detection. From KITTI-C [125] and nuScenes-C [125], it can be seen that Multi-modal 3D object detection is more robust compared to mono-modal 3D object detection (Camera-only and LiDAR-only), with smaller RCE. In KITTI-C, representative articles LoGoNet [121] for Auto-Projection-based and VirConv [99] for Unified-Feature-based exhibit

greater robustness, while EPNet [104] for Point-Projection-based and Focals Conv [110] for Feature-Projection-based show slightly weaker performance. Additionally, in nuScenes-C, among Non-Projection-based methods, FUTR3D [106], TransFusion [108], BEVFusion [109], and DeepInteraction [116] all demonstrate strong robustness. It is worth noting that MetaBEV [430] explores the problem of modal loss caused by feature misalignments and sensor failures in BEV features of LiDAR and camera through deformable attention based on BEVFusion [109]. ObjectFusion [117] proposes a novel object-centric fusion to align object-centric features of different modalities. GraphBEV [349] mitigates misalignment issues by matching neighbor depth features through graph matching.

## VI. FUTURE OUTLOOKS

Through reviewing all the literature and analyzing the research trends of the past few years, we make some predictions on the future research direction of 3D object detection from the perspective of robustness.

### A. 3D Object Detection with Large Models

Inspired by the success of large language models (LLMs) such as ChatGPT [434] and vision foundation models (VFMs) like SAM, many researchers have focused on related research of large models. Compared to conventional methods, a large autonomous driving model based on LLM can mainly solve the following two problems. Firstly, it is the endless corner case problem. LLMs have a common sense ability and may become a new paradigm for solving corner cases in autonomous driving problems. Secondly, the current methods lack intuitive reasoning and provide textual explanations, and LLMs happen to be the best in this direction. It is worth researching how to combine large models with 3D object detection to enhance robustness and generalization and improve the ability of corner cases. However, there is currently limited research on combining large models and 3D object detection. For example, RoboFusion [330] has integrated TransFusion [108] and Focals Conv [110] with VFMs like SAM [435] to enhance its ability in harsh weather conditions. SEAL [436] uses VFMs like SAM [435] to segment different car point cloud sequences and can segment any car point cloud by encouraging spatial and temporal consistency during the representation learning stage. CLIP-BEVFormer [281] combines CLIP [437] and BEVFormer [16], leveraging the universal capabilities of CLIP [437] to enhance generalization on corner cases. VisLED [438] is a language-driven active learning framework for open-set 3D object detection, which utilizes active learning techniques to query various information-rich data samples from unlabeled pools. Almost all existing work is proposed and evaluated on close-range datasets. Although these datasets may be large and diverse, they are still insufficient for real-world applications. In the real world, the generalization and robustness of corner cases are of utmost importance, and 3D object detection with large models is a good starting point for solving open-set 3D object detection. In addition, current 3D object detection algorithms lack interpretability, and LLMs can bring hope for more robust 3D object detection and avoid unexpected situations caused by black box detectors.

### B. 3D Object Detection in End-to-End Autonomous Driving

UniAD [439] undoubtedly brought another hot topic to the field of autonomous driving after winning the CVPR Best Paper Award: end-to-end autonomous driving. End-to-end autonomous driving is a fully differentiable machine learning system that takes raw sensor input data and other metadata as prior information and directly outputs the control signals or trajectory planning for vehicles [440]. Generally, the autonomous drive system integrates multiple tasks, such as detection, tracking, online mapping, motion prediction, and planning. 3D object detection is closely related to other perception tasks and downstream tasks such as prediction and planning. Therefore, pursuing high accuracy in 3D object detection may not be optimal when considering the autonomous drive system. Although impressive progress has been made in end-to-end research, we believe three areas can be further improved in current 3D object detection for end-to-end autonomous driving. First, 3D object detection can guide more effective multi-modal environmental perception, allowing for better data integration from multi-modal sources. Second, the current inference capabilities of end-to-end autonomous driving are concerning. Third, 3D object detection enhanced with large language models (LLMs) provides stronger explanatory power, leading to enhanced explanatory power for subsequent tasks.

## VII. CONCLUSION

3D object detection plays a crucial role in autonomous driving perception. In recent years, this field has witnessed rapid development, yielding many research results. Based on the diverse data forms generated by sensors, these methods are primarily categorized into three types: image-based, point cloud-based, and multi-modal. The primary metrics for evaluation in these methods are high accuracy and low latency. Numerous reviews have summarized these approaches, focusing on the core principles of ‘high accuracy and low latency’ in delineating their technical trajectories. However, in the transition of autonomous driving technology from breakthroughs to practical applications, existing reviews have not prioritized safety perception as a central concern, failing to encompass the current technological pathways related to safety perception. For instance, recent Multi-modal fusion methods typically undergo robustness testing during the experimental phase, a facet not adequately considered in current reviews. Therefore, in this study, we re-examine 3D object detection algorithms with a central focus on the key aspects of ‘Accuracy, Latency, and Robustness’. We reclassify previous reviews, placing particular emphasis on re-segmenting from the perspective of safety perception. We aim for this work to offer new insights for future research in 3D object detection, transcending the confines of high-accuracy exploration.

## REFERENCES

[1] E. Arnold, O. Y. Al-Jarrah, M. Dianati, S. Fallah, D. Oxtoby, and A. Mouzakitis, “A survey on 3d object detection methods for autonomous driving applications,” *IEEE Transactions on Intelligent Transportation Systems*, vol. 20, no. 10, pp. 3782–3795, 2019.

[2] J. Liu, H. Wang, L. Peng, Z. Cao, D. Yang, and J. Li, “Pnnud: Perception neural networks uncertainty aware decision-making for autonomous vehicle,” *IEEE Transactions on Intelligent Transportation Systems*, vol. 23, no. 12, pp. 24355–24368, 2022.

[3] K. Yang, B. Li, W. Shao, X. Tang, X. Liu, and H. Wang, “Prediction failure risk-aware decision-making for autonomous vehicles on signalized intersections,” *IEEE Transactions on Intelligent Transportation Systems*, 2023.

[4] L. Wang, X. Zhang, Z. Song, J. Bi, G. Zhang, H. Wei, L. Tang, L. Yang, J. Li, C. Jia *et al.*, “Multi-modal 3d object detection in autonomous driving: A survey and taxonomy,” *IEEE Transactions on Intelligent Vehicles*, 2023.

[5] Y. Cao, H. Zhang, Y. Li, C. Ren, and C. Lang, “Cman: Leaning global structure correlation for monocular 3d object detection,” *IEEE Transactions on Intelligent Transportation Systems*, vol. 23, no. 12, pp. 24727–24737, 2022.

[6] Y. Wang, W.-L. Chao, D. Garg, B. Hariharan, M. Campbell, and K. Q. Weinberger, “Pseudo-lidar from visual depth estimation: Bridging the gap in 3d object detection for autonomous driving,” in *Proceedings of the IEEE/CVF Conference on Computer Vision and Pattern Recognition*, 2019, pp. 8445–8453.

[7] P. Li, H. Zhao, P. Liu, and F. Cao, “Rtm3d: Real-time monocular 3d detection from object keypoints for autonomous driving,” in *European Conference on Computer Vision*. Springer, 2020, pp. 644–660.

[8] Y. Zhang, J. Lu, and J. Zhou, “Objects are different: Flexible monocular 3d object detection,” in *Proceedings of the IEEE/CVF Conference on Computer Vision and Pattern Recognition*, 2021, pp. 3289–3298.

[9] A. Simonelli, S. R. Buló, L. Porzi, M. López-Antequera, and P. Kotschieder, “Disentangling monocular 3d object detection,” in *Proceedings of the IEEE/CVF International Conference on Computer Vision*, 2019, pp. 1991–1999.

[10] Q. Lian, P. Li, and X. Chen, “Monojsg: Joint semantic and geometric cost volume for monocular 3d object detection,” in *Proceedings of the IEEE/CVF Conference on Computer Vision and Pattern Recognition*, 2022, pp. 1070–1079.

[11] G. Brazil and X. Liu, “M3d-rpn: Monocular 3d region proposal network for object detection,” in *Proceedings of the IEEE/CVF International Conference on Computer Vision*, 2019, pp. 9287–9296.

[12] Y. Cai, B. Li, Z. Jiao, H. Li, X. Zeng, and X. Wang, “Monocular 3d object detection with decoupled structured polygon estimation and height-guided depth estimation,” in *Proceedings of the AAAI Conference on Artificial Intelligence*, vol. 34, no. 07, 2020, pp. 10478–10485.

[13] Y. Chen, L. Tai, K. Sun, and M. Li, “Monopair: Monocular 3d object detection using pairwise spatial relationships,” in *Proceedings of the IEEE/CVF Conference on Computer Vision and Pattern Recognition*, 2020, pp. 12093–12102.

[14] Y. Liu, L. Wang, and M. Liu, “Yolostereo3d: A step back to 2d for efficient stereo 3d detection,” in *2021 IEEE International Conference on Robotics and Automation (ICRA)*. IEEE, 2021, pp. 13018–13024.

[15] Y. Li, Z. Ge, G. Yu, J. Yang, Z. Wang, Y. Shi, J. Sun, and Z. Li, “Bevdepth: Acquisition of reliable depth for multi-view 3d object detection,” in *Proceedings of the AAAI Conference on Artificial Intelligence*, vol. 37, no. 2, 2023, pp. 1477–1485.

[16] Z. Li, W. Wang, H. Li, E. Xie, C. Sima, T. Lu, Y. Qiao, and J. Dai, “Bevformer: Learning bird’s-eye-view representation from multi-camera images via spatiotemporal transformers,” in *European conference on computer vision*. Springer, 2022, pp. 1–18.

[17] Y. Chen, S. Liu, X. Shen, and J. Jia, “Dsgn: Deep stereo geometry network for 3d object detection,” in *Proceedings of the IEEE/CVF conference on computer vision and pattern recognition*, 2020, pp. 12536–12545.

[18] L. Liu, J. Lu, C. Xu, Q. Tian, and J. Zhou, “Deep fitting degree scoring network for monocular 3d object detection,” in *Proceedings of the IEEE/CVF conference on computer vision and pattern recognition*, 2019, pp. 1057–1066.

[19] X. Shi, Z. Chen, and T.-K. Kim, “Distance-normalized unified representation for monocular 3d object detection,” in *Computer Vision—ECCV 2020: 16th European Conference, Glasgow, UK, August 23–28, 2020, Proceedings, Part XXIX 16*. Springer, 2020, pp. 91–107.

[20] X. Ma, Z. Wang, H. Li, P. Zhang, W. Ouyang, and X. Fan, “Accurate monocular 3d object detection via color-embedded 3d reconstruction for autonomous driving,” in *Proceedings of the IEEE/CVF International Conference on Computer Vision*, 2019, pp. 6851–6860.

[21] J. Ku, A. D. Pon, and S. L. Waslander, “Monocular 3d object detection leveraging accurate proposals and shape reconstruction,” in *Proceed-*

- ings of the *IEEE/CVF conference on computer vision and pattern recognition*, 2019, pp. 11 867–11 876.
- [22] C. Reading, A. Harakeh, J. Chae, and S. L. Waslander, “Categorical depth distribution network for monocular 3d object detection,” in *Proceedings of the IEEE/CVF Conference on Computer Vision and Pattern Recognition*, 2021, pp. 8555–8564.
- [23] K.-C. Huang, T.-H. Wu, H.-T. Su, and W. H. Hsu, “Monodtr: Monocular 3d object detection with depth-aware transformer,” in *Proceedings of the IEEE/CVF Conference on Computer Vision and Pattern Recognition*, 2022, pp. 4012–4021.
- [24] T. Wang, X. Zhu, J. Pang, and D. Lin, “Fcos3d: Fully convolutional one-stage monocular 3d object detection,” in *Proceedings of the IEEE/CVF International Conference on Computer Vision*, 2021, pp. 913–922.
- [25] T. Wang, Z. Xinge, J. Pang, and D. Lin, “Probabilistic and geometric depth: Detecting objects in perspective,” in *Conference on Robot Learning*. PMLR, 2022, pp. 1475–1485.
- [26] Y. Lu, X. Ma, L. Yang, T. Zhang, Y. Liu, Q. Chu, J. Yan, and W. Ouyang, “Geometry uncertainty projection network for monocular 3d object detection,” in *Proceedings of the IEEE/CVF International Conference on Computer Vision*, 2021, pp. 3111–3121.
- [27] D. Park, R. Ambrus, V. Guizilini, J. Li, and A. Gaidon, “Is pseudo-lidar needed for monocular 3d object detection?” in *Proceedings of the IEEE/CVF International Conference on Computer Vision*, 2021, pp. 3142–3152.
- [28] L. Yang, X. Zhang, J. Li, L. Wang, M. Zhu, C. Zhang, and H. Liu, “Mix-teaching: A simple, unified and effective semi-supervised learning framework for monocular 3d object detection,” *IEEE Transactions on Circuits and Systems for Video Technology*, 2023.
- [29] R. Zhang, H. Qiu, T. Wang, Z. Guo, X. Xu, Y. Qiao, P. Gao, and H. Li, “Monodetr: depth-guided transformer for monocular 3d object detection,” *arXiv preprint arXiv:2203.13310*, 2022.
- [30] Y. Wang, V. C. Guizilini, T. Zhang, Y. Wang, H. Zhao, and J. Solomon, “Detr3d: 3d object detection from multi-view images via 3d-to-2d queries,” in *Conference on Robot Learning*. PMLR, 2022, pp. 180–191.
- [31] Y. Liu, T. Wang, X. Zhang, and J. Sun, “Petr: Position embedding transformation for multi-view 3d object detection,” in *European Conference on Computer Vision*. Springer, 2022, pp. 531–548.
- [32] Y. Liu, J. Yan, F. Jia, S. Li, A. Gao, T. Wang, and X. Zhang, “Petrv2: A unified framework for 3d perception from multi-camera images,” in *Proceedings of the IEEE/CVF International Conference on Computer Vision*, 2023, pp. 3262–3272.
- [33] J. Huang and G. Huang, “Bevdet4d: Exploit temporal cues in multi-camera 3d object detection,” *arXiv preprint arXiv:2203.17054*, 2022.
- [34] H. Liu, Y. Teng, T. Lu, H. Wang, and L. Wang, “Sparsebev: High-performance sparse 3d object detection from multi-camera videos,” in *Proceedings of the IEEE/CVF International Conference on Computer Vision*, 2023, pp. 18 580–18 590.
- [35] L. Yang, T. Tang, J. Li, P. Chen, K. Yuan, L. Wang, Y. Huang, X. Zhang, and K. Yu, “Bevheight++: Toward robust visual centric 3d object detection,” *arXiv preprint arXiv:2309.16179*, 2023.
- [36] Z. Song, H. Wei, C. Jia, Y. Xia, X. Li, and C. Zhang, “Vp-net: Voxels as points for 3d object detection,” *IEEE Transactions on Geoscience and Remote Sensing*, 2023.
- [37] G. Wang, B. Tian, Y. Ai, T. Xu, L. Chen, and D. Cao, “Centernet3d: An anchor free object detector for autonomous driving,” *Cornell University - arXiv, Cornell University - arXiv*, Jul 2020.
- [38] Y. Hu, Z. Ding, R. Ge, W. Shao, L. Huang, K. Li, and Q. Liu, “Afdetv2: Rethinking the necessity of the second stage for object detection from point clouds,” *Proceedings of the AAAI Conference on Artificial Intelligence*, p. 969–979, Jul 2022.
- [39] R. Ge, Z. Ding, Y. Hu, Y. Wang, S. Chen, L. Huang, and Y. Li, “Afdet: Anchor free one stage 3d object detection,” *arXiv preprint arXiv:2006.12671*, 2020.
- [40] Z. Yang, Y. Sun, S. Liu, and J. Jia, “3dssd: Point-based 3d single stage object detector,” in *Proceedings of the IEEE/CVF conference on computer vision and pattern recognition*, 2020, pp. 11 040–11 048.
- [41] J. H. Yoo, Y. Kim, J. Kim, and J. W. Choi, “3d-cvf: Generating joint camera and lidar features using cross-view spatial feature fusion for 3d object detection,” in *Computer Vision—ECCV 2020: 16th European Conference, Glasgow, UK, August 23–28, 2020, Proceedings, Part XXVII 16*. Springer, 2020, pp. 720–736.
- [42] Y. Zhou and O. Tuzel, “Voxelnet: End-to-end learning for point cloud based 3d object detection,” in *Proceedings of the IEEE conference on computer vision and pattern recognition*, 2018, pp. 4490–4499.
- [43] Y. Yan, Y. Mao, and B. Li, “Second: Sparsely embedded convolutional detection,” *Sensors*, vol. 18, no. 10, p. 3337, 2018.
- [44] W. Shi and R. Rajkumar, “Point-gnn: Graph neural network for 3d object detection in a point cloud,” in *Proceedings of the IEEE/CVF conference on computer vision and pattern recognition*, 2020, pp. 1711–1719.
- [45] S. Shi, X. Wang, and H. Li, “Pointcnn: 3d object proposal generation and detection from point cloud,” in *Proceedings of the IEEE/CVF conference on computer vision and pattern recognition*, 2019, pp. 770–779.
- [46] Y. Chen, J. Liu, X. Zhang, X. Qi, and J. Jia, “Voxelnext: Fully sparse voxelnet for 3d object detection and tracking.”
- [47] J. Deng, S. Shi, P. Li, W. Zhou, Y. Zhang, and H. Li, “Voxel r-cnn: Towards high performance voxel-based 3d object detection,” in *Proceedings of the AAAI Conference on Artificial Intelligence*, vol. 35, no. 2, 2021, pp. 1201–1209.
- [48] H. Kuang, B. Wang, J. An, M. Zhang, and Z. Zhang, “Voxel-fpn: Multi-scale voxel feature aggregation for 3d object detection from lidar point clouds,” *Sensors*, vol. 20, no. 3, p. 704, 2020.
- [49] Z. Liu, H. Tang, Y. Lin, and S. Han, “Point-voxel cnn for efficient 3d deep learning,” *Advances in Neural Information Processing Systems*, vol. 32, 2019.
- [50] S. Shi, L. Jiang, J. Deng, Z. Wang, C. Guo, J. Shi, X. Wang, and H. Li, “Pv-rnn++: Point-voxel feature set abstraction with local vector representation for 3d object detection,” *International Journal of Computer Vision*, vol. 131, no. 2, pp. 531–551, 2023.
- [51] A. H. Lang, S. Vora, H. Caesar, L. Zhou, J. Yang, and O. Beijbom, “Pointpillars: Fast encoders for object detection from point clouds,” in *Proceedings of the IEEE/CVF conference on computer vision and pattern recognition*, 2019, pp. 12 697–12 705.
- [52] J. Li, C. Luo, X. Yang, and Q. Qcraft, “Pillarnext: Rethinking network designs for 3d object detection in lidar point clouds.”
- [53] J. S. Hu, T. Kuai, and S. L. Waslander, “Point density-aware voxels for lidar 3d object detection,” in *Proceedings of the IEEE/CVF Conference on Computer Vision and Pattern Recognition*, 2022, pp. 8469–8478.
- [54] H. Wu, C. Wen, W. Li, X. Li, R. Yang, and C. Wang, “Transformation-equivariant 3d object detection for autonomous driving,” Nov 2022.
- [55] L. Fan, Z. Pang, T. Zhang, Y.-X. Wang, H. Zhao, F. Wang, N. Wang, and Z. Zhang, “Embracing single stride 3d object detector with sparse transformer,” in *2022 IEEE/CVF Conference on Computer Vision and Pattern Recognition (CVPR)*, Jun 2022.
- [56] L. Fan, F. Wang, N. Wang, and Z.-X. ZHANG, “Fully sparse 3d object detection,” *Advances in Neural Information Processing Systems*, vol. 35, pp. 351–363, 2022.
- [57] T. Yin, X. Zhou, and P. Krahenbuhl, “Center-based 3d object detection and tracking,” in *2021 IEEE/CVF Conference on Computer Vision and Pattern Recognition (CVPR)*, Jun 2021.
- [58] J. Mao, Y. Xue, M. Niu, H. Bai, J. Feng, X. Liang, H. Xu, and C. Xu, “Voxel transformer for 3d object detection,” in *Proceedings of the IEEE/CVF International Conference on Computer Vision*, 2021, pp. 3164–3173.
- [59] C. He, R. Li, S. Li, and L. Zhang, “Voxel set transformer: A set-to-set approach to 3d object detection from point clouds.”
- [60] Y. Chen, J. Liu, X. Zhang, X. Qi, and J. Jia, “Largekernel3d: Scaling up kernels in 3d sparse cnns,” in *Proceedings of the IEEE/CVF Conference on Computer Vision and Pattern Recognition*, 2023, pp. 13 488–13 498.
- [61] T. Lu, X. Ding, H. Liu, G. Wu, and L. Wang, “Link: Linear kernel for lidar-based 3d perception,” in *Proceedings of the IEEE/CVF Conference on Computer Vision and Pattern Recognition*, 2023, pp. 1105–1115.
- [62] X. Lai, Y. Chen, F. Lu, J. Liu, and J. Jia, “Spherical transformer for lidar-based 3d recognition,” in *Proceedings of the IEEE/CVF Conference on Computer Vision and Pattern Recognition*, 2023, pp. 17 545–17 555.
- [63] Q. He, Z. Wang, H. Zeng, Y. Zeng, and Y. Liu, “Svga-net: Sparse voxel-graph attention network for 3d object detection from point clouds,” *Proceedings of the AAAI Conference on Artificial Intelligence*, p. 870–878, Jul 2022.
- [64] P. Sun, M. Tan, W. Wang, C. Liu, F. Xia, Z. Leng, and D. Anguelov, “Swformer: Sparse window transformer for 3d object detection in point clouds,” Oct 2022.
- [65] Y. Li, Y. Chen, X. Qi, Z. Li, J. Sun, and J. Jia, “Unifying voxel-based representation with transformer for 3d object detection,” *Advances in Neural Information Processing Systems*, vol. 35, pp. 18 442–18 455, 2022.

- [66] X. Pan, Z. Xia, S. Song, L. E. Li, and G. Huang, "3d object detection with pointformer," in *Proceedings of the IEEE/CVF Conference on Computer Vision and Pattern Recognition*, 2021, pp. 7463–7472.
- [67] H. Sheng, S. Cai, Y. Liu, B. Deng, J. Huang, X.-S. Hua, and M.-J. Zhao, "Improving 3d object detection with channel-wise transformer," in *Proceedings of the IEEE/CVF International Conference on Computer Vision*, 2021, pp. 2743–2752.
- [68] Q. Xu, Y. Zhong, and U. Neumann, "Behind the curtain: Learning occluded shapes for 3d object detection," in *Proceedings of the AAAI Conference on Artificial Intelligence*, vol. 36, no. 3, 2022, pp. 2893–2901.
- [69] W. Zheng, W. Tang, L. Jiang, and C.-W. Fu, "Se-ssd: Self-ensembling single-stage object detector from point cloud," in *Proceedings of the IEEE/CVF Conference on Computer Vision and Pattern Recognition*, 2021, pp. 14 494–14 503.
- [70] Z. Yang, Y. Sun, S. Liu, X. Shen, and J. Jia, "Ipod: Intensive point-based object detector for point cloud," *arXiv preprint arXiv:1812.05276*, 2018.
- [71] L. Du, X. Ye, X. Tan, J. Feng, Z. Xu, E. Ding, and S. Wen, "Associate-3ddet: Perceptual-to-conceptual association for 3d point cloud object detection," in *Proceedings of the IEEE/CVF conference on computer vision and pattern recognition*, 2020, pp. 13 329–13 338.
- [72] J. Li, H. Dai, L. Shao, and Y. Ding, "From voxel to point: Iou-guided 3d object detection for point cloud with voxel-to-point decoder," in *Proceedings of the 29th ACM International Conference on Multimedia*, 2021, pp. 4622–4631.
- [73] Z. Li, Y. Yao, Z. Quan, W. Yang, and J. Xie, "Sienet: spatial information enhancement network for 3d object detection from point cloud," *arXiv preprint arXiv:2103.15396*, 2021.
- [74] D. Zhang, D. Liang, Z. Zou, J. Li, X. Ye, Z. Liu, X. Tan, and X. Bai, "A simple vision transformer for weakly semi-supervised 3d object detection," in *Proceedings of the IEEE/CVF International Conference on Computer Vision*, 2023, pp. 8373–8383.
- [75] B. Zhu, Z. Jiang, X. Zhou, Z. Li, and G. Yu, "Class-balanced grouping and sampling for point cloud 3d object detection," *arXiv preprint arXiv:1908.09492*, 2019.
- [76] M. Ye, S. Xu, and T. Cao, "Hvnet: Hybrid voxel network for lidar based 3d object detection," in *Proceedings of the IEEE/CVF conference on computer vision and pattern recognition*, 2020, pp. 1631–1640.
- [77] W. Zheng, W. Tang, S. Chen, L. Jiang, and C.-W. Fu, "Cia-ssd: Confident iou-aware single-stage object detector from point cloud," in *Proceedings of the AAAI conference on artificial intelligence*, vol. 35, no. 4, 2021, pp. 3555–3562.
- [78] Q. Chen, L. Sun, E. Cheung, and A. Yuille, "Every view counts: Cross-view consistency in 3d object detection with hybrid-cylindrical-spherical voxelization," *Neural Information Processing Systems, Neural Information Processing Systems*, Jan 2020.
- [79] T. Wang, X. Zhu, and D. Lin, "Reconfigurable voxels: A new representation for lidar-based point clouds," *arXiv: Computer Vision and Pattern Recognition, arXiv: Computer Vision and Pattern Recognition*, Apr 2020.
- [80] Y. Wang and J. Solomon, "Object dgcn: 3d object detection using dynamic graphs."
- [81] X. Zhu, Y. Ma, T. Wang, Y. Xu, J. Shi, and D. Lin, *SSN: Shape Signature Networks for Multi-class Object Detection from Point Clouds*, Jan 2020, p. 581–597.
- [82] Z. Miao, J. Chen, H. Pan, R. Zhang, K. Liu, P. Hao, J. Zhu, Y. Wang, and X. Zhan, "Pvgnnet: A bottom-up one-stage 3d object detector with integrated multi-level features," in *2021 IEEE/CVF Conference on Computer Vision and Pattern Recognition (CVPR)*, Jun 2021.
- [83] J. Noh, S. Lee, and B. Ham, "Hvpr: Hybrid voxel-point representation for single-stage 3d object detection," in *2021 IEEE/CVF Conference on Computer Vision and Pattern Recognition (CVPR)*, Jun 2021.
- [84] T. Guan, J. Wang, S. Lan, R. Chandra, Z. Wu, L. Davis, and D. Manocha, "M3detr: Multi-representation, multi-scale, mutual-relation 3d object detection with transformers," in *Proceedings of the IEEE/CVF winter conference on applications of computer vision*, 2022, pp. 772–782.
- [85] J. Wang, S. Lan, M. Gao, and L. S. Davis, "Infofocus: 3d object detection for autonomous driving with dynamic information modeling," in *Computer Vision—ECCV 2020: 16th European Conference, Glasgow, UK, August 23–28, 2020, Proceedings, Part X 16*. Springer, 2020, pp. 405–420.
- [86] J. Mao, M. Niu, H. Bai, X. Liang, H. Xu, and C. Xu, "Pyramid r-cnn: Towards better performance and adaptability for 3d object detection," in *Proceedings of the IEEE/CVF International Conference on Computer Vision*, 2021, pp. 2723–2732.
- [87] Z. Liang, M. Zhang, Z. Zhang, X. Zhao, and S. Pu, "Rangercnn: Towards fast and accurate 3d object detection with range image representation."
- [88] A. Bewley, P. Sun, T. Mensink, D. Anguelov, and C. Sminchisescu, "Range conditioned dilated convolutions for scale invariant 3d object detection," *Conference on Robot Learning, Conference on Robot Learning*, May 2020.
- [89] Z. Liang, Z. Zhang, M. Zhang, X. Zhao, and S. Pu, "Rangeioudet: Range image based real-time 3d object detector optimized by intersection over union," in *2021 IEEE/CVF Conference on Computer Vision and Pattern Recognition (CVPR)*, Jun 2021.
- [90] L. Fan, X. Xiong, F. Wang, N. Wang, and Z. Zhang, "Rangedet:in defense of range view for lidar-based 3d object detection," in *2021 IEEE/CVF International Conference on Computer Vision (ICCV)*, Oct 2021.
- [91] X. Feng, H. Du, H. Fan, Y. Duan, and Y. Liu, "Seformer: Structure embedding transformer for 3d object detection," in *Proceedings of the AAAI Conference on Artificial Intelligence*, vol. 37, no. 1, 2023, pp. 632–640.
- [92] H. Wu, J. Deng, C. Wen, X. Li, C. Wang, and J. Li, "Casa: A cascade attention network for 3-d object detection from lidar point clouds," *IEEE Transactions on Geoscience and Remote Sensing*, vol. 60, pp. 1–11, 2022.
- [93] G. Shi, R. Li, and C. Ma, "Pillarnet: Real-time and high-performance pillar-based 3d object detection," in *European Conference on Computer Vision*. Springer, 2022, pp. 35–52.
- [94] C. Chen, Z. Chen, J. Zhang, and D. Tao, "Sasa: Semantics-augmented set abstraction for point-based 3d object detection," in *Proceedings of the AAAI Conference on Artificial Intelligence*, vol. 36, no. 1, 2022, pp. 221–229.
- [95] H. Wang, S. Shi, Z. Yang, R. Fang, Q. Qian, H. Li, B. Schiele, and L. Wang, "Rbgnet: Ray-based grouping for 3d object detection," in *Proceedings of the IEEE/CVF Conference on Computer Vision and Pattern Recognition*, 2022, pp. 1110–1119.
- [96] Z. Wang and K. Jia, "Frustum convnet: Sliding frustums to aggregate local point-wise features for amodal 3d object detection," in *2019 IEEE/RSJ International Conference on Intelligent Robots and Systems (IROS)*. IEEE, 2019, pp. 1742–1749.
- [97] H. Tang, Z. Liu, S. Zhao, Y. Lin, J. Lin, H. Wang, and S. Han, "Searching efficient 3d architectures with sparse point-voxel convolution," in *European conference on computer vision*. Springer, 2020, pp. 685–702.
- [98] Z. Yang, Y. Sun, S. Liu, X. Shen, and J. Jia, "Std: Sparse-to-dense 3d object detector for point cloud," in *Proceedings of the IEEE/CVF international conference on computer vision*, 2019, pp. 1951–1960.
- [99] H. Wu, C. Wen, S. Shi, X. Li, and C. Wang, "Virtual sparse convolution for multimodal 3d object detection," Mar 2023.
- [100] S. Vora, A. H. Lang, B. Helou, and O. Beijbom, "Pointpainting: Sequential fusion for 3d object detection," in *Proceedings of the IEEE/CVF conference on computer vision and pattern recognition*, 2020, pp. 4604–4612.
- [101] Y. Xie, C. Xu, M.-J. Rakotosaona, P. Rim, F. Tombari, K. Keutzer, M. Tomizuka, and W. Zhan, "Sparsefusion: Fusing multi-modal sparse representations for multi-sensor 3d object detection," *arXiv preprint arXiv:2304.14340*, 2023.
- [102] Z. Yu, W. Wan, M. Ren, X. Zheng, and Z. Fang, "Sparsefusion3d: Sparse sensor fusion for 3d object detection by radar and camera in environmental perception," *IEEE Transactions on Intelligent Vehicles*, pp. 1–14, 2023.
- [103] J. Yan, Y. Liu, J. Sun, F. Jia, S. Li, T. Wang, and X. Zhang, "Cross modal transformer via coordinates encoding for 3d object detection," *arXiv preprint arXiv:2301.01283*, 2023.
- [104] T. Huang, Z. Liu, X. Chen, and X. Bai, "Epnet: Enhancing point features with image semantics for 3d object detection," in *European Conference on Computer Vision*. Springer, 2020, pp. 35–52.
- [105] Z. Liu, T. Huang, B. Li, X. Chen, X. Wang, and X. Bai, "Epnet++: Cascade bi-directional fusion for multi-modal 3d object detection," *IEEE Transactions on Pattern Analysis and Machine Intelligence*, vol. 45, no. 7, pp. 8324–8341, 2023.
- [106] X. Chen, T. Zhang, Y. Wang, Y. Wang, and H. Zhao, "Futr3d: A unified sensor fusion framework for 3d detection."
- [107] Y. Zhou, P. Sun, Y. Zhang, D. Anguelov, J. Gao, T. Ouyang, J. Guo, J. Ngiam, and V. Vasudevan, "End-to-end multi-view fusion for 3d object detection in lidar point clouds," *Conference on Robot Learning, Conference on Robot Learning*, Jan 2019.

- [108] X. Bai, Z. Hu, X. Zhu, Q. Huang, Y. Chen, H. Fu, and C.-L. Tai, "Transfusion: Robust lidar-camera fusion for 3d object detection with transformers."
- [109] T. Liang, H. Xie, K. Yu, Z. Xia, Z. Lin, Y. Wang, T. Tang, B. Wang, and Z. Tang, "Bevfusion: A simple and robust lidar-camera fusion framework," *Advances in Neural Information Processing Systems*, vol. 35, pp. 10421–10434, 2022.
- [110] Y. Chen, Y. Li, X. Zhang, J. Sun, and J. Jia, "Focal sparse convolutional networks for 3d object detection," in *Proceedings of the IEEE/CVF Conference on Computer Vision and Pattern Recognition*, 2022, pp. 5428–5437.
- [111] Z. Song, H. Wei, L. Bai, L. Yang, and C. Jia, "Graphalign: Enhancing accurate feature alignment by graph matching for multi-modal 3d object detection," in *Proceedings of the IEEE/CVF International Conference on Computer Vision*, 2023, pp. 3358–3369.
- [112] Z. Song, C. Jia, L. Yang, H. Wei, and L. Liu, "Graphalign++: An accurate feature alignment by graph matching for multi-modal 3d object detection," *IEEE Transactions on Circuits and Systems for Video Technology*, 2023.
- [113] H. Yang, Z. Liu, X. Wu, W. Wang, W. Qian, X. He, and D. Cai, "Graph r-cnn: Towards accurate 3d object detection with semantic-decorated local graph."
- [114] X. Wu, L. Peng, H. Yang, L. Xie, C. Huang, C. Deng, H. Liu, and D. Cai, "Sparse fuse dense: Towards high quality 3d detection with depth completion," in *Proceedings of the IEEE/CVF Conference on Computer Vision and Pattern Recognition*, 2022, pp. 5418–5427.
- [115] Y. Li, A. Yu, T. Meng, B. Caine, J. Ngiam, D. Peng, J. Shen, B. Wu, Y. Lu, D. Zhou, Q. Le, A. Yuille, and M. Tan, "Deepfusion: Lidar-camera deep fusion for multi-modal 3d object detection."
- [116] Z. Yang, J. Chen, Z. Miao, W. Li, X. Zhu, and L. Zhang, "Deepinteraction: 3d object detection via modality interaction," Aug 2022.
- [117] Q. Cai, Y. Pan, T. Yao, C.-W. Ngo, and T. Mei, "Objectfusion: Multimodal 3d object detection with object-centric fusion," in *Proceedings of the IEEE/CVF International Conference on Computer Vision (ICCV)*, October 2023, pp. 18 067–18 076.
- [118] Y. Qin, C. Wang, Z. Kang, N. Ma, Z. Li, and R. Zhang, "Supfusion: Supervised lidar-camera fusion for 3d object detection," in *Proceedings of the IEEE/CVF International Conference on Computer Vision (ICCV)*, October 2023, pp. 22 014–22 024.
- [119] R. Qian, X. Lai, and X. Li, "3d object detection for autonomous driving: A survey," *Pattern Recognition*, vol. 130, p. 108796, 2022.
- [120] X. Li, B. Shi, Y. Hou, X. Wu, T. Ma, Y. Li, and L. He, "Homogeneous multi-modal feature fusion and interaction for 3d object detection," in *European Conference on Computer Vision*. Springer, 2022, pp. 691–707.
- [121] X. Li, T. Ma, Y. Hou, B. Shi, Y. Yang, Y. Liu, X. Wu, Q. Chen, Y. Li, Y. Qiao, and L. He, "Logonet: Towards accurate 3d object detection with local-to-global cross-modal fusion," Mar 2023.
- [122] Z. Song, G. Zhang, J. Xie, L. Liu, C. Jia, S. Xu, and Z. Wang, "Voxelnetfusion: A simple, unified, and effective voxel fusion framework for multimodal 3-d object detection," *IEEE Transactions on Geoscience and Remote Sensing*, vol. 61, pp. 1–12, 2023.
- [123] Y. Wang, Q. Mao, H. Zhu, J. Deng, Y. Zhang, J. Ji, H. Li, and Y. Zhang, "Multi-modal 3d object detection in autonomous driving: a survey," *International Journal of Computer Vision*, pp. 1–31, 2023.
- [124] S. Xie, L. Kong, W. Zhang, J. Ren, L. Pan, K. Chen, and Z. Liu, "Robobev: Towards robust bird's eye view perception under corruptions," Apr 2023.
- [125] Y. Dong, C. Kang, J. Zhang, Z. Zhu, Y. Wang, X. Yang, H. Su, X. Wei, and J. Zhu, "Benchmarking robustness of 3d object detection to common corruptions in autonomous driving," Mar 2023.
- [126] J. Mao, S. Shi, X. Wang, and H. Li, "3d object detection for autonomous driving: A comprehensive survey," *International Journal of Computer Vision*, pp. 1–55, 2023.
- [127] S. Y. Alaba and J. E. Ball, "Deep learning-based image 3-d object detection for autonomous driving," *IEEE Sensors Journal*, vol. 23, no. 4, pp. 3378–3394, 2023.
- [128] A. Singh and V. Bankiti, "Surround-view vision-based 3d detection for autonomous driving: A survey," *arXiv preprint arXiv:2302.06650*, 2023.
- [129] A. Singh, "Transformer-based sensor fusion for autonomous driving: A survey," *arXiv preprint arXiv:2302.11481*, 2023.
- [130] X. Wang, K. Li, and A. Chehri, "Multi-sensor fusion technology for 3d object detection in autonomous driving: A review," *IEEE Transactions on Intelligent Transportation Systems*, 2023.
- [131] Y. Peng, Y. Qin, X. Tang, Z. Zhang, and L. Deng, "Survey on image and point-cloud fusion-based object detection in autonomous vehicles," *IEEE Transactions on Intelligent Transportation Systems*, vol. 23, no. 12, pp. 22 772–22 789, 2022.
- [132] Y. Wu, Y. Wang, S. Zhang, and H. Ogai, "Deep 3d object detection networks using lidar data: A review," *IEEE Sensors Journal*, vol. 21, no. 2, pp. 1152–1171, 2020.
- [133] A. Geiger, P. Lenz, and R. Urtasun, "Are we ready for autonomous driving? the kitti vision benchmark suite," in *2012 IEEE conference on computer vision and pattern recognition*. IEEE, 2012, pp. 3354–3361.
- [134] H. Caesar, V. Bankiti, A. H. Lang, S. Vora, V. E. Liong, Q. Xu, A. Krishnan, Y. Pan, G. Baldan, and O. Beijbom, "nusenes: A multimodal dataset for autonomous driving," in *Proceedings of the IEEE/CVF conference on computer vision and pattern recognition*, 2020, pp. 11 621–11 631.
- [135] P. Sun, H. Kretschmar, X. Dotiwalla, A. Chouard, V. Patnaik, P. Tsui, J. Guo, Y. Zhou, Y. Chai, B. Caine *et al.*, "Scalability in perception for autonomous driving: Waymo open dataset," in *Proceedings of the IEEE/CVF conference on computer vision and pattern recognition*, 2020, pp. 2446–2454.
- [136] C. Sakaridis, D. Dai, and L. Van Gool, "Semantic foggy scene understanding with synthetic data," *International Journal of Computer Vision*, vol. 126, pp. 973–992, 2018.
- [137] B. Cai, X. Xu, K. Jia, C. Qing, and D. Tao, "Dehazenet: An end-to-end system for single image haze removal," *IEEE transactions on image processing*, vol. 25, no. 11, pp. 5187–5198, 2016.
- [138] T. Ort, I. Gilitschenski, and D. Rus, "Grounded: The localizing ground penetrating radar evaluation dataset," in *Robotics: Science and Systems*, vol. 2, 2021.
- [139] M. Pitropov, D. E. Garcia, J. Rebello, M. Smart, C. Wang, K. Czarnecki, and S. Waslander, "Canadian adverse driving conditions dataset," *The International Journal of Robotics Research*, vol. 40, no. 4-5, pp. 681–690, 2021.
- [140] X. Huang, P. Wang, X. Cheng, D. Zhou, Q. Geng, and R. Yang, "The apolloscape open dataset for autonomous driving and its application," *IEEE transactions on pattern analysis and machine intelligence*, vol. 42, no. 10, pp. 2702–2719, 2019.
- [141] C. A. Diaz-Ruiz, Y. Xia, Y. You, J. Nino, J. Chen, J. Monica, X. Chen, K. Luo, Y. Wang, M. Emond *et al.*, "Ithaca365: Dataset and driving perception under repeated and challenging weather conditions," in *Proceedings of the IEEE/CVF Conference on Computer Vision and Pattern Recognition*, 2022, pp. 21 383–21 392.
- [142] D. Hendrycks and T. Dietterich, "Benchmarking neural network robustness to common corruptions and perturbations," *arXiv preprint arXiv:1903.12261*, 2019.
- [143] S. Xie, Z. Li, Z. Wang, and C. Xie, "On the adversarial robustness of camera-based 3d object detection," *arXiv preprint arXiv:2301.10766*, 2023.
- [144] J. Sun, Y. Cao, Q. A. Chen, and Z. M. Mao, "Towards robust {LiDAR-based} perception in autonomous driving: General black-box adversarial sensor attack and countermeasures," in *29th USENIX Security Symposium (USENIX Security 20)*, 2020, pp. 877–894.
- [145] D. Liu, R. Yu, and H. Su, "Extending adversarial attacks and defenses to deep 3d point cloud classifiers," in *2019 IEEE International Conference on Image Processing (ICIP)*. IEEE, 2019, pp. 2279–2283.
- [146] S. Li, Z. Wang, F. Juefei-Xu, Q. Guo, X. Li, and L. Ma, "Common corruption robustness of point cloud detectors: Benchmark and enhancement," *IEEE Transactions on Multimedia*, 2023.
- [147] K. Yu, T. Tao, H. Xie, Z. Lin, Z. Wu, Z. Xia, T. Liang, H. Sun, J. Deng, D. Hao, Y. Wang, X. Liang, and B. Wang, "Benchmarking the robustness of lidar-camera fusion for 3d object detection."
- [148] L. Kong, Y. Liu, X. Li, R. Chen, W. Zhang, J. Ren, L. Pan, K. Chen, and Z. Liu, "Robo3d: Towards robust and reliable 3d perception against corruptions," in *Proceedings of the IEEE/CVF International Conference on Computer Vision*, 2023, pp. 19 994–20 006.
- [149] L. Kong, S. Xie, H. Hu, L. X. Ng, B. R. Cottreau, and W. T. Ooi, "Robodepth: Robust out-of-distribution depth estimation under corruptions," *arXiv preprint arXiv:2310.15171*, 2023.
- [150] R. Kesten, M. Usman, J. Houston, T. Pandya, K. Nadhamuni, A. Ferreira, M. Yuan, B. Low, A. Jain, P. Ondruska *et al.*, "Lyft level 5 av dataset 2019," [urlhttps://level5.lyft.com/dataset](https://level5.lyft.com/dataset), vol. 1, p. 3, 2019.
- [151] A. Patil, S. Malla, H. Gang, and Y.-T. Chen, "The h3d dataset for full-surround 3d multi-object detection and tracking in crowded urban scenes," in *2019 International Conference on Robotics and Automation (ICRA)*. IEEE, 2019, pp. 9552–9557.



- [152] X. Huang, P. Wang, X. Cheng, D. Zhou, Q. Geng, and R. Yang, "The apollo scape open dataset for autonomous driving and its application," *IEEE transactions on pattern analysis and machine intelligence*, vol. 42, no. 10, pp. 2702–2719, 2019.
- [153] M.-F. Chang, J. Lambert, P. Sangkloy, J. Singh, S. Bak, A. Hartnett, D. Wang, P. Carr, S. Lucey, D. Ramanan *et al.*, "Argoverse: 3d tracking and forecasting with rich maps," in *Proceedings of the IEEE/CVF Conference on Computer Vision and Pattern Recognition*, 2019, pp. 8748–8757.
- [154] Q.-H. Pham, P. Sevestre, R. S. Pahwa, H. Zhan, C. H. Pang, Y. Chen, A. Mustafa, V. Chandrasekhar, and J. Lin, "A 3d dataset: Towards autonomous driving in challenging environments," in *2020 IEEE International conference on Robotics and Automation (ICRA)*. IEEE, 2020, pp. 2267–2273.
- [155] J. Geyer, Y. Kassahun, M. Mahmudi, X. Ricou, R. Durgesh, A. S. Chung, L. Hauswald, V. H. Pham, M. Mühlegg, S. Dorn *et al.*, "A2d2: Audi autonomous driving dataset," *arXiv preprint arXiv:2004.06320*, 2020.
- [156] P. Xiao, Z. Shao, S. Hao, Z. Zhang, X. Chai, J. Jiao, Z. Li, J. Wu, K. Sun, K. Jiang *et al.*, "Pandaset: Advanced sensor suite dataset for autonomous driving," in *2021 IEEE International Intelligent Transportation Systems Conference (ITSC)*. IEEE, 2021, pp. 3095–3101.
- [157] Y. Liao, J. Xie, and A. Geiger, "Kitti-360: A novel dataset and benchmarks for urban scene understanding in 2d and 3d," *IEEE Transactions on Pattern Analysis and Machine Intelligence*, vol. 45, no. 3, pp. 3292–3310, 2022.
- [158] Z. Wang, S. Ding, Y. Li, J. Fenn, S. Roychowdhury, A. Wallin, L. Martin, S. Rytola, G. Sapiro, and Q. Qiu, "Cirrus: A long-range bi-pattern lidar dataset," in *2021 IEEE International Conference on Robotics and Automation (ICRA)*. IEEE, 2021, pp. 5744–5750.
- [159] J. Mao, M. Niu, C. Jiang, H. Liang, J. Chen, X. Liang, Y. Li, C. Ye, W. Zhang, Z. Li *et al.*, "One million scenes for autonomous driving: Once dataset," *arXiv preprint arXiv:2106.11037*, 2021.
- [160] L. Chen, C. Sima, Y. Li, Z. Zheng, J. Xu, X. Geng, H. Li, C. He, J. Shi, Y. Qiao *et al.*, "Persformer: 3d lane detection via perspective transformer and the openlane benchmark," in *European Conference on Computer Vision*. Springer, 2022, pp. 550–567.
- [161] J. Ren, L. Pan, and Z. Liu, "Benchmarking and analyzing point cloud classification under corruptions," in *International Conference on Machine Learning*. PMLR, 2022, pp. 18 559–18 575.
- [162] F. Chabot, M. Chaouch, J. Rabarisoa, C. Teuliere, and T. Chateau, "Deep manta: A coarse-to-fine many-task network for joint 2d and 3d vehicle analysis from monocular image," in *Proceedings of the IEEE conference on computer vision and pattern recognition*, 2017, pp. 2040–2049.
- [163] T. He and S. Soatto, "Mono3d++: Monocular 3d vehicle detection with two-scale 3d hypotheses and task priors," in *Proceedings of the AAAI Conference on Artificial Intelligence*, vol. 33, no. 01, 2019, pp. 8409–8416.
- [164] A. Kundu, Y. Li, and J. M. Rehg, "3d-rcnn: Instance-level 3d object reconstruction via render-and-compare," in *Proceedings of the IEEE conference on computer vision and pattern recognition*, 2018, pp. 3559–3568.
- [165] F. Manhardt, W. Kehl, and A. Gaidon, "Roi-10d: Monocular lifting of 2d detection to 6d pose and metric shape," in *Proceedings of the IEEE/CVF Conference on Computer Vision and Pattern Recognition*, 2019, pp. 2069–2078.
- [166] D. Beker, H. Kato, M. A. Morariu, T. Ando, T. Matsuoka, W. Kehl, and A. Gaidon, "Monocular differentiable rendering for self-supervised 3d object detection," in *Computer Vision—ECCV 2020: 16th European Conference, Glasgow, UK, August 23–28, 2020, Proceedings, Part XXI 16*. Springer, 2020, pp. 514–529.
- [167] S. Zakharov, W. Kehl, A. Bhargava, and A. Gaidon, "Autolabeling 3d objects with differentiable rendering of sdf shape priors," in *Proceedings of the IEEE/CVF Conference on Computer Vision and Pattern Recognition*, 2020, pp. 12 224–12 233.
- [168] Y. Xiang, W. Choi, Y. Lin, and S. Savarese, "Data-driven 3d voxel patterns for object category recognition," in *Proceedings of the IEEE conference on computer vision and pattern recognition*, 2015, pp. 1903–1911.
- [169] A. Mousavian, D. Anguelov, J. Flynn, and J. Kosecka, "3d bounding box estimation using deep learning and geometry," in *Proceedings of the IEEE conference on Computer Vision and Pattern Recognition*, 2017, pp. 7074–7082.
- [170] A. Naiden, V. Paunescu, G. Kim, B. Jeon, and M. Leordeanu, "Shift r-cnn: Deep monocular 3d object detection with closed-form geometric constraints," in *2019 IEEE international conference on image processing (ICIP)*. IEEE, 2019, pp. 61–65.
- [171] Q. Lian, B. Ye, R. Xu, W. Yao, and T. Zhang, "Exploring geometric consistency for monocular 3d object detection," in *Proceedings of the IEEE/CVF Conference on Computer Vision and Pattern Recognition*, 2022, pp. 1685–1694.
- [172] Z. Qin and X. Li, "Monoground: Detecting monocular 3d objects from the ground," in *Proceedings of the IEEE/CVF Conference on Computer Vision and Pattern Recognition*, 2022, pp. 3793–3802.
- [173] Z. Wu, Y. Gan, L. Wang, G. Chen, and J. Pu, "Monopgc: Monocular 3d object detection with pixel geometry contexts," in *2023 IEEE International Conference on Robotics and Automation (ICRA)*. IEEE, 2023, pp. 4842–4849.
- [174] M. Zhu, L. Ge, P. Wang, and H. Peng, "Monoedge: Monocular 3d object detection using local perspectives," in *Proceedings of the IEEE/CVF Winter Conference on Applications of Computer Vision*, 2023, pp. 643–652.
- [175] F. Yang, X. Xu, H. Chen, Y. Guo, Y. He, K. Ni, and G. Ding, "Gpro3d: Deriving 3d bbox from ground plane in monocular 3d object detection," *Neurocomputing*, vol. 562, p. 126894, 2023.
- [176] L. Yang, J. Yu, X. Zhang, J. Li, L. Wang, Y. Huang, C. Zhang, H. Wang, and Y. Li, "Monogae: Roadside monocular 3d object detection with ground-aware embeddings," *arXiv preprint arXiv:2310.00400*, 2023.
- [177] Y. Lu, X. Ma, L. Yang, T. Zhang, Y. Liu, Q. Chu, T. He, Y. Li, and W. Ouyang, "Gupnet++: Geometry uncertainty propagation network for monocular 3d object detection," *arXiv preprint arXiv:2310.15624*, 2023.
- [178] Z. Min, B. Zhuang, S. Schulter, B. Liu, E. Dunn, and M. Chandraker, "Neurocs: Neural nocs supervision for monocular 3d object localization," in *Proceedings of the IEEE/CVF Conference on Computer Vision and Pattern Recognition*, 2023, pp. 21 404–21 414.
- [179] Z. Liu, Z. Wu, and R. Tóth, "Smoke: Single-stage monocular 3d object detection via keypoint estimation," in *Proceedings of the IEEE/CVF Conference on Computer Vision and Pattern Recognition Workshops*, 2020, pp. 996–997.
- [180] G. Brazil, G. Pons-Moll, X. Liu, and B. Schiele, "Kinematic 3d object detection in monocular video," in *Computer Vision—ECCV 2020: 16th European Conference, Glasgow, UK, August 23–28, 2020, Proceedings, Part XXIII 16*. Springer, 2020, pp. 135–152.
- [181] A. Simonelli, S. R. Buló, L. Porzi, E. Ricci, and P. Kotschieder, "Towards generalization across depth for monocular 3d object detection," in *Computer Vision—ECCV 2020: 16th European Conference, Glasgow, UK, August 23–28, 2020, Proceedings, Part XXII 16*. Springer, 2020, pp. 767–782.
- [182] B. Li, W. Ouyang, L. Sheng, X. Zeng, and X. Wang, "Gs3d: An efficient 3d object detection framework for autonomous driving," in *Proceedings of the IEEE/CVF Conference on Computer Vision and Pattern Recognition*, 2019, pp. 1019–1028.
- [183] Z. Qin, J. Wang, and Y. Lu, "Monogrnet: A geometric reasoning network for monocular 3d object localization," in *Proceedings of the AAAI conference on artificial intelligence*, vol. 33, no. 01, 2019, pp. 8851–8858.
- [184] X. Shi, Q. Ye, X. Chen, C. Chen, Z. Chen, and T.-K. Kim, "Geometry-based distance decomposition for monocular 3d object detection," in *Proceedings of the IEEE/CVF International Conference on Computer Vision*, 2021, pp. 15 172–15 181.
- [185] W. Bao, B. Xu, and Z. Chen, "Monofenet: Monocular 3d object detection with feature enhancement networks," *IEEE Transactions on Image Processing*, vol. 29, pp. 2753–2765, 2019.
- [186] X. Liu, N. Xue, and T. Wu, "Learning auxiliary monocular contexts helps monocular 3d object detection," in *Proceedings of the AAAI Conference on Artificial Intelligence*, vol. 36, no. 2, 2022, pp. 1810–1818.
- [187] X. Liu, C. Zheng, K. B. Cheng, N. Xue, G.-J. Qi, and T. Wu, "Monocular 3d object detection with bounding box denoising in 3d by perceiver," in *Proceedings of the IEEE/CVF International Conference on Computer Vision*, 2023, pp. 6436–6446.
- [188] Z. Zhou, L. Du, X. Ye, Z. Zou, X. Tan, L. Zhang, X. Xue, and J. Feng, "Sgm3d: Stereo guided monocular 3d object detection," *IEEE Robotics and Automation Letters*, vol. 7, no. 4, pp. 10 478–10 485, 2022.
- [189] L. Peng, X. Wu, Z. Yang, H. Liu, and D. Cai, "Did-m3d: Decoupling instance depth for monocular 3d object detection," in *European Conference on Computer Vision*. Springer, 2022, pp. 71–88.
- [190] J. Xu, L. Peng, H. Cheng, H. Li, W. Qian, K. Li, W. Wang, and D. Cai, "Mononerf: Nerf-like representations for monocular 3d object detection," in *Proceedings of the IEEE/CVF International Conference on Computer Vision*, 2023, pp. 6814–6824.

- [191] C. Xia, W. Zhao, H. Han, Z. Tao, B. Ge, X. Gao, K.-C. Li, and Y. Zhang, "Monosaid: Monocular 3d object detection based on scene-level adaptive instance depth estimation," *Journal of Intelligent & Robotic Systems*, vol. 110, no. 1, p. 2, 2024.
- [192] R. Tao, W. Han, Z. Qiu, C.-z. Xu, and J. Shen, "Weakly supervised monocular 3d object detection using multi-view projection and direction consistency," in *Proceedings of the IEEE/CVF Conference on Computer Vision and Pattern Recognition*, 2023, pp. 17 482–17 492.
- [193] X. Wu, D. Ma, X. Qu, X. Jiang, and D. Zeng, "Depth dynamic center difference convolutions for monocular 3d object detection," *Neurocomputing*, vol. 520, pp. 73–81, 2023.
- [194] C. Huang, T. He, H. Ren, W. Wang, B. Lin, and D. Cai, "Obmo: One bounding box multiple objects for monocular 3d object detection," *IEEE Transactions on Image Processing*, vol. 32, pp. 6570–6581, 2023.
- [195] L. Chen, J. Sun, Y. Xie, S. Zhang, Q. Shuai, Q. Jiang, G. Zhang, H. Bao, and X. Zhou, "Shape prior guided instance disparity estimation for 3d object detection," *IEEE Transactions on Pattern Analysis and Machine Intelligence*, vol. 44, no. 9, pp. 5529–5540, 2021.
- [196] L. Yang, X. Zhang, J. Li, L. Wang, M. Zhu, and L. Zhu, "Lite-fpn for keypoint-based monocular 3d object detection," *Knowledge-Based Systems*, vol. 271, p. 110517, 2023.
- [197] C. Park, H. Kim, J. Jang, and J. Paik, "Odd-m3d: Object-wise dense depth estimation for monocular 3d object detection," *IEEE Transactions on Consumer Electronics*, 2024.
- [198] X. Li, J. Liu, Y. Lei, L. Ma, X. Fan, and R. Liu, "Monotdp: Twin depth perception for monocular 3d object detection in adverse scenes," *arXiv preprint arXiv:2305.10974*, 2023.
- [199] G. Brazil, A. Kumar, J. Straub, N. Ravi, J. Johnson, and G. Gkioxari, "Omni3d: A large benchmark and model for 3d object detection in the wild," in *Proceedings of the IEEE/CVF conference on computer vision and pattern recognition*, 2023, pp. 13 154–13 164.
- [200] J. U. Kim, H.-I. Kim, and Y. M. Ro, "Stereoscopic vision recalling memory for monocular 3d object detection," *IEEE Transactions on Image Processing*, 2023.
- [201] X. Ma, S. Liu, Z. Xia, H. Zhang, X. Zeng, and W. Ouyang, *Rethinking Pseudo-LiDAR Representation*, Jan 2020, p. 311–327.
- [202] J. Chang and G. Wetzstein, "Deep optics for monocular depth estimation and 3d object detection," in *Proceedings of the IEEE/CVF International Conference on Computer Vision*, 2019, pp. 10 193–10 202.
- [203] H.-I. Liu, C. Wu, J.-H. Cheng, W. Chai, S.-Y. Wang, G. Liu, J.-N. Hwang, H.-H. Shuai, and W.-H. Cheng, "Monotakd: Teaching assistant knowledge distillation for monocular 3d object detection," *arXiv preprint arXiv:2404.04910*, 2024.
- [204] Y. Kim, S. Kim, S. Sim, J. W. Choi, and D. Kum, "Boosting monocular 3d object detection with object-centric auxiliary depth supervision," *IEEE Transactions on Intelligent Transportation Systems*, vol. 24, no. 2, pp. 1801–1813, 2022.
- [205] L. Wang, L. Du, X. Ye, Y. Fu, G. Guo, X. Xue, J. Feng, and L. Zhang, "Depth-conditioned dynamic message propagation for monocular 3d object detection," in *Proceedings of the IEEE/CVF Conference on Computer Vision and Pattern Recognition*, 2021, pp. 454–463.
- [206] M. Ding, Y. Huo, H. Yi, Z. Wang, J. Shi, Z. Lu, and P. Luo, "Learning depth-guided convolutions for monocular 3d object detection," in *Proceedings of the IEEE/CVF Conference on computer vision and pattern recognition workshops*, 2020, pp. 1000–1001.
- [207] Z. Wu, Y. Wu, J. Pu, X. Li, and X. Wang, "Attention-based depth distillation with 3d-aware positional encoding for monocular 3d object detection," in *Proceedings of the AAAI Conference on Artificial Intelligence*, vol. 37, no. 3, 2023, pp. 2892–2900.
- [208] H. Sheng, S. Cai, N. Zhao, B. Deng, M.-J. Zhao, and G. H. Lee, "Pdr: Progressive depth regularization for monocular 3d object detection," *IEEE Transactions on Circuits and Systems for Video Technology*, 2023.
- [209] C. Tao, J. Cao, C. Wang, Z. Zhang, and Z. Gao, "Pseudo-mono for monocular 3d object detection in autonomous driving," *IEEE Transactions on Circuits and Systems for Video Technology*, 2023.
- [210] A. Kumar, G. Brazil, E. Corona, A. Parchami, and X. Liu, "Deviant: Depth equivariant network for monocular 3d object detection," in *European Conference on Computer Vision*. Springer, 2022, pp. 664–683.
- [211] W. Zhang, D. Liu, C. Ma, and W. Cai, "Alleviating foreground sparsity for semi-supervised monocular 3d object detection," in *Proceedings of the IEEE/CVF Winter Conference on Applications of Computer Vision*, 2024, pp. 7542–7552.
- [212] Z. Wu, Y. Gan, Y. Wu, R. Wang, X. Wang, and J. Pu, "Fd3d: Exploiting foreground depth map for feature-supervised monocular 3d object detection," in *Proceedings of the AAAI Conference on Artificial Intelligence*, vol. 38, no. 6, 2024, pp. 6189–6197.
- [213] S. Wang and J. Zheng, "Monoskd: General distillation framework for monocular 3d object detection via spearman correlation coefficient," *arXiv preprint arXiv:2310.11316*, 2023.
- [214] J. Sun, L. Chen, Y. Xie, S. Zhang, Q. Jiang, X. Zhou, and H. Bao, "Disp r-cnn: Stereo 3d object detection via shape prior guided instance disparity estimation," in *Proceedings of the IEEE/CVF conference on computer vision and pattern recognition*, 2020, pp. 10 548–10 557.
- [215] Z. Qin, J. Wang, and Y. Lu, "Triangulation learning network: from monocular to stereo 3d object detection," in *Proceedings of the IEEE/CVF Conference on Computer Vision and Pattern Recognition*, 2019, pp. 7615–7623.
- [216] Z. Xu, W. Zhang, X. Ye, X. Tan, W. Yang, S. Wen, E. Ding, A. Meng, and L. Huang, "Zoomnet: Part-aware adaptive zooming neural network for 3d object detection," in *Proceedings of the AAAI Conference on Artificial Intelligence*, vol. 34, no. 07, 2020, pp. 12 557–12 564.
- [217] W. Peng, H. Pan, H. Liu, and Y. Sun, "Ida-3d: Instance-depth-aware 3d detector from stereo vision for autonomous driving," in *Proceedings of the IEEE/CVF Conference on Computer Vision and Pattern Recognition*, 2020, pp. 13 015–13 024.
- [218] X. Peng, X. Zhu, T. Wang, and Y. Ma, "Side: center-based stereo 3d detector with structure-aware instance depth estimation," in *Proceedings of the IEEE/CVF Winter Conference on Applications of Computer Vision*, 2022, pp. 119–128.
- [219] C.-H. Wang, H.-W. Chen, Y. Chen, P.-Y. Hsiao, and L.-C. Fu, "Vopifnet: Voxel-pixel fusion network for multi-class 3d object detection," *IEEE Transactions on Intelligent Transportation Systems*, pp. 1–11, 2024.
- [220] Y. Wu, Z. Liu, Y. Chen, X. Zheng, Q. Zhang, M. Yang, and G. Tang, "Fcnet: Stereo 3d object detection with feature correlation networks," *Entropy*, vol. 24, no. 8, p. 1121, 2022.
- [221] M. Feng, J. Cheng, H. Jia, L. Liu, G. Xu, and X. Yang, "Mc-stereo: Multi-peak lookup and cascade search range for stereo matching," *arXiv preprint arXiv:2311.02340*, 2023.
- [222] Z. Shen, Y. Dai, X. Song, Z. Rao, D. Zhou, and L. Zhang, "Pcw-net: Pyramid combination and warping cost volume for stereo matching," in *European conference on computer vision*. Springer, 2022, pp. 280–297.
- [223] O.-H. Kwon and E. Zell, "Image-coupled volume propagation for stereo matching," in *2023 IEEE International Conference on Image Processing (ICIP)*. IEEE, 2023, pp. 2510–2514.
- [224] Z. Chen, W. Long, H. Yao, Y. Zhang, B. Wang, Y. Qin, and J. Wu, "Mocha-stereo: Motif channel attention network for stereo matching," *arXiv preprint arXiv:2404.06842*, 2024.
- [225] Z. Shen, X. Song, Y. Dai, D. Zhou, Z. Rao, and L. Zhang, "Digging into uncertainty-based pseudo-label for robust stereo matching," *IEEE Transactions on Pattern Analysis and Machine Intelligence*, 2023.
- [226] G. Xu, X. Wang, X. Ding, and X. Yang, "Iterative geometry encoding volume for stereo matching," in *Proceedings of the IEEE/CVF Conference on Computer Vision and Pattern Recognition*, 2023, pp. 21 919–21 928.
- [227] T. Guan, C. Wang, and Y.-H. Liu, "Neural markov random field for stereo matching," *arXiv preprint arXiv:2403.11193*, 2024.
- [228] Y. You, Y. Wang, W.-L. Chao, D. Garg, G. Pleiss, B. Hariharan, M. Campbell, and K. Q. Weinberger, "Pseudo-lidar++: Accurate depth for 3d object detection in autonomous driving," in *ICLR*, 2020.
- [229] R. Qian, D. Garg, Y. Wang, Y. You, S. Belongie, B. Hariharan, M. Campbell, K. Q. Weinberger, and W.-L. Chao, "End-to-end pseudo-lidar for image-based 3d object detection," in *Proceedings of the IEEE/CVF Conference on Computer Vision and Pattern Recognition*, 2020, pp. 5881–5890.
- [230] C. Li, J. Ku, and S. L. Waslander, "Confidence guided stereo 3d object detection with split depth estimation," in *2020 IEEE/RSJ International Conference on Intelligent Robots and Systems (IROS)*. IEEE, 2020, pp. 5776–5783.
- [231] P. Li, S. Su, and H. Zhao, "Rts3d: Real-time stereo 3d detection from 4d feature-consistency embedding space for autonomous driving," in *Proceedings of the AAAI Conference on Artificial Intelligence*, vol. 35, no. 3, 2021, pp. 1930–1939.
- [232] H. Königshof, N. O. Salscheider, and C. Stiller, "Realtime 3d object detection for automated driving using stereo vision and semantic information," in *2019 IEEE Intelligent Transportation Systems Conference (ITSC)*. IEEE, 2019, pp. 1405–1410.
- [233] H. Königshof and C. Stiller, "Learning-based shape estimation with grid map patches for realtime 3d object detection for automated

- driving,” in *2020 IEEE 23rd International conference on intelligent transportation systems (ITSC)*. IEEE, 2020, pp. 1–6.
- [234] D. Garg, Y. Wang, B. Hariharan, M. Campbell, K. Q. Weinberger, and W.-L. Chao, “Wasserstein distances for stereo disparity estimation,” *Advances in Neural Information Processing Systems*, vol. 33, pp. 22 517–22 529, 2020.
- [235] A. Kendall, H. Martirosyan, S. Dasgupta, P. Henry, R. Kennedy, A. Bachrach, and A. Bry, “End-to-end learning of geometry and context for deep stereo regression,” in *Proceedings of the IEEE international conference on computer vision*, 2017, pp. 66–75.
- [236] A. Gao, Y. Pang, J. Nie, Z. Shao, J. Cao, Y. Guo, and X. Li, “Esgn: Efficient stereo geometry network for fast 3d object detection,” *IEEE Transactions on Circuits and Systems for Video Technology*, 2022.
- [237] Y. Chen, S. Huang, S. Liu, B. Yu, and J. Jia, “Dsgn++: Exploiting visual-spatial relation for stereo-based 3d detectors,” *IEEE Transactions on Pattern Analysis and Machine Intelligence*, vol. 45, no. 4, pp. 4416–4429, 2022.
- [238] X. Guo, S. Shi, X. Wang, and H. Li, “Liga-stereo: Learning lidar geometry aware representations for stereo-based 3d detector,” in *Proceedings of the IEEE/CVF International Conference on Computer Vision*, 2021, pp. 3153–3163.
- [239] Y. Wang, B. Yang, R. Hu, M. Liang, and R. Urtaun, “Plumenet: Efficient 3d object detection from stereo images,” in *2021 IEEE/RSJ International Conference on Intelligent Robots and Systems (IROS)*. IEEE, 2021, pp. 3383–3390.
- [240] X. Wang, G. Xu, H. Jia, and X. Yang, “Selective-stereo: Adaptive frequency information selection for stereo matching,” *arXiv preprint arXiv:2403.00486*, 2024.
- [241] C.-W. Liu, Q. Chen, and R. Fan, “Playing to vision foundation model’s strengths in stereo matching,” *arXiv preprint arXiv:2404.06261*, 2024.
- [242] B. Liu, H. Yu, and Y. Long, “Local similarity pattern and cost self-reassembling for deep stereo matching networks,” in *Proceedings of the AAAI Conference on Artificial Intelligence*, vol. 36, no. 2, 2022, pp. 1647–1655.
- [243] Y. Shi, “Rethinking iterative stereo matching from diffusion bridge model perspective,” *arXiv preprint arXiv:2404.09051*, 2024.
- [244] T. Yuan, J. Hu, S. Ou, W. Yang, and Y. Hei, “Hourglass cascaded recurrent stereo matching network,” *Image and Vision Computing*, p. 105074, 2024.
- [245] X. Cheng, Y. Zhong, M. Harandi, Y. Dai, X. Chang, H. Li, T. Drummond, and Z. Ge, “Hierarchical neural architecture search for deep stereo matching,” *Advances in neural information processing systems*, vol. 33, pp. 22 158–22 169, 2020.
- [246] J. Li, P. Wang, P. Xiong, T. Cai, Z. Yan, L. Yang, J. Liu, H. Fan, and S. Liu, “Practical stereo matching via cascaded recurrent network with adaptive correlation,” in *Proceedings of the IEEE/CVF conference on computer vision and pattern recognition*, 2022, pp. 16 263–16 272.
- [247] X. Li, Y. Fan, G. Lv, and H. Ma, “Area-based correlation and non-local attention network for stereo matching,” *The Visual Computer*, vol. 38, no. 11, pp. 3881–3895, 2022.
- [248] Y. Zhang, Y. Chen, X. Bai, S. Yu, K. Yu, Z. Li, and K. Yang, “Adaptive unimodal cost volume filtering for deep stereo matching,” in *Proceedings of the AAAI Conference on Artificial Intelligence*, vol. 34, no. 07, 2020, pp. 12 926–12 934.
- [249] S. Chen, B. Li, W. Wang, H. Zhang, H. Li, and Z. Wang, “Cost affinity learning network for stereo matching,” in *ICASSP 2021-2021 IEEE International Conference on Acoustics, Speech and Signal Processing (ICASSP)*. IEEE, 2021, pp. 2120–2124.
- [250] Z. Shen, Y. Dai, and Z. Rao, “Cfnet: Cascade and fused cost volume for robust stereo matching,” in *Proceedings of the IEEE/CVF Conference on Computer Vision and Pattern Recognition*, 2021, pp. 13 906–13 915.
- [251] K. Zeng, Y. Wang, Q. Zhu, J. Mao, and H. Zhang, “Deep progressive fusion stereo network,” *IEEE Transactions on Intelligent Transportation Systems*, vol. 23, no. 12, pp. 25 437–25 447, 2021.
- [252] M. Tahmasebi, S. Huq, K. Meehan, and M. McAfee, “Dcvsmnet: Double cost volume stereo matching network,” *arXiv preprint arXiv:2402.16473*, 2024.
- [253] Y. Deng, J. Xiao, S. Z. Zhou, and J. Feng, “Detail preserving coarse-to-fine matching for stereo matching and optical flow,” *IEEE Transactions on Image Processing*, vol. 30, pp. 5835–5847, 2021.
- [254] G. Xu, J. Cheng, P. Guo, and X. Yang, “Attention concatenation volume for accurate and efficient stereo matching,” in *Proceedings of the IEEE/CVF conference on computer vision and pattern recognition*, 2022, pp. 12 981–12 990.
- [255] J. Huang, G. Huang, Z. Zhu, Y. Ye, and D. Du, “Bevdet: High-performance multi-camera 3d object detection in bird-eye-view,” *arXiv preprint arXiv:2112.11790*, 2021.
- [256] J. Phillion and S. Fidler, “Lift, splat, shoot: Encoding images from arbitrary camera rigs by implicitly unprojecting to 3d,” in *Computer Vision—ECCV 2020: 16th European Conference, Glasgow, UK, August 23–28, 2020, Proceedings, Part XIV 16*. Springer, 2020, pp. 194–210.
- [257] L. Yang, K. Yu, T. Tang, J. Li, K. Yuan, L. Wang, X. Zhang, and P. Chen, “Bevheight: A robust framework for vision-based roadside 3d object detection,” in *Proceedings of the IEEE/CVF Conference on Computer Vision and Pattern Recognition*, 2023, pp. 21 611–21 620.
- [258] X. Chi, J. Liu, M. Lu, R. Zhang, Z. Wang, Y. Guo, and S. Zhang, “Bevsan: Accurate bev 3d object detection via slice attention networks,” in *Proceedings of the IEEE/CVF Conference on Computer Vision and Pattern Recognition*, 2023, pp. 17 461–17 470.
- [259] J. Liu, R. Zhang, X. Chi, X. Li, M. Lu, Y. Guo, and S. Zhang, “Multi-latent space alignments for unsupervised domain adaptation in multi-view 3d object detection,” *arXiv preprint arXiv:2211.17126*, 2022.
- [260] J. Huang and G. Huang, “Bevpoolv2: A cutting-edge implementation of bevdet toward deployment,” *arXiv preprint arXiv:2211.17111*, 2022.
- [261] Y. Li, H. Bao, Z. Ge, J. Yang, J. Sun, and Z. Li, “Bevstereo: Enhancing depth estimation in multi-view 3d object detection with temporal stereo,” in *Proceedings of the AAAI Conference on Artificial Intelligence*, vol. 37, no. 2, 2023, pp. 1486–1494.
- [262] Y. Li, J. Yang, J. Sun, H. Bao, Z. Ge, and L. Xiao, “Bevstereo++: Accurate depth estimation in multi-view 3d object detection via dynamic temporal stereo,” *arXiv preprint arXiv:2304.04185*, 2023.
- [263] P. Huang, L. Liu, R. Zhang, S. Zhang, X. Xu, B. Wang, and G. Liu, “Tig-bev: Multi-view bev 3d object detection via target inner-geometry learning,” *arXiv preprint arXiv:2212.13979*, 2022.
- [264] S. Wang, X. Zhao, H.-M. Xu, Z. Chen, D. Yu, J. Chang, Z. Yang, and F. Zhao, “Towards domain generalization for multi-view 3d object detection in bird-eye-view,” in *Proceedings of the IEEE/CVF Conference on Computer Vision and Pattern Recognition*, 2023, pp. 13 333–13 342.
- [265] P. Dong, Z. Kong, X. Meng, P. Yu, Y. Gong, G. Yuan, H. Tang, and Y. Wang, “Hotbev: Hardware-oriented transformer-based multi-view 3d detector for bev perception,” *Advances in Neural Information Processing Systems*, vol. 36, 2024.
- [266] Z. Li, S. Lan, J. M. Alvarez, and Z. Wu, “Bevnext: Reviving dense bev frameworks for 3d object detection,” *arXiv preprint arXiv:2312.01696*, 2023.
- [267] Y. Jiang, L. Zhang, Z. Miao, X. Zhu, J. Gao, W. Hu, and Y.-G. Jiang, “Polarformer: Multi-camera 3d object detection with polar transformer,” in *Proceedings of the AAAI Conference on Artificial Intelligence*, vol. 37, no. 1, 2023, pp. 1042–1050.
- [268] Y. Wang, Y. Chen, and Z. Zhang, “Frustrumformer: Adaptive instance-aware resampling for multi-view 3d detection,” in *Proceedings of the IEEE/CVF Conference on Computer Vision and Pattern Recognition*, 2023, pp. 5096–5105.
- [269] Z. Luo, C. Zhou, G. Zhang, and S. Lu, “Detr4d: Direct multi-view 3d object detection with sparse attention,” *arXiv preprint arXiv:2212.07849*, 2022.
- [270] X. Lin, T. Lin, Z. Pei, L. Huang, and Z. Su, “Sparse4d: Multi-view 3d object detection with sparse spatial-temporal fusion,” *arXiv preprint arXiv:2211.10581*, 2022.
- [271] —, “Sparse4d v2: Recurrent temporal fusion with sparse model,” *arXiv preprint arXiv:2305.14018*, 2023.
- [272] X. Lin, Z. Pei, T. Lin, L. Huang, and Z. Su, “Sparse4d v3: Advancing end-to-end 3d detection and tracking,” *arXiv preprint arXiv:2311.11722*, 2023.
- [273] J. Park, C. Xu, S. Yang, K. Keutzer, K. Kitani, M. Tomizuka, and W. Zhan, “Time will tell: New outlooks and a baseline for temporal multi-view 3d object detection,” *arXiv preprint arXiv:2210.02443*, 2022.
- [274] K. Xiong, S. Gong, X. Ye, X. Tan, J. Wan, E. Ding, J. Wang, and X. Bai, “Cape: Camera view position embedding for multi-view 3d object detection,” in *Proceedings of the IEEE/CVF Conference on Computer Vision and Pattern Recognition*, 2023, pp. 21 570–21 579.
- [275] D. Chen, J. Li, V. Guizilini, R. A. Ambrus, and A. Gaidon, “Viewpoint equivariance for multi-view 3d object detection,” in *Proceedings of the IEEE/CVF Conference on Computer Vision and Pattern Recognition*, 2023, pp. 9213–9222.
- [276] Z. Chen, Z. Li, S. Zhang, L. Fang, Q. Jiang, and F. Zhao, “Graphdetr3d: rethinking overlapping regions for multi-view 3d object detection,” in *Proceedings of the 30th ACM International Conference on Multimedia*, 2022, pp. 5999–6008.
- [277] C. Shu, J. Deng, F. Yu, and Y. Liu, “3dppc: 3d point positional encoding for transformer-based multi-camera 3d object detection,” in *Proceedings of the IEEE/CVF International Conference on Computer Vision*, 2023, pp. 3580–3589.

- [278] Z. Chen, Z. Li, S. Zhang, L. Fang, Q. Jiang, and F. Zhao, “Bevdistill: Cross-modal bev distillation for multi-view 3d object detection,” *arXiv preprint arXiv:2211.09386*, 2022.
- [279] S. Wang, Y. Liu, T. Wang, Y. Li, and X. Zhang, “Exploring object-centric temporal modeling for efficient multi-view 3d object detection,” *arXiv preprint arXiv:2303.11926*, 2023.
- [280] X. Jiang, S. Li, Y. Liu, S. Wang, F. Jia, T. Wang, L. Han, and X. Zhang, “Far3d: Expanding the horizon for surround-view 3d object detection,” *arXiv preprint arXiv:2308.09616*, 2023.
- [281] C. Pan, B. Yaman, S. Velipasalar, and L. Ren, “Clip-bevformer: Enhancing multi-view image-based bev detector with ground truth flow,” *arXiv preprint arXiv:2403.08919*, 2024.
- [282] C. Yang, Y. Chen, H. Tian, C. Tao, X. Zhu, Z. Zhang, G. Huang, H. Li, Y. Qiao, L. Lu *et al.*, “Befvformer v2: Adapting modern image backbones to bird’s-eye-view recognition via perspective supervision,” in *Proceedings of the IEEE/CVF Conference on Computer Vision and Pattern Recognition*, 2023, pp. 17 830–17 839.
- [283] Y. Zhou, H. Zhu, Q. Liu, S. Chang, and M. Guo, “Monoatt: Online monocular 3d object detection with adaptive token transformer,” in *Proceedings of the IEEE/CVF Conference on Computer Vision and Pattern Recognition*, 2023, pp. 17 493–17 503.
- [284] L. Yan, P. Yan, S. Xiong, X. Xiang, and Y. Tan, “Monocd: Monocular 3d object detection with complementary depths,” in *CVPR*, 2024.
- [285] P. Li, X. Chen, and S. Shen, “Stereo r-cnn based 3d object detection for autonomous driving,” in *Proceedings of the IEEE/CVF Conference on Computer Vision and Pattern Recognition*, 2019, pp. 7644–7652.
- [286] A. D. Pon, J. Ku, C. Li, and S. L. Waslander, “Object-centric stereo matching for 3d object detection,” in *2020 IEEE International Conference on Robotics and Automation (ICRA)*. IEEE, 2020, pp. 8383–8389.
- [287] J. Sun, L. Chen, Y. Xie, S. Zhang, Q. Jiang, X. Zhou, and H. Bao, “Disp r-cnn: Stereo 3d object detection via shape prior guided instance disparity estimation,” in *Proceedings of the IEEE/CVF conference on computer vision and pattern recognition*, 2020, pp. 10 548–10 557.
- [288] S. Li, Z. Liu, Z. Shen, and K.-T. Cheng, “Stereo neural vernier caliper,” in *Proceedings of the AAAI Conference on Artificial Intelligence*, vol. 36, no. 2, 2022, pp. 1376–1385.
- [289] Z. Liu, X. Ye, X. Tan, E. Ding, and X. Bai, “Stereodistill: Pick the cream from lidar for distilling stereo-based 3d object detection,” *arXiv preprint arXiv:2301.01615*, 2023.
- [290] Z. Wang, D. Li, C. Luo, C. Xie, and X. Yang, “Distillbev: Boosting multi-camera 3d object detection with cross-modal knowledge distillation,” in *Proceedings of the IEEE/CVF International Conference on Computer Vision*, 2023, pp. 8637–8646.
- [291] B. Yang, W. Luo, and R. Urtasun, “Pixor: Real-time 3d object detection from point clouds,” in *Proceedings of the IEEE conference on Computer Vision and Pattern Recognition*, 2018, pp. 7652–7660.
- [292] B. Yang, M. Liang, and R. Urtasun, “Hdnet: Exploiting hd maps for 3d object detection,” in *Conference on Robot Learning*. PMLR, 2018, pp. 146–155.
- [293] J. Beltrán, C. Guindel, F. M. Moreno, D. Cruzado, F. Garcia, and A. De La Escalera, “Birdnet: a 3d object detection framework from lidar information,” in *2018 21st International Conference on Intelligent Transportation Systems (ITSC)*. IEEE, 2018, pp. 3517–3523.
- [294] J. Zarzar, S. Giancola, and B. Ghanem, “Pointrgcn: Graph convolution networks for 3d vehicles detection refinement,” *arXiv: Computer Vision and Pattern Recognition*, arXiv: *Computer Vision and Pattern Recognition*, Nov 2019.
- [295] J. Ngiam, B. Caine, W. Han, B. Yang, Y. Chai, P. Sun, Y. Zhou, X. Yi, O. Alsharif, P. Nguyen, Z. Chen, J. Shlens, and V. Vasudevan, “Starnet: Targeted computation for object detection in point clouds,” *Cornell University - arXiv, Cornell University - arXiv*, Aug 2019.
- [296] L. Xie, C. Xiang, Z. Yu, G. Xu, Z. Yang, D. Cai, and X. He, “Pi-rnn: An efficient multi-sensor 3d object detector with point-based attentive cont-conv fusion module,” in *Proceedings of the AAAI conference on artificial intelligence*, vol. 34, no. 07, 2020, pp. 12 460–12 467.
- [297] Q. Wang, J. Chen, J. Deng, and X. Zhang, “3d-centernet: 3d object detection network for point clouds with center estimation priority,” *Pattern Recognition*, p. 107884, Jul 2021.
- [298] Y. Zhang, D. Huang, and Y. Wang, “Pc-rgnn: Point cloud completion and graph neural network for 3d object detection,” in *Proceedings of the AAAI conference on artificial intelligence*, vol. 35, no. 4, 2021, pp. 3430–3437.
- [299] Y. Zhang, Q. Hu, G. Xu, Y. Ma, J. Wan, and Y. Guo, “Not all points are equal: Learning highly efficient point-based detectors for 3d lidar point clouds,” in *Proceedings of the IEEE/CVF Conference on Computer Vision and Pattern Recognition*, 2022, pp. 18 953–18 962.
- [300] I. Koo, I. Lee, S.-H. Kim, H.-S. Kim, W.-j. Jeon, and C. Kim, “Pgrcnn: Semantic surface point generation for 3d object detection,” in *Proceedings of the IEEE/CVF International Conference on Computer Vision*, 2023, pp. 18 142–18 151.
- [301] B. Zhu, Z. Jiang, X. Zhou, Z. Li, and G. Yu, “Class-balanced grouping and sampling for point cloud 3d object detection,” *arXiv preprint arXiv:1908.09492*, 2019.
- [302] S. Shi, Z. Wang, J. Shi, X. Wang, and H. Li, “From points to parts: 3d object detection from point cloud with part-aware and part-aggregation network,” *IEEE transactions on pattern analysis and machine intelligence*, vol. 43, no. 8, pp. 2647–2664, 2020.
- [303] Z. Liu, X. Zhao, T. Huang, R. Hu, Y. Zhou, and X. Bai, “Tanet: Robust 3d object detection from point clouds with triple attention,” in *Proceedings of the AAAI Conference on Artificial Intelligence*, vol. 34, no. 07, 2020, pp. 11 677–11 684.
- [304] Q. Chen, L. Sun, E. Cheung, and A. L. Yuille, “Every view counts: Cross-view consistency in 3d object detection with hybrid-cylindrical-spherical voxelization,” *Advances in Neural Information Processing Systems*, vol. 33, pp. 21 224–21 235, 2020.
- [305] H. Yi, S. Shi, M. Ding, J. Sun, K. Xu, H. Zhou, Z. Wang, S. Li, and G. Wang, “Segvoxelnet: Exploring semantic context and depth-aware features for 3d vehicle detection from point cloud,” in *2020 IEEE International Conference on Robotics and Automation (ICRA)*, May 2020.
- [306] Q. Chen, L. Sun, Z. Wang, K. Jia, and A. Yuille, “Object as hotspots: An anchor-free 3d object detection approach via firing of hotspots,” in *Computer Vision—ECCV 2020: 16th European Conference, Glasgow, UK, August 23–28, 2020, Proceedings, Part XXI 16*. Springer, 2020, pp. 68–84.
- [307] C. Yu, J. Lei, B. Peng, H. Shen, and Q. Huang, “Siev-net: A structure-information enhanced voxel network for 3d object detection from lidar point clouds,” *IEEE Transactions on Geoscience and Remote Sensing*, vol. 60, pp. 1–11, 2022.
- [308] S. Shi, C. Guo, L. Jiang, Z. Wang, J. Shi, X. Wang, and H. Li, “Pv-rnn: Point-voxel feature set abstraction for 3d object detection,” in *Proceedings of the IEEE/CVF Conference on Computer Vision and Pattern Recognition*, 2020, pp. 10 529–10 538.
- [309] C. He, H. Zeng, J. Huang, X.-S. Hua, and L. Zhang, “Structure aware single-stage 3d object detection from point cloud,” in *Proceedings of the IEEE/CVF conference on computer vision and pattern recognition*, 2020, pp. 11 873–11 882.
- [310] T. Jiang, N. Song, H. Liu, R. Yin, Y. Gong, and J. Yao, “Vic-net: voxelization information compensation network for point cloud 3d object detection,” in *2021 IEEE International Conference on Robotics and Automation (ICRA)*. IEEE, 2021, pp. 13 408–13 414.
- [311] H. Zhang, G. Luo, X. Wang, Y. Li, W. Ding, and F.-Y. Wang, “Sasan: Shape-adaptive set abstraction network for point-voxel 3d object detection,” *IEEE Transactions on Neural Networks and Learning Systems*, 2023.
- [312] H. Yang, W. Wang, M. Chen, B. Lin, T. He, H. Chen, X. He, and W. Ouyang, “Pvt-ssd: Single-stage 3d object detector with point-voxel transformer,” in *Proceedings of the IEEE/CVF Conference on Computer Vision and Pattern Recognition*, 2023, pp. 13 476–13 487.
- [313] B. Fan, K. Zhang, and J. Tian, “Hcpvf: Hierarchical cascaded point-voxel fusion for 3d object detection,” *IEEE Transactions on Circuits and Systems for Video Technology*, 2023.
- [314] J. Cao, C. Tao, Z. Zhang, Z. Gao, X. Luo, S. Zheng, and Y. Zhu, “Accelerating point-voxel representation of 3d object detection for automatic driving,” *IEEE Transactions on Artificial Intelligence*, 2023.
- [315] C. Feng, C. Xiang, X. Xie, Y. Zhang, M. Yang, and X. Li, “Hpv-rnn: Hybrid point-voxel two-stage network for lidar based 3-d object detection,” *IEEE Transactions on Computational Social Systems*, 2023.
- [316] V. A. Sindagi, Y. Zhou, and O. Tuzel, “Mvx-net: Multimodal voxelnet for 3d object detection,” in *2019 International Conference on Robotics and Automation (ICRA)*. IEEE, 2019, pp. 7276–7282.
- [317] K. Shin, Y. P. Kwon, and M. Tomizuka, “Roarnet: A robust 3d object detection based on region approximation refinement,” in *2019 IEEE intelligent vehicles symposium (IV)*. IEEE, 2019, pp. 2510–2515.
- [318] M. Simon, K. Amende, A. Kraus, J. Honer, T. Samann, H. Kaulbersch, S. Milz, and H. Michael Gross, “Complexer-yolo: Real-time 3d object detection and tracking on semantic point clouds,” in *Proceedings of the IEEE/CVF Conference on Computer Vision and Pattern Recognition Workshops*, 2019, pp. 0–0.
- [319] C. Wang, C. Ma, M. Zhu, and X. Yang, “Pointaugmenting: Cross-modal augmentation for 3d object detection,” in *Proceedings of the IEEE/CVF Conference on Computer Vision and Pattern Recognition*, 2021, pp. 11 794–11 803.

- [320] S. Xu, D. Zhou, J. Fang, J. Yin, Z. Bin, and L. Zhang, "Fusionpainting: Multimodal fusion with adaptive attention for 3d object detection," in *2021 IEEE International Intelligent Transportation Systems Conference (ITSC)*. IEEE, 2021, pp. 3047–3054.
- [321] G. P. Meyer, J. Charland, D. Hegde, A. Laddha, and C. Vallespi-Gonzalez, "Sensor fusion for joint 3d object detection and semantic segmentation," in *Proceedings of the IEEE/CVF conference on computer vision and pattern recognition workshops*, 2019, pp. 0–0.
- [322] R. Nabati and H. Qi, "Centerfusion: Center-based radar and camera fusion for 3d object detection," in *Proceedings of the IEEE/CVF Winter Conference on Applications of Computer Vision*, 2021, pp. 1527–1536.
- [323] S. Xu, F. Li, Z. Song, J. Fang, S. Wang, and Z.-X. Yang, "Multi-sem fusion: Multimodal semantic fusion for 3d object detection," 2023.
- [324] G. Xie, Z. Chen, M. Gao, M. Hu, and X. Qin, "Ppf-det: Point-pixel fusion for multi-modal 3d object detection," *IEEE Transactions on Intelligent Transportation Systems*, 2024.
- [325] M. Liang, B. Yang, S. Wang, and R. Urtaun, "Deep continuous fusion for multi-sensor 3d object detection," in *Proceedings of the European conference on computer vision (ECCV)*, 2018, pp. 641–656.
- [326] M. Liang, B. Yang, Y. Chen, R. Hu, and R. Urtaun, "Multi-task multi-sensor fusion for 3d object detection," in *Proceedings of the IEEE/CVF Conference on Computer Vision and Pattern Recognition*, 2019, pp. 7345–7353.
- [327] Y. Li, X. Qi, Y. Chen, L. Wang, Z. Li, J. Sun, and J. Jia, "Voxel field fusion for 3d object detection," in *Proceedings of the IEEE/CVF Conference on Computer Vision and Pattern Recognition*, 2022, pp. 1120–1129.
- [328] Y. Chen, J. Liu, X. Zhang, X. Qi, and J. Jia, "Largekernel3d: Scaling up kernels in 3d sparse cnns," in *Proceedings of the IEEE/CVF Conference on Computer Vision and Pattern Recognition*, 2023, pp. 13488–13498.
- [329] Y. Qin, C. Wang, Z. Kang, N. Ma, Z. Li, and R. Zhang, "Supfusion: Supervised lidar-camera fusion for 3d object detection," in *Proceedings of the IEEE/CVF International Conference on Computer Vision*, 2023, pp. 22014–22024.
- [330] Z. Song, G. Zhang, L. Liu, L. Yang, S. Xu, C. Jia, F. Jia, and L. Wang, "Robofusion: Towards robust multi-modal 3d object detection via sam," *arXiv preprint arXiv:2401.03907*, 2024.
- [331] Y. Kim, K. Park, M. Kim, D. Kum, and J. W. Choi, "3d dual-fusion: Dual-domain dual-query camera-lidar fusion for 3d object detection," *arXiv preprint arXiv:2211.13529*, 2022.
- [332] Z. Chen, Z. Li, S. Zhang, L. Fang, Q. Jiang, and F. Zhao, "Autoalignv2: Deformable feature aggregation for dynamic multi-modal 3d object detection," Jul 2022.
- [333] S. Pang, D. Morris, and H. Radha, "Clocs: Camera-lidar object candidates fusion for 3d object detection," in *2020 IEEE/RSJ International Conference on Intelligent Robots and Systems (IROS)*. IEEE, 2020, pp. 10386–10393.
- [334] J. Ku, M. Mozifian, J. Lee, A. Harakeh, and S. L. Waslander, "Joint 3d proposal generation and object detection from view aggregation," in *2018 IEEE/RSJ International Conference on Intelligent Robots and Systems (IROS)*. IEEE, 2018, pp. 1–8.
- [335] X. Chen, H. Ma, J. Wan, B. Li, and T. Xia, "Multi-view 3d object detection network for autonomous driving," in *Proceedings of the IEEE conference on Computer Vision and Pattern Recognition*, 2017, pp. 1907–1915.
- [336] C. R. Qi, W. Liu, C. Wu, H. Su, and L. J. Guibas, "Frustum pointnets for 3d object detection from rgb-d data," in *Proceedings of the IEEE conference on computer vision and pattern recognition*, 2018, pp. 918–927.
- [337] A. Paigwar, D. Sierra-Gonzalez, Ö. Erkent, and C. Laugier, "Frustum-pointpillars: A multi-stage approach for 3d object detection using rgb camera and lidar," in *Proceedings of the IEEE/CVF international conference on computer vision*, 2021, pp. 2926–2933.
- [338] S. Pang, D. Morris, and H. Radha, "Fast-clocs: Fast camera-lidar object candidates fusion for 3d object detection," in *Proceedings of the IEEE/CVF Winter Conference on Applications of Computer Vision*, 2022, pp. 187–196.
- [339] Z. Chen, Z. Li, S. Zhang, L. Fang, Q. Jiang, F. Zhao, B. Zhou, and H. Zhao, "Autoalign: Pixel-instance feature aggregation for multi-modal 3d object detection," in *Proceedings of the Thirty-First International Joint Conference on Artificial Intelligence*, Jul 2022.
- [340] H. Zhang, L. Liang, P. Zeng, X. Song, and Z. Wang, "Sparselif: High-performance sparse lidar-camera fusion for 3d object detection," *arXiv preprint arXiv:2403.07284*, 2024.
- [341] C. Hu, H. Zheng, K. Li, J. Xu, W. Mao, M. Luo, L. Wang, M. Chen, K. Liu, Y. Zhao *et al.*, "Fusionformer: A multi-sensory fusion in bird's-eye-view and temporal consistent transformer for 3d object detection," *arXiv preprint arXiv:2309.05257*, 2023.
- [342] Y. Li, L. Fan, Y. Liu, Z. Huang, Y. Chen, N. Wang, and Z. Zhang, "Fully sparse fusion for 3d object detection," *IEEE Transactions on Pattern Analysis and Machine Intelligence*, pp. 1–15, 2024.
- [343] Z. Liu, H. Tang, A. Amini, X. Yang, H. Mao, D. L. Rus, and S. Han, "Bevfusion: Multi-task multi-sensor fusion with unified bird's-eye view representation," pp. 2774–2781, 2023.
- [344] H. Hu, F. Wang, J. Su, L. Hu, T. Feng, Z. Zhang, and W. Zhang, "Eabev: Edge-aware bird's-eye-view projector for 3d object detection."
- [345] H. Cai, Z. Zhang, Z. Zhou, Z. Li, W. Ding, and J. Zhao, "Bevfusion4d: Learning lidar-camera fusion under bird's-eye-view via cross-modality guidance and temporal aggregation," *arXiv preprint arXiv:2303.17099*, 2023.
- [346] "Focusing on hard instance for 3d object detection," Aug 2023.
- [347] H. Wang, H. Tang, S. Shi, A. Li, Z. Li, B. Schiele, and L. Wang, "Unitr: A unified and efficient multi-modal transformer for bird's-eye-view representation," in *Proceedings of the IEEE/CVF International Conference on Computer Vision*, 2023, pp. 6792–6802.
- [348] Y. Jiao, Z. Jie, S. Chen, J. Chen, X. Wei, L. Ma, and Y.-G. Jiang, "Msmdfusion: Fusing lidar and camera at multiple scales with multi-depth seeds for 3d object detection," Sep 2022.
- [349] Z. Song, L. Yang, S. Xu, L. Liu, D. Xu, C. Jia, F. Jia, and L. Wang, "Graphbev: Towards robust bev feature alignment for multi-modal 3d object detection," *arXiv preprint arXiv:2403.11848*, 2024.
- [350] Z. Song, F. Jia, H. Pan, Y. Luo, C. Jia, G. Zhang, L. Liu, Y. Ji, L. Yang, and L. Wang, "Contrastalign: Toward robust bev feature alignment via contrastive learning for multi-modal 3d object detection," *arXiv preprint arXiv:2405.16873*, 2024.
- [351] J. Yin, J. Shen, R. Chen, W. Li, R. Yang, P. Frossard, and W. Wang, "Is-fusion: Instance-scene collaborative fusion for multimodal 3d object detection," *arXiv preprint arXiv:2403.15241*, 2024.
- [352] M. Zeeshan Zia, M. Stark, and K. Schindler, "Are cars just 3d boxes?-jointly estimating the 3d shape of multiple objects," in *Proceedings of the IEEE Conference on Computer Vision and Pattern Recognition*, 2014, pp. 3678–3685.
- [353] H. Chen, Y. Huang, W. Tian, Z. Gao, and L. Xiong, "Monorun: Monocular 3d object detection by reconstruction and uncertainty propagation," in *Proceedings of the IEEE/CVF Conference on Computer Vision and Pattern Recognition*, 2021, pp. 10379–10388.
- [354] J. Ku, A. Pon, and S. Waslander, "Monocular 3d object detection leveraging accurate proposals and shape reconstruction," *Cornell University - arXiv,Cornell University - arXiv*, Apr 2019.
- [355] J. J. Park, P. Florence, J. Straub, R. Newcombe, and S. Lovegrove, "DeepSDF: Learning continuous signed distance functions for shape representation," in *2019 IEEE/CVF Conference on Computer Vision and Pattern Recognition (CVPR)*, Jun 2019.
- [356] E. Jørgensen, C. Zach, and F. Kahl, "Monocular 3d object detection and box fitting trained end-to-end using intersection-over-union loss." *Cornell University - arXiv,Cornell University - arXiv*, Jun 2019.
- [357] H.-N. Hu, Q.-Z. Cai, D. Wang, J. Lin, M. Sun, P. Krahenbuhl, T. Darrell, and F. Yu, "Joint monocular 3d vehicle detection and tracking," in *Proceedings of the IEEE/CVF International Conference on Computer Vision*, 2019, pp. 5390–5399.
- [358] C. Godard, O. Mac Aodha, and G. J. Brostow, "Unsupervised monocular depth estimation with left-right consistency," in *Proceedings of the IEEE conference on computer vision and pattern recognition*, 2017, pp. 270–279.
- [359] X. Chu, J. Deng, Y. Li, Z. Yuan, Y. Zhang, J. Ji, and Y. Zhang, "Neighbor-vote: Improving monocular 3d object detection through neighbor distance voting," *Cornell University - arXiv,Cornell University - arXiv*, Jul 2021.
- [360] Y. Hong, H. Dai, and Y. Ding, "Cross-modality knowledge distillation network for monocular 3d object detection," in *European Conference on Computer Vision*. Springer, 2022, pp. 87–104.
- [361] X. Weng and K. Kitani, "Monocular 3d object detection with pseudo-lidar point cloud," in *Proceedings of the IEEE/CVF International Conference on Computer Vision Workshops*, 2019, pp. 0–0.
- [362] X. Wang, W. Yin, T. Kong, Y. Jiang, L. Li, and C. Shen, "Task-aware monocular depth estimation for 3d object detection," in *Proceedings of the AAAI Conference on Artificial Intelligence*, vol. 34, no. 07, 2020, pp. 12257–12264.
- [363] X. Ye, L. Du, Y. Shi, Y. Li, X. Tan, J. Feng, E. Ding, and S. Wen, "Monocular 3d object detection via feature domain adaptation," in *Computer Vision—ECCV 2020: 16th European Conference, Glasgow, UK, August 23–28, 2020, Proceedings, Part IX 16*. Springer, 2020, pp. 17–34.

- [364] L. Wang, L. Zhang, Y. Zhu, Z. Zhang, T. He, M. Li, and X. Xue, "Progressive coordinate transforms for monocular 3d object detection," *Advances in Neural Information Processing Systems*, vol. 34, pp. 13 364–13 377, 2021.
- [365] H. Meng, C. Li, G. Chen, L. Chen *et al.*, "Efficient 3d object detection based on pseudo-lidar representation," *IEEE Transactions on Intelligent Vehicles*, 2023.
- [366] X. Guo, K. Yang, W. Yang, X. Wang, and H. Li, "Group-wise correlation stereo network," in *Proceedings of the IEEE/CVF conference on computer vision and pattern recognition*, 2019, pp. 3273–3282.
- [367] P. Cao, H. Chen, Y. Zhang, and G. Wang, "Multi-view frustum pointnet for object detection in autonomous driving," in *2019 IEEE International Conference on Image Processing (ICIP)*. IEEE, 2019, pp. 3896–3899.
- [368] C. Xu, B. Wu, J. Hou, S. Tsai, R. Li, J. Wang, W. Zhan, Z. He, P. Vajda, K. Keutzer *et al.*, "Nerf-det: Learning geometry-aware volumetric representation for multi-view 3d object detection," in *Proceedings of the IEEE/CVF International Conference on Computer Vision*, 2023, pp. 23 320–23 330.
- [369] D. Wang, X. Cui, X. Chen, Z. Zou, T. Shi, S. Salcudean, Z. J. Wang, and R. Ward, "Multi-view 3d reconstruction with transformers," in *Proceedings of the IEEE/CVF International Conference on Computer Vision*, 2021, pp. 5722–5731.
- [370] A. Vaswani, N. Shazeer, N. Parmar, J. Uszkoreit, L. Jones, A. N. Gomez, L. Kaiser, and I. Polosukhin, "Attention is all you need," *Advances in neural information processing systems*, vol. 30, 2017.
- [371] Z. Liu, Y. Lin, Y. Cao, H. Hu, Y. Wei, Z. Zhang, S. Lin, and B. Guo, "Swin transformer: Hierarchical vision transformer using shifted windows." in *2021 IEEE/CVF International Conference on Computer Vision (ICCV)*, Oct 2021.
- [372] A. Dosovitskiy, L. Beyer, A. Kolesnikov, D. Weissenborn, X. Zhai, T. Unterthiner, M. Dehghani, M. Minderer, G. Heigold, S. Gelly *et al.*, "An image is worth 16x16 words: Transformers for image recognition at scale," *arXiv preprint arXiv:2010.11929*, 2020.
- [373] X. Zhu, W. Su, L. Lu, B. Li, X. Wang, and J. Dai, "Deformable detr: Deformable transformers for end-to-end object detection," *arXiv preprint arXiv:2010.04159*, 2020.
- [374] N. Carion, F. Massa, G. Synnaeve, N. Usunier, A. Kirillov, and S. Zagoruyko, "End-to-end object detection with transformers," in *European conference on computer vision*. Springer, 2020, pp. 213–229.
- [375] H. Li, C. Sima, J. Dai, W. Wang, L. Lu, H. Wang, J. Zeng, Z. Li, J. Yang, H. Deng *et al.*, "Delving into the devils of bird's-eye-view perception: A review, evaluation and recipe," *IEEE Transactions on Pattern Analysis and Machine Intelligence*, 2023.
- [376] X. Liu, N. Xue, and T. Wu, "Learning auxiliary monocular contexts helps monocular 3d object detection," in *Proceedings of the AAAI Conference on Artificial Intelligence*, vol. 36, no. 2, 2022, pp. 1810–1818.
- [377] Z. Chong, X. Ma, H. Zhang, Y. Yue, H. Li, Z. Wang, and W. Ouyang, "Monodistill: Learning spatial features for monocular 3d object detection," *arXiv preprint arXiv:2201.10830*, 2022.
- [378] J. Chen, Q. Wang, W. Peng, H. Xu, X. Li, and W. Xu, "Disparity-based multiscale fusion network for transportation detection," *IEEE Transactions on Intelligent Transportation Systems*, vol. 23, no. 10, pp. 18 855–18 863, 2022.
- [379] X. Zhou, D. Wang, and P. Krähenbühl, "Objects as points," *arXiv: Computer Vision and Pattern Recognition, arXiv: Computer Vision and Pattern Recognition*, Apr 2019.
- [380] J. Li, S. Luo, Z. Zhu, H. Dai, A. S. Krylov, Y. Ding, and L. Shao, "3d iou-net: Iou guided 3d object detector for point clouds," *arXiv preprint arXiv:2004.04962*, 2020.
- [381] Z. Li, F. Wang, and N. Wang, "Lidar r-cnn: An efficient and universal 3d object detector," in *Proceedings of the IEEE/CVF Conference on Computer Vision and Pattern Recognition*, 2021, pp. 7546–7555.
- [382] C. Zhang, H. Wang, Y. Cai, L. Chen, Y. Li, M. A. Sotelo, and Z. Li, "Robust-fusionnet: Deep multimodal sensor fusion for 3-d object detection under severe weather conditions," *IEEE Transactions on Instrumentation and Measurement*, vol. 71, pp. 1–13, 2022.
- [383] C. Chen, L. Z. Fragonara, and A. Tsourdos, "Roifusion: 3d object detection from lidar and vision," *IEEE Access*, vol. 9, pp. 51710–51 721, 2021.
- [384] S. Pang, D. Morris, and H. Radha, "Clocs: Camera-lidar object candidates fusion for 3d object detection," in *2020 IEEE/RSJ International Conference on Intelligent Robots and Systems (IROS)*. IEEE, 2020, pp. 10 386–10 393.
- [385] Y. Zhang, J. Chen, and D. Huang, "Cat-det: Contrastively augmented transformer for multi-modal 3d object detection," in *Proceedings of the IEEE/CVF Conference on Computer Vision and Pattern Recognition (CVPR)*, June 2022, pp. 908–917.
- [386] L. N. Smith and N. Topin, "Super-convergence: Very fast training of neural networks using large learning rates," in *Artificial intelligence and machine learning for multi-domain operations applications*, vol. 11006. SPIE, 2019, pp. 369–386.
- [387] H. Meng, C. Li, G. Chen, Z. Gu, and A. Knoll, "Er3d: An efficient real-time 3d object detection framework for autonomous driving," in *29th IEEE International Conference on Parallel and Distributed Systems*, 2023.
- [388] C. Li, H. Meng, G. Chen, and L. Chen, "Real-time pseudo-lidar 3d object detection with geometric constraints," in *2022 IEEE 25th International Conference on Intelligent Transportation Systems (ITSC)*. IEEE, 2022, pp. 3298–3303.
- [389] H. Meng, C. Li, C. Zhong, J. Gu, G. Chen, and A. Knoll, "Fastfusion: Deep stereo-lidar fusion for real-time high-precision dense depth sensing," *Journal of Field Robotics*, vol. 40, no. 7, pp. 1804–1816, 2023.
- [390] Z. Zhu, Y. Zhang, H. Chen, Y. Dong, S. Zhao, W. Ding, J. Zhong, and S. Zheng, "Understanding the robustness of 3d object detection with bird's-eye-view representations in autonomous driving," in *Proceedings of the IEEE/CVF Conference on Computer Vision and Pattern Recognition*, 2023, pp. 21 600–21 610.
- [391] Y. Zhang, J. Hou, and Y. Yuan, "A comprehensive study of the robustness for lidar-based 3d object detectors against adversarial attacks," *International Journal of Computer Vision*, pp. 1–33, 2023.
- [392] Z. Liu, X. Zhao, T. Huang, R. Hu, Y. Zhou, and X. Bai, "Tanet: Robust 3d object detection from point clouds with triple attention," in *Proceedings of the AAAI conference on artificial intelligence*, vol. 34, no. 07, 2020, pp. 11 677–11 684.
- [393] D. Rukhovich, A. Vorontsova, and A. Konushin, "Imvoxelnet: Image to voxels projection for monocular and multi-view general-purpose 3d object detection," in *Proceedings of the IEEE/CVF Winter Conference on Applications of Computer Vision*, 2022, pp. 2397–2406.
- [394] G. P. Meyer, A. Laddha, E. Kee, C. Vallespi-Gonzalez, and C. K. Wellington, "Lasernet: An efficient probabilistic 3d object detector for autonomous driving," in *Proceedings of the IEEE/CVF conference on computer vision and pattern recognition*, 2019, pp. 12 677–12 686.
- [395] G. P. Meyer, J. Charland, S. Pandey, A. Laddha, S. Gautam, C. Vallespi-Gonzalez, and C. K. Wellington, "Laserflow: Efficient and probabilistic object detection and motion forecasting," *IEEE Robotics and Automation Letters*, vol. 6, no. 2, pp. 526–533, 2020.
- [396] B. Li, T. Zhang, and T. Xia, "Vehicle detection from 3d lidar using fully convolutional network," *arXiv preprint arXiv:1608.07916*, 2016.
- [397] Y. Su, W. Liu, Z. Yuan, M. Cheng, Z. Zhang, X. Shen, and C. Wang, "Dla-net: Learning dual local attention features for semantic segmentation of large-scale building facade point clouds," *Pattern Recognition*, vol. 123, p. 108372, 2022.
- [398] O. Ronneberger, P. Fischer, and T. Brox, "U-net: Convolutional networks for biomedical image segmentation," in *International Conference on Medical image computing and computer-assisted intervention*. Springer, 2015, pp. 234–241.
- [399] P. Sun, W. Wang, Y. Chai, G. Elsayed, A. Bewley, X. Zhang, C. Sminchisescu, and D. Anguelov, "Rsn: Range sparse net for efficient, accurate lidar 3d object detection," in *Proceedings of the IEEE/CVF Conference on Computer Vision and Pattern Recognition*, 2021, pp. 5725–5734.
- [400] S. Ren, K. He, R. Girshick, and J. Sun, "Faster r-cnn: Towards real-time object detection with region proposal networks," *IEEE Transactions on Pattern Analysis and Machine Intelligence*, p. 1137–1149, Jun 2017.
- [401] T.-Y. Lin, P. Dollár, R. Girshick, K. He, B. Hariharan, and S. Belongie, "Feature pyramid networks for object detection," in *2017 IEEE Conference on Computer Vision and Pattern Recognition (CVPR)*, Jul 2017.
- [402] Y. Chai, P. Sun, J. Ngiam, W. Wang, B. Caine, V. Vasudevan, X. Zhang, and D. Anguelov, "To the point: Efficient 3d object detection in the range image with graph convolution kernels," in *Proceedings of the IEEE/CVF conference on computer vision and pattern recognition*, 2021, pp. 16 000–16 009.
- [403] A. Barrera, C. Guindel, J. Beltrán, and F. García, "Birdnet+: End-to-end 3d object detection in lidar bird's eye view," in *2020 IEEE 23rd International Conference on Intelligent Transportation Systems (ITSC)*. IEEE, 2020, pp. 1–6.

- [404] H. Zhou, X. Zhu, X. Song, Y. Ma, Z. Wang, H. Li, and D. Lin, "Cylinder3d: An effective 3d framework for driving-scene lidar semantic segmentation," *arXiv preprint arXiv:2008.01550*, 2020.
- [405] C. R. Qi, H. Su, K. Mo, and L. J. Guibas, "Pointnet: Deep learning on point sets for 3d classification and segmentation," in *Proceedings of the IEEE conference on computer vision and pattern recognition*, 2017, pp. 652–660.
- [406] J. Redmon and A. Farhadi, "Yolov3: An incremental improvement," *arXiv preprint arXiv:1804.02767*, 2018.
- [407] K. He, X. Zhang, S. Ren, and J. Sun, "Deep residual learning for image recognition," in *2016 IEEE Conference on Computer Vision and Pattern Recognition (CVPR)*, Jun 2016.
- [408] B. Graham, "Spatially-sparse convolutional neural networks," *arXiv preprint arXiv:1409.6070*, 2014.
- [409] B. Graham, M. Engelcke, and L. v. d. Maaten, "3d semantic segmentation with submanifold sparse convolutional networks," in *2018 IEEE/CVF Conference on Computer Vision and Pattern Recognition*, Jun 2018.
- [410] C. R. Qi, L. Yi, H. Su, and L. J. Guibas, "Pointnet++: Deep hierarchical feature learning on point sets in a metric space," *Advances in neural information processing systems*, vol. 30, 2017.
- [411] M. Feng, S. Z. Gilani, Y. Wang, L. Zhang, and A. Mian, "Relation graph network for 3d object detection in point clouds," *IEEE Transactions on Image Processing*, p. 92–107, Jan 2021.
- [412] Z. Liu, Z. Zhang, Y. Cao, H. Hu, and X. Tong, "Group-free 3d object detection via transformers," Apr 2021.
- [413] H. Zhao, L. Jiang, J. Jia, P. Torr, and V. Koltun, "Point transformer," in *2021 IEEE/CVF International Conference on Computer Vision (ICCV)*, Oct 2021.
- [414] J. Liu, T. He, H. Yang, R. Su, J. Tian, J. Wu, H. Guo, K. Xu, and W. Ouyang, "3d-queryvis: A query-based framework for 3d instance segmentation," Nov 2022.
- [415] Y. Chen, S. Liu, X. Shen, and J. Jia, "Fast point r-cnn," in *Proceedings of the IEEE/CVF international conference on computer vision*, 2019, pp. 9775–9784.
- [416] Q. Hu, D. Liu, and W. Hu, "Density-insensitive unsupervised domain adaption on 3d object detection," in *Proceedings of the IEEE/CVF Conference on Computer Vision and Pattern Recognition*, 2023, pp. 17 556–17 566.
- [417] J. Yuan, B. Zhang, X. Yan, T. Chen, B. Shi, Y. Li, and Y. Qiao, "Bi3d: Bi-domain active learning for cross-domain 3d object detection," in *Proceedings of the IEEE/CVF Conference on Computer Vision and Pattern Recognition*, 2023, pp. 15 599–15 608.
- [418] G. P. Meyer, A. Laddha, E. Kee, C. Vallespi-Gonzalez, and C. K. Wellington, "Lasernet: An efficient probabilistic 3d object detector for autonomous driving," in *Proceedings of the IEEE/CVF conference on computer vision and pattern recognition*, 2019, pp. 12 677–12 686.
- [419] D. Xu, D. Anguelov, and A. Jain, "Pointfusion: Deep sensor fusion for 3d bounding box estimation," in *Proceedings of the IEEE conference on computer vision and pattern recognition*, 2018, pp. 244–253.
- [420] B. Ding, J. Xie, and J. Nie, "C2bn: Cross-modality and cross-scale balance network for multi-modal 3d object detection," in *ICASSP 2023-2023 IEEE International Conference on Acoustics, Speech and Signal Processing (ICASSP)*. IEEE, 2023, pp. 1–5.
- [421] C. Lin, D. Tian, X. Duan, J. Zhou, D. Zhao, and D. Cao, "Cl3d: Camera-lidar 3d object detection with point feature enhancement and point-guided fusion," *IEEE Transactions on Intelligent Transportation Systems*, vol. 23, no. 10, pp. 18 040–18 050, 2022.
- [422] Z. Song, L. Peng, J. Hu, D. Yao, and Y. Zhang, "A re-calibration method for object detection with multi-modal alignment bias in autonomous driving," *arXiv preprint arXiv:2405.16848*, 2024.
- [423] M. Liu, Y. Chen, J. Xie, Y. Zhu, Y. Zhang, L. Yao, Z. Bing, G. Zhuang, K. Huang, and J. T. Zhou, "Menet: Multi-modal mapping enhancement network for 3d object detection in autonomous driving," *IEEE Transactions on Intelligent Transportation Systems*, 2024.
- [424] Z. Wu, Y. Wu, X. Wang, Y. Gan, and J. Pu, "A robust diffusion modeling framework for radar camera 3d object detection," in *Proceedings of the IEEE/CVF Winter Conference on Applications of Computer Vision*, 2024, pp. 3282–3292.
- [425] C. Zhang, H. Wang, L. Chen, Y. Li, and Y. Cai, "Mixedfusion: An efficient multimodal data fusion framework for 3-d object detection and tracking," *IEEE Transactions on Neural Networks and Learning Systems*, pp. 1–15, 2023.
- [426] J. Hou, Z. Liu, Z. Zou, X. Ye, X. Bai *et al.*, "Query-based temporal fusion with explicit motion for 3d object detection," *Advances in Neural Information Processing Systems*, vol. 36, 2024.
- [427] Z. Liu, X. Ye, Z. Zou, X. He, X. Tan, E. Ding, J. Wang, and X. Bai, "Multi-modal 3d object detection by box matching," *arXiv preprint arXiv:2305.07713*, 2023.
- [428] L. Zheng, S. Li, B. Tan, L. Yang, S. Chen, L. Huang, J. Bai, X. Zhu, and Z. Ma, "Rcfusion: Fusing 4d radar and camera with bird's-eye view features for 3d object detection," *IEEE Transactions on Instrumentation and Measurement*, 2023.
- [429] Y. Zeng, C. Ma, M. Zhu, Z. Fan, and X. Yang, "Cross-modal 3d object detection and tracking for auto-driving," in *2021 IEEE/RSJ International Conference on Intelligent Robots and Systems (IROS)*. IEEE, 2021, pp. 3850–3857.
- [430] C. Ge, J. Chen, E. Xie, Z. Wang, L. Hong, H. Lu, Z. Li, and P. Luo, "Metabev: Solving sensor failures for bev detection and map segmentation," *arXiv preprint arXiv:2304.09801*, 2023.
- [431] T. Zhou, J. Chen, Y. Shi, K. Jiang, M. Yang, and D. Yang, "Bridging the view disparity between radar and camera features for multi-modal fusion 3d object detection," *IEEE Transactions on Intelligent Vehicles*, vol. 8, no. 2, pp. 1523–1535, 2023.
- [432] Z. Wang, W. Zhan, and M. Tomizuka, "Fusing bird view lidar point cloud and front view camera image for deep object detection," *Cornell University - arXiv, Cornell University - arXiv*, Nov 2017.
- [433] S. Jiang, S. Xu, L. Liu, Z. Song, Y. Bo, Z.-X. Yang *et al.*, "Sparseinteraction: Sparse semantic guidance for radar and camera 3d object detection," in *ACM Multimedia 2024*.
- [434] J. Achiam, S. Adler, S. Agarwal, L. Ahmad, I. Akkaya, F. L. Aleman, D. Almeida, J. Altenschmidt, S. Altman, S. Anadkat *et al.*, "Gpt-4 technical report," *arXiv preprint arXiv:2303.08774*, 2023.
- [435] A. Kirillov, E. Mintun, N. Ravi, H. Mao, C. Rolland, L. Gustafson, T. Xiao, S. Whitehead, A. C. Berg, W.-Y. Lo *et al.*, "Segment anything," in *Proceedings of the IEEE/CVF International Conference on Computer Vision*, 2023, pp. 4015–4026.
- [436] Y. Liu, L. Kong, J. Cen, R. Chen, W. Zhang, L. Pan, K. Chen, and Z. Liu, "Segment any point cloud sequences by distilling vision foundation models," *Advances in Neural Information Processing Systems*, vol. 36, 2024.
- [437] A. Radford, J. W. Kim, C. Hallacy, A. Ramesh, G. Goh, S. Agarwal, G. Sastry, A. Askell, P. Mishkin, J. Clark *et al.*, "Learning transferable visual models from natural language supervision," in *International conference on machine learning*. PMLR, 2021, pp. 8748–8763.
- [438] R. Greer, B. Antoniusen, A. Møgelmoose, and M. Trivedi, "Language-driven active learning for diverse open-set 3d object detection," *arXiv preprint arXiv:2404.12856*, 2024.
- [439] Y. Hu, J. Yang, L. Chen, K. Li, C. Sima, X. Zhu, S. Chai, S. Du, T. Lin, W. Wang *et al.*, "Planning-oriented autonomous driving," in *Proceedings of the IEEE/CVF Conference on Computer Vision and Pattern Recognition*, 2023, pp. 17 853–17 862.
- [440] D. Xu, H. Li, Q. Wang, Z. Song, L. Chen, and H. Deng, "M2da: Multi-modal fusion transformer incorporating driver attention for autonomous driving," *arXiv preprint arXiv:2403.12552*, 2024.



**Ziyang Song**, was born in Xingtai, Hebei Province, China in 1997. He received the B.S. degree from Hebei Normal University of Science and Technology (China) in 2019. He received a master's degree major in Hebei University of Science and Technology (China) in 2022. He is now a PhD student majoring in Computer Science and Technology at Beijing Jiaotong University (China), with a research focus on Computer Vision.



**Lin Liu** was born in Jinzhou, Liaoning Province, China, in 2001. He is now a college student majoring in Computer Science and Technology at China University of Geosciences(Beijing). Since Dec. 2022, he has been recommended for a master's degree in Computer Science and Technology at Beijing Jiaotong University. His research interests are in computer vision.



**Lei Yang (Graduate Student Member, IEEE)** received his B.E. degree from Taiyuan University of Technology, Taiyuan, China, and the M.S. degree from the Robotics Institute at Beihang University, in 2018. Then he joined the Autonomous Driving R&D Department of JD.COM as an algorithm researcher from 2018 to 2020. He is now a Ph.D. student in the School of Vehicle and Mobility at Tsinghua University since 2020. His current research interests include computer vision, 3D scene understanding and autonomous driving.



**Feiyang Jia** was born in Yinchuan, Ningxia Province, China, in 1998. He received his B.S. degree from Beijing Jiaotong University (China) in 2020. He received a master's degree from Beijing Technology and Business University (China) in 2023. He is now a Ph.D. student majoring in Computer Science and Technology at Beijing Jiaotong University (China), with research focus on Computer Vision.



**Yadan Luo** (Member, IEEE) received the BS degree in computer science from the University of Electronic Engineering and Technology of China, and the PhD degree from the University of Queensland. Her research interests include machine learning, computer vision, and multimedia data analysis. She is now a lecturer with the University of Queensland.



**Li Wang** was born in Shangqiu, Henan Province, China in 1990. He received his Ph.D. degree in mechatronic engineering at the State Key Laboratory of Robotics and System, Harbin Institute of Technology, in 2020. He was a visiting scholar at Nanyang Technology of University for two years. He was a postdoctoral fellow in the State Key Laboratory of Automotive Safety and Energy, and the School of Vehicle and Mobility, Tsinghua University. Currently, he is an assistant professor at School of Mechanical Engineering, Beijing Institute

of Technology. His research interests include autonomous driving perception, 3D robot vision, and Multi-modal fusion.



**Caiyan Jia**, born on March 2, 1976, is a lecturer and a postdoctoral fellow of the Chinese Computer Society. she graduated from Ningxia University in 1998 with a bachelor's degree in mathematics, Xiangtan University in 2001 with a master's degree in computational mathematics, specializing in intelligent information processing, and the Institute of Computing Technology of the Chinese Academy of Sciences in 2004 with a doctorate degree in engineering, specializing in data mining. she has received her D. degree in 2004. Since 2002, she has

been a reviewer for several papers in AAAI, IJCAI, NeurIPS TKDE, etc.



**Guoxin Zhang**, was born in 1998 in Xingtai, Hebei Province, China. He received his bachelor's and Master's degrees from Hebei University of Science and Technology in 2021 and 2024, respectively. He is now a Ph.D. student in the School of Computer Science at Beijing University of Posts and Telecommunications (China) since 2024. His research interests are in computer vision.